RADC-TR-79-285
Final Technical Report
November 1979

LEVEL II

POLARIZATION PROCESSING TECHNIQUES STUDY

ITT Gilfillan

Mr. Albert Klein
Dr. David Hammers
Mr. Masaaki (Tom) Fujita
Dr. George Ioannidis
Dr. Nhan Levan
Dr. Jeffery Bell
Mr. Charles Lucas

ROME AIR DEVELOPMENT CENTER
Air Force Systems Command
Griffiss Air Force Base, New York 13441

This report has been reviewed by the RADC Public Affairs Office (PA) and is releasable to the National Technical Information Service (NTIS). At NTIS it will be releasable to the general public, including foreign nations.

RADC-TR-79-285 has been reviewed and is approved for publication.

APPROVED: Russell D. Brown

RUSSELL D. BROWN
Project Engineer

APPROVED: Frank J. Rehm

FRANK J. REHM
Technical Director
Surveillance Division

FOR THE COMMANDER: John P. Huss

JOHN P. HUSS
Acting Chief, Plans Office

If your address has changed or if you wish to be removed from the RADC mailing list, or if the addressee is no longer employed by your organization, please notify RADC (OCTS), Griffiss AFB NY 13441. This will assist us in maintaining a current mailing list.

Do not return this copy. Retain or destroy.

UNCLASSIFIED

SECURITY CLASSIFICATION OF THIS PAGE (When Data Entered)

REPORT DOCUMENTATION PAGE

READ INSTRUCTIONS BEFORE COMPLETING FORM

1 REPORT NUMBER: RADC-TR-79-285	2 GOVT ACCESSION NO. / 3 RECIPIENT'S CATALOG NUMBER
4 TITLE (and Subtitle): POLARIZATION PROCESSING TECHNIQUES STUDY	5 TYPE OF REPORT & PERIOD COVERED: Final Technical Report. Mar 78 — Mar 79
	6 PERFORMING ORG. REPORT NUMBER: 9532-F
7 AUTHOR(s): Mr. Albert Klein; Dr. David Hammers; Mr. Masaaki (Tom) Fujita; Dr. George Ioannidis; Dr. Nhan Levan; Dr. Jeffery Bell; Mr. Charles Lucas	8 CONTRACT OR GRANT NUMBER(s): F30602-78-C-0119
9 PERFORMING ORGANIZATION NAME AND ADDRESS: ITT Gilfillan, 7821 Orion Avenue, Van Nuys CA 91409	10 PROGRAM ELEMENT, PROJECT, TASK AREA & WORK UNIT NUMBERS: 62702F; 45061136
11 CONTROLLING OFFICE NAME AND ADDRESS: Rome Air Development Center (OCTS), Griffiss AFB NY 13441	12 REPORT DATE: November 1979
	13 NUMBER OF PAGES: 152
14 MONITORING AGENCY NAME & ADDRESS (if different from Controlling Office): Same	15 SECURITY CLASS. (of this report): UNCLASSIFIED
	15a DECLASSIFICATION/DOWNGRADING SCHEDULE: N/A

16 DISTRIBUTION STATEMENT (of this Report)

Approved for public release; distribution unlimited.

17 DISTRIBUTION STATEMENT (of the abstract entered in Block 20, if different from Report)

Same

18 SUPPLEMENTARY NOTES

RADC Project Engineer: Russell D. Brown (OCTS)

19 KEY WORDS (Continue on reverse side if necessary and identify by block number)

Radar Detection
Signal Processing
Clutter Modeling
Polarization Processing
Dual Channel Radar
Mathematics and Statistics

20 ABSTRACT (Continue on reverse side if necessary and identify by block number)

Polarization serves as a discriminant between radar targets and surrounding chaff and clutter. A dual channel system is required to utilize polarization information which exists in the target scattering matrix. Several methods are presented for designing an optimum polarization codes transmit waveform and matched coherent receiver based on target and clutter statistics. Simulation results for various target models against chaff show a significant increase in detectability for the two-channel system.

DD FORM 1 JAN 73 1473

UNCLASSIFIED

SECURITY CLASSIFICATION OF THIS PAGE (When Data Entered)

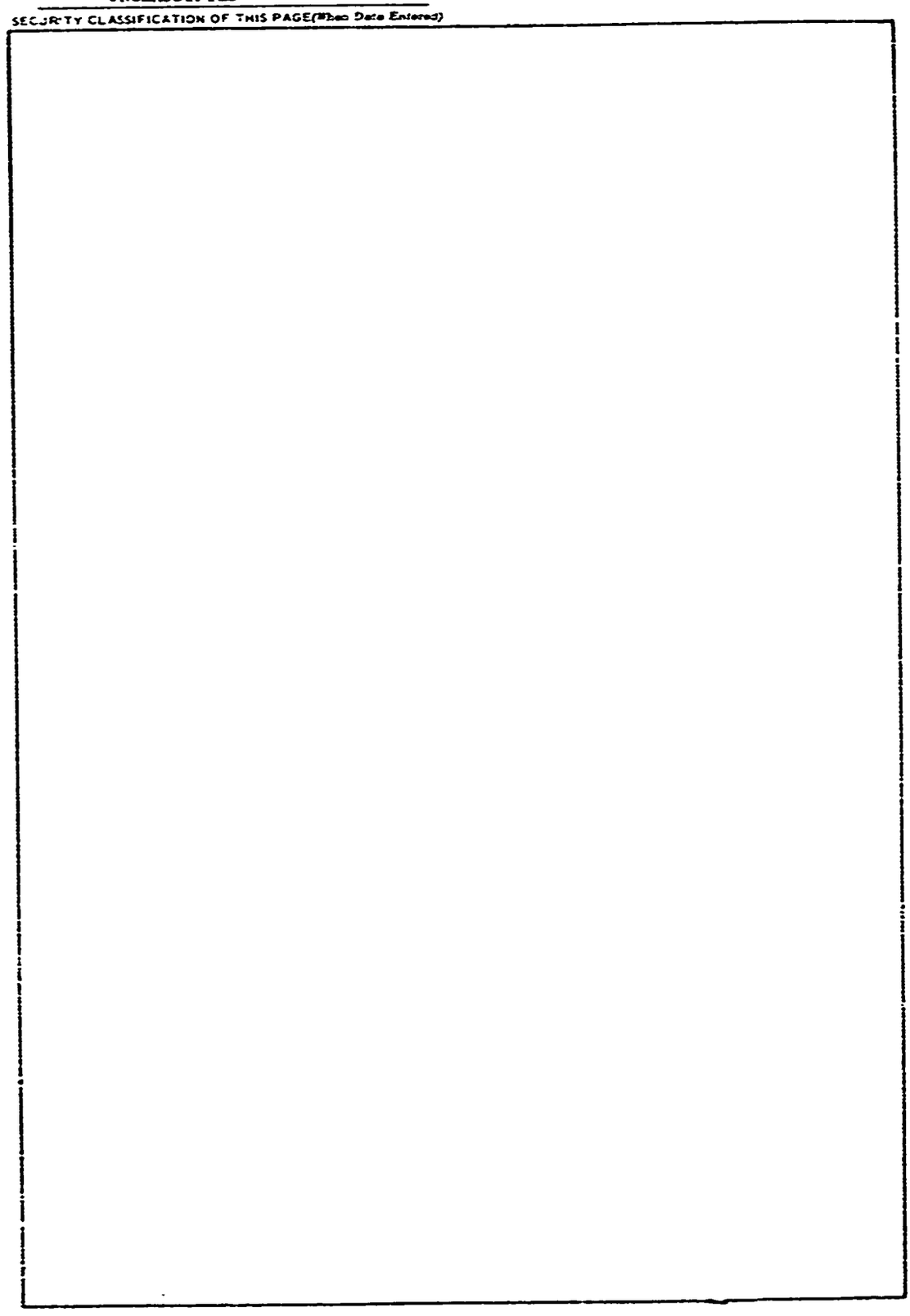

PREFACE

This report describes work performed by ITT Gilfillan for Rome Air Development Center (RADC) under Contract No. F30602-78-C-0119. The Project Engineers for RADC were Mr. Vincent Vannicola and Russell Brown. The objective of this study was to optimize radar systems by using the properties of the scattering matrix, including polarization and statistical, to design the waveform and receiver. The report contains results of computer simulations which compare target detection performance for derived dual channel systems which incorporate processing techniques utilizing the scattering matrix, against that of conventional single channel systems.

Analytical and systematic approaches are described for five techniques which lead to dual channel optimum processing. Finally, the statistical target and chaff models are formulated and described as they are applied to computer simulation for system evaluation.

The report was edited by Mr. Albert Klein who also contributed to Sections 3, 5, and 6. Dr. David Hammers supervised the signal processing and analysis tasks, which were performed by Mr. Masaaki (Tom) Fujita, Dr. George Ioannidis, and Dr. Nhan Levan. Dr. Jeffery Bell wrote Section 4 on modeling and simulation and contributed to Sections 1 and 2. Mr. Charles Lucas was responsible for the signal processor design.

TABLE OF CONTENTS

Section			Page
	FOREWORD		ii
1	INTRODUCTORY SUMMARY		1-1
	1.1	Background and Problem	1-1
	1.2	Approach	1-1
	1.3	Results and Conclusions	1-2
2	PROBLEM FORMULATION		2-1
	2.1	Polarization Properties of Targets and Clutter	2-1
	2.2	Scattering System Formulation	2-3
	2.3	Computation of Return Signal Covariance Matrix	2-5
		2.3.1 Definitions of Important Matrices	2-5
		2.3.2 First Method	2-6
		2.3.3 Second Method	2-7
		2.3.4 Further Notes	2-8
	2.4	Covariance Matrices of Point Target in Chaff	2-10
3	OPTIMAL TRANSMIT WAVEFORM AND RECEIVER DEVELOPMENT		3-1
	3.1	Finite Dimensional Space	3-2
		3.1.1 Generalized Vector Approach	3-2
		3.1.2 Vector Approach Waveform Design	3-6
		3.1.3 Generalized Matrix Approach	3-8
		3.1.4 Maximum Likelihood Detector	3-14
		3.1.5 Preliminary Design of the Processor	3-17
	3.2	The State Space Approach	3-21
		3.2.1 State Space Modeling of Radar Targets and Clutter	3-21
		3.2.2 Optimum Receiver Design: The Case of a Point Target in a Cloud of Chaff Dipoles	3-26
		3.2.3 State Space Summary	3-31
	3.3	The Fredholm Integral Equation Approach	3-31
		3.3.1 Integral Equation for the Filter Q_0	3-32
		3.3.2 The System of Fredholm Integral Equations for $D_0(t, u) = [D_0^{ij}(t, u)]$	3-33

TABLE OF CONTENTS (Continued)

Section			Page
		3.3.3 Integral Equation for the Filter E_0	3-33
		3.3.4 Approach to Solving Equations	3-34
		3.3.5 Fredholm Approach Summary	3-35
	3.4	Stokes Formalism	3-35
		3.4.1 Stokes Model	3-35
4		MODELING AND SIMULATION	4-1
	4.1	Target Models	4-1
		4.1.1 Methodology	4-1
		4.1.2 Target: A Collection of Scatters	4-1
		4.1.3 Radar Cross Section Validation	4-4
		4.1.4 Covariance Matrix	4-8
	4.2	Chaff	4-8
		4.2.1 The Dipole Chaff Cloud Model	4-8
		4.2.2 Theoretical Covariance Matrix	4-8
		4.2.3 Stochastic Model Derived From Autoregressive Process	4-12
		4.2.4 Covariance Matrix Validation	4-18
	4.3	Simulation	4-18
		4.3.1 Overview	4-18
		4.3.2 Target	4-18
		4.3.3 Chaff	4-23
		4.3.4 Processing Algorithms	4-23
5		COMPUTER SIMULATION RESULTS	5-1
	5.1	Simulation Parameters	5-1
		5.1.1 Target and Chaff Models	5-1
		5.1.2 Definition of s/c Ratio	5-3
		5.1.3 Qualitative Assessment	5-3
	5.2	Stokes Approach Results	5-4
	5.3	Vector Approach Results	5-5
	5.4	Matrix Approach Results	5-6
		5.4.1 Dual Channel Results	5-6
		5.4.2 Matrix Dual vs Single Channel Results	5-8
		5.4.3 Transmit Waveform Selection	5-13
		5.4.4 Receiver Matrix	5-14

TABLE OF CONTENTS (Continued)

Section		Page
6	CONCLUSIONS AND RECOMMENDATIONS	6-1
	REFERENCES	6-4
Appendix		
A	A MODEL FOR THE SIMULATION OF THE SPECTRAL AND POLARIZATION CHARACTERISTICS OF CHAFF	A-1
B	LIKELIHOOD DETECTION	B-1
C	CONSTRAINED OPTIMIZATION OF S/C	C-1
D	SIMULTANEOUS DIAGONALIZATION OF TWO COVARIANCE MATRICES	D-1
E	BHATTACHARYYA DISTANCE B FOR GAUSSIAN DENSITIES	E-1
F	AUTOREGRESSIVE MODELING	F-1

EVALUATION

Air Force radar systems must operate against natural and man-made interference, particularly clutter and chaff. This program has investigated new methods of target detection in dual polarization radar systems. Contrasting scatter in polarization between targets and chaff is exploited to enhance target detection.

Of significance in this study are design methods for polarization coded transmit waveforms and matched receivers. A simulation was performed for analysis of potential improvement factor. This contract supports TPO R4B, Surveillance ECCM.

Russell D. Brown
RUSSELL D. BROWN
Project Engineer

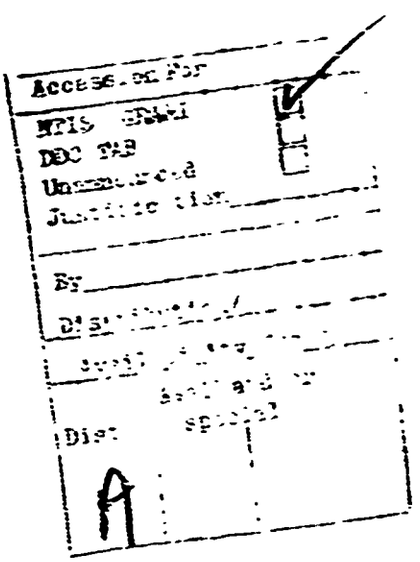

Section 1

INTRODUCTORY SUMMARY

1.1 BACKGROUND AND PROBLEM

Conventional radar signal processing techniques use Doppler and polarization information in discriminating target returns from chaff and other forms of interference. These two discriminants are used independently; most often in single channel systems. For example, the polarizations of the transmit and receive antennas are fixed and determined by the combiner. On the other hand, spectral processing is performed by the receiver processor on signals that have already been combined by the antenna. As a result, such systems do not exploit the statistical properties of the target and chaff scattering matrices, which include both spectral and polarization information.

The utilization of this information which exists in the scattering matrix should be more fully exploitable in a dual-channel system, relative to the more conventional single channel system. Thus the basic objective of this effort was to explore the merits of performing the signal processing in a dual-channel system, to develop the optimum combined spectral and polarization processing approach. This involves determining the optimum transmit waveform and coherent receive polarization and time weights for each pulse in a burst. The criterion of optimality is to maximize the probability of target detection for a given false alarm rate attributed to the interference.

1.2 APPROACH

The basis of our approach was to formulate the system in an operator theoretic manner, such that the resulting approach would be readily amenable to be validated by computer simulation. We started by developing a range/Doppler spread dual channel scattering formulation, since this affords complete information on the target operator. However, we reduced the problem to a Doppler spread point target in a dual channel formulation for computer simulation, and concentrated on this during the bulk of the study.

Several system models were developed and used in the analysis. They include a matrix receiver weighting method, a vector receiver weighting method (essentially a subset of the matrix method) a state space approach, a Fredholm integral approach, and a Stokes vector approach. (The Stokes approach is a single pulse polarization processing scheme, which has no spectral processing capability. It was investigated in a prior study and reported here only for the sake of completeness.) The matrix and vector methods, as well as the Stokes approach were simulated on a digital computer to evaluate their performance. The state space approach was carried to the point of an optimum receiver design, given the transmit waveform and target/clutter scattering properties. The Fredholm integral equations were formulated to the extent of developing the system of equations with target/clutter scattering matrices.

In order to perform the simulations, it was necessary to have adequate models of the target and chaff. We chose the BQM-34A as our target model since we have validated simulated rcs plots with actual measurement data. This target model is deterministic, and consists of mathematical expressions for the elements of the scattering matrix which are functions of the target orientation with respect to the radar, and to the carrier frequency of the emitted signal.

Chaff was modeled as a collection of dipoles with selectable preferred orientations. The dipole cloud was further described by Doppler and dipole rotation statistics. From the distribution of the dipole orientations and the spectral statistics, a theoretical covariance matrix was derived. This matrix was then used in conjunction with the chaff model. Simulated signatures were derived from the target model by sampling its scattering matrix at various aspect angles corresponding to a trajectory. The simulated chaff signatures were derived from the same sample rates. Once these simulated signatures were generated, correlation functions (covariance matrices) were created. The optimum dual-channel waveforms and receivers were then computed through application of the various techniques developed (matrix, vector, and Stokes approaches).

The figures of merit used in the evaluation were probability of detection and target-to-chaff ratio improvement. The various optimum dual channel systems were simulated and compared with single channel simulation results, and with the single pulse Stokes formulation results.

1.3 RESULTS AND CONCLUSIONS

The most significant results are plots of probability of detection vs signal-to-chaff power ratio generated from simulation outputs which compares dual channel performance against single channel. An example is shown in Figure 1-1. Here we see the probability of detection vs input signal-to-chaff ratio for a dual channel system using matrix receiver weighting. Three curves are also shown for conventional single channel systems. The conventional systems are assumed to have the same polarization during both transmit and receive. Vertical, horizontal, and right circular polarizations are shown. Each of the conventional systems is assumed to have a filter matched to the transmit waveform. The dipole distribution of ±45 degrees means that the dipoles in the chaff cloud are uniformly distributed between ±45 degrees from the horizontal; yielding a partially preferred orientation in that direction. The pulse sample rate was 3 msec, such that the target model scattering matrix is reasonably decorrelated pulse-to-pulse (approaching a Swerling II model). The curves show that the probability of detection is far greater in the dual channel system than in any of the three conventional single channel systems.

All of the simulation results reported upon yield to the same basic conclusion; that is, the exploitation of the polarization and spectral spread scattering properties of the target and chaff in a dual channel matrix configuration, provides superior target detection performance compared to conventional single channel matched filter systems. The degree of target detection enhancement is a strong function of the pulse-to-pulse

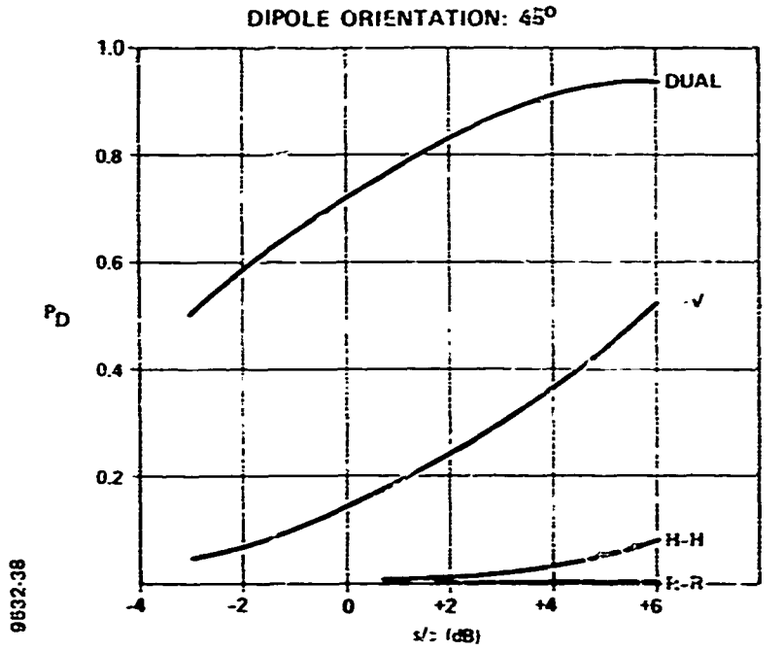

Figure 1-1. Dual vs Single Channel RT3 Target

correlation property of the target scattering covariance matrix. A Swerling II type target which is uncorrelated pulse-to-pulse, will perform better than a Swerling I, which is completely correlated pulse-to-pulse. In the latter case however, dual channel performance is still better than the conventional single channel.

In view of the results, it is recommended that further study be performed to more fully define the practical advantages of the dual channel configuration. This would involve application of a typical surveillance radar implementation incorporating MTI type processing in conjunction with the polarization discriminant. A preliminary design of the dual channel system would be undertaken to provide qualitative cost assessment against single channel systems.

Further analytical work is also recommended to develop the state space approach for waveform design and computer simulation. Finally, the range spread properties of the target should be considered as an added discriminant toward optimizing target detection in clutter.

Section 2

PROBLEM FORMULATION

The purpose of this section is to mathematically formulate the problem with the aid of scattering operator theory. Using this approach, we treat the target as a system which is characterized by a scattering matrix (operator). The function of this scattering matrix is to operate on incoming or incident radar signals (waves) to produce backscattered or output signals. This represents a linear coherent dual or two port system which can account for the horizontal and vertical polarizations. If the transmitted radar signal is a two-element polarization vector which is operated on by the 2 x 2 target scattering matrix, then the corresponding two-element vector scattered back to the radar is considered to be the radar receiver input. This receiver input is then operated on by the radar in processing the signal.

A block diagram of this total process is depicted in Figure 2-1. Here we see dual channel signal modulation during the transmitting process. Likewise, the dual channel receiver process is shown operating on the backscattered signal from both the desired target and the undesired clutter. The basic problem treated in this study is to determine the optimum combination of dual channel signal waveform (including the transmit antenna polarization) and the dual channel signal processing (including the receive antenna polarization). By optimum we mean that which yields the maximum probability of detection for a given false alarm rate.

The approach is to solve for the dual channel transmit waveform (optimum) which provides the maximum separation of received target and clutter covariance functions. This requires a vector form of the scattering operator to effectively manipulate the mathematical functions inherent in the covariance matrices, so as to properly isolate the clutter return from the target plus clutter return. Once this is obtained, the receiver function is derived to maximize the probability of detection.

Since a key element in designing the optimum dual channel system is knowledge of the target and chaff covariance matrices, we will also develop a methodology in this section for computing these matrices for use in optimizing the system design.

2.1 POLARIZATION PROPERTIES OF TARGETS AND CLUTTER

It should be fairly obvious that more information about a target and background exists in a dual channel polarization sensitive system than in the conventional single channel system. Since our goal here is to include dual channel scattering characteristics into a system design, let us briefly review a few important known polarization sensitive characteristics about targets and clutter.

In the area of clutter suppression we know that polarization sensitivity of rain has been well established, and that circular polarization can be used to cancel isotropic rain. More recent approaches [Beguin (1975), Nathanson (1975)] have improved on this by estimating

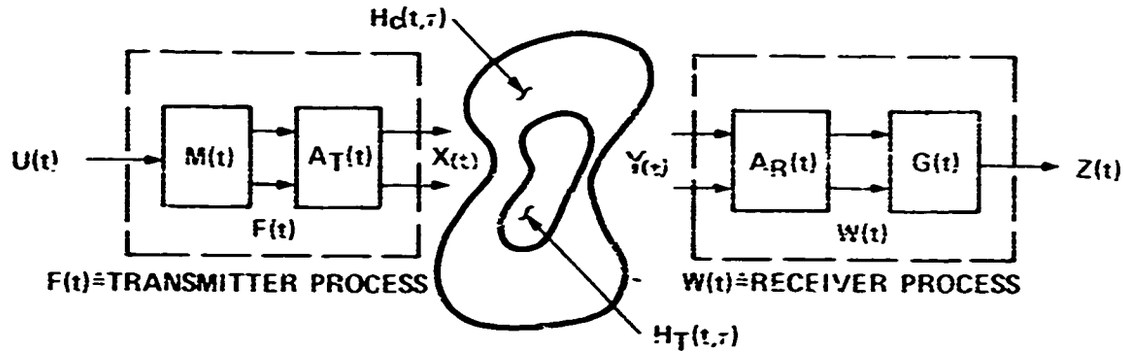

U(t) ≡ BASIC UNMODULATED CARRIER SIGNAL
M(t) ≡ DUAL CHANNEL TRANSMITTED SIGNAL MODULATION OPERATOR
$A_T(t)$ ≡ TRANSMITTED ANTENNA POLARIZATION OPERATOR

$H_T(t,\tau)$ ≡ TIME-RANGE TARGET SCATTERING OPERATOR
$H_c(t,\tau)$ ≡ TIME-RANGE CLUTTER SCATTERING OPERATOR

$A_R(t)$ ≡ RECEIVED ANTENNA POLARIZATION OPERATOR
G(t) ≡ DUAL CHANNEL RECEIVER SIGNAL PROCESSOR OPERATOR
Z(t) ≡ DETECTED SIGNAL

Figure 2-1. Dual Channel Scattering System

the ellipticity of nonisotropic rain and then adaptively varying the horizontal and vertical polarized receive channel to enhance suppression. For target enhancement, it has been found that pulse-to-pulse variation of polarization of a transmitted signal will tend to decorrelate target returns in a manner similar to that achieved by frequency variation. Poelman (1978) analyzes this problem relative to simple targets and shows that considerable improvement can be achieved in target detectability through polarization agility. The same concept has also been applied to improve angle estimation in a multipath environment [Ewell, et al. (1971)].

The pulse-to-pulse correlation phenomena for targets and rain may also be extended to other types of ground and sea clutter. For example, backscatter from manmade clutter, such as buildings (cities), tends to exhibit much variability (10 to 20 dB) between H and V responses, whereas mountainous areas tend not to exhibit such deviations. Angles of incidence and wavelength influence this heavily. More variability exists at smaller aspect angles and lower frequencies. For example, at angles of incidence less than 10 degrees, the variation in the VV/HH ratio has been measured at C-band to be about 14 dB [Daley (1968), city of Phoenix].

Chaff drops (of interest in this study) are characterized by metallic type dipoles which are cut to resonate at the radiated frequencies of the radars they are designed to confuse. As with target scattering surfaces, maximum backscattering occurs when the majority of the dropped dipoles are oriented parallel to the E-field of the transmitted signal. After the chaff has been dropped dispersion occurs (due either to air conditions or by design) so that the principle plane of the dipoles in the chaff cloud changes with respect to space and time. The changes that occur can be correlated with wind characteristics. Relative to sampling time, it is possible for a polarization diverse radar to make estimates of the polarization properties and thus adapt in such a way as to maximize the target-to-clutter ratio. The bases for utilization of these polarization properties are formulated in the following sections.

2.2 SCATTERING SYSTEM FORMULATION

The relationship between the polarization sensitivity of targets and background as applied to radar systems, can be described by a dual channel (or 2-port) operator as shown in Figure 2-1. In this formulation we consider changes in the wideband range dependent scattering properties as well as longer time (pulse-to-pulse) scattering properties due to motion. As a result, both interpulse and intrapulse signal modulation and the corresponding optimum receiver can be derived to maximize the signal-to-background ratio.

Referring to Figure 2-1, we find that the transmitted signal is the 2 x 1 complex vector $X(t)$ where elements $x_1(t)$ – the vertically polarized component – and $x_2(t)$ – the horizontally polarized component – are functions of the time variable t, $-\infty < t < \infty$. Similarly, the received signal will be a 2 x 1 vector denoted by $Y(t)$.

The ***scattering matrix*** – which relates the relative amplitude and phase of the incident and backscattered electric field vectors – of a complex radar target is given by a 2 x 2 matrix of the form:

$$H(t,\tau) = \begin{bmatrix} h_{11}(t,\tau) & h_{12}(t,\tau) \\ h_{21}(t,\tau) & h_{22}(t,\tau) \end{bmatrix} \tag{2-1}$$

Here, the entries $h_{ij}(t,\tau)$, i, j = 1,2, are taken to be complex Gaussian processes, t is the time variable, and τ is the space variable – measured in units of two-way travel time to the reflection point on the target.

From the scattering approach, a complex radar target then admits the input-output ***dual channel or two-port*** description:

$$Y(t) = \int_{-\infty}^{\infty} H(t,\tau)\, X(t-\tau)\, d\tau, \tag{2-2}$$

$$= \int_{-\infty}^{\infty} H(t,t-\tau)\, X(\tau)\, d\tau. \tag{2-3}$$

These equations form the familiar linear relationship between the input signal (X) and output (Y) when operated on by a system. At this point it is convenient to introduce a ***scattering vector*** which has the same elements as the matrix $H(t,\tau)$ and is defined by:

$$\tilde{S}(t,\tau) = [h_{11}(t,\tau),\ h_{12}(t,\tau),\ h_{21}(t,\tau),\ h_{22}(t,\tau)] \tag{2-4}$$

where $\sim$ denotes matrix transposition.

It then follows that (2-2) can be written as

$$Y(t) = \int_{-\infty}^{\infty} \begin{bmatrix} x_1(t-\tau)\ x_2(t-\tau) & 0 & 0 \\ 0 & 0 & x_1(t-\tau)\ x_2(t-\tau) \end{bmatrix} \begin{bmatrix} h_{11}(t,\tau) \\ h_{12}(t,\tau) \\ h_{21}(t,\tau) \\ h_{22}(t,\tau) \end{bmatrix} d\tau$$

or,

$$Y(t) = \int_{-\infty}^{\infty} \underline{\underline{X}}(t-\tau)S(t,\tau)d\tau \text{ (say).} \tag{2-5}$$

where

$$\underline{\underline{X}}(t-\tau) = \begin{bmatrix} x_1(t-\tau) & x_2(t-\tau) & 0 & 0 \\ 0 & 0 & x_1(t-\tau) & x_2(t-\tau) \end{bmatrix} \tag{2-6}$$

Similarly, (2-3) can be written as

$$Y(t) = \int_{-\infty}^{\infty} \underline{\underline{X}}(\tau)S(t,t-\tau)d\tau. \tag{2-7}$$

Equations (2-5) and (2-7) now define the received signal vector Y in terms of the transmit matrix $\underline{\underline{X}}$ and the scattering vector S.

2.3 COMPUTATION OF RETURN SIGNAL COVARIANCE MATRIX

2.3.1 Definitions of Important Matrices

Since knowledge of the covariance matrix of the target and clutter returns are of major importance in designing the optimum system, we will, in this subsection, define the covariance matrix and devise two approaches for computing it. Here we define a general expression for the covariance matrix $K_y(t,w)$ of the received signal $Y(t)$ – which is a complex Gaussian process with zero mean. Thus, let $E(\cdot)$ denote the expectation operation and * stand for the complex conjugate transpose, then

$$K_y(t,w) = E[Y(t)Y(w)^*]$$

$$= \begin{bmatrix} E[y_1(t)y_1(w)^*] & E[y_1(t)y_2(w)^*] \\ E[y_2(t)y_1(w)^*] & E[y_2(t)y_2(w)^*] \end{bmatrix} \tag{2-8}$$

Before proceeding to derive the two methods of computing the covariance matrix, it is instructive to define two new matrices which have the same information as the scattering matrix $H(t,\tau)$, Equation (2-1). They are

$$M(t,\tau) = \begin{bmatrix} h_{11}(t,\tau)I_2 & h_{12}(t,\tau)I_2 \\ h_{21}(t,\tau)I_2 & h_{22}(t,\tau)I_2 \end{bmatrix} \tag{2-9}$$

and

$$N(t,\tau) = \begin{bmatrix} H(t,\tau) & 0_2 \\ 0_2 & H(t,\tau) \end{bmatrix} \tag{2-10}$$

where I_2 is the 2 X 2 identity matrix, while 0_2 is the 2 X 2 zero matrix.

2.3.2 First Method

We now present the first method of computing $K_Y(t,w)$ using the target scattering vector $S(t,\tau)$. For this we define the ***scattering vector covariance matrix*** $K_S(t,\tau,w,\sigma)$ as

$$K_S(t,\tau,w,\sigma) = E[S(t,\tau) \cdot S(w,\sigma)^*] \tag{2-11}$$

Next, we have

$$M(t,\tau)\begin{bmatrix}1\\0\\0\\1\end{bmatrix} = \begin{bmatrix}h_{11} & 0 & h_{12} & 0\\ 0 & h_{11} & 0 & h_{12}\\ h_{21} & 0 & h_{22} & 0\\ 0 & h_{21} & 0 & h_{22}\end{bmatrix}\begin{bmatrix}1\\0\\0\\1\end{bmatrix} = \begin{bmatrix}h_{11}\\h_{12}\\h_{21}\\h_{22}\end{bmatrix} = S(t,\tau) \tag{2-12}$$

where the h_{ij}'s are functions of t and τ. Similarly, it is easy to verify that

$$\tilde{N}(t,\tau)\begin{bmatrix}1\\0\\0\\1\end{bmatrix} = S(t,\tau) \tag{2-13}$$

Therefore

$$S(t,\tau) \cdot S(w,\sigma)^* = M(t,\tau)\begin{bmatrix}1\\0\\0\\1\end{bmatrix}[1\ \ 0\ \ 0\ \ 1]\ \ \bar{N}(w,\sigma)$$

or

$$S(t,\tau) \cdot S(w,\sigma)^* = M(t,\tau) \cdot \underline{1} \cdot \bar{N}(w,\sigma) = \tilde{N}(t,\tau) \cdot \underline{1} \cdot M(w,\sigma)^*, \tag{2-14}$$

where $-$ indicates complex conjugate and

where

$$\underline{I} = \begin{bmatrix} 1 & 0 & 0 & 1 \\ 0 & 0 & 0 & 0 \\ 0 & 0 & 0 & 0 \\ 1 & 0 & 0 & 1 \end{bmatrix} \tag{2-15}$$

Consequently,

$$K_S(t,\tau,w,\sigma) = E[(M(t,\tau) \cdot \underline{I} \cdot \overline{N}(w,\sigma)] = E[\tilde{N}(t,\tau) \cdot \underline{I} \cdot M(w,\sigma)^*] \tag{2-16}$$

It then follows from Equations (2-5) and (2-8) that the covariance matrix $K_y(t,w)$ of the received signal $Y(t)$ is given by

$$K_y(t,w) = \int_{-\infty}^{\infty} \int_{-\infty}^{\infty} \underline{\underline{X}}(t-\tau) \cdot K_S(t,\tau,w,\sigma) \cdot \underline{\underline{X}}(w-\sigma)^* \, d\sigma d\tau \, , \tag{2-17}$$

where $K_S(\cdot)$ is the target scattering vector covariance matrix and $\underline{\underline{X}}(\cdot)$ is the transmitted signal matrix defined in Equation (2-5).

2.3.3 Second Method

The second method does not lead to a direct computation of the covariance matrix. Instead, a vector is computed, which has the same elements as those found in the covariance matrix. This covariance vector, as we will call it, is 4x1 and defined by

$$\tilde{\kappa}_y(t,w) = [K_{y_{11}}(t,w), K_{y_{12}}(t,w), K_{y_{21}}(t,w), K_{y_{22}}(t,w)] \tag{2-18}$$

where $K_{y_{ij}}(t,w)$ are the elements of the covariance matrix in Equation (2-8).

If we further define the vector

$$\tilde{X}(t-\tau,w-\sigma) = [x_1(t-\tau)\overline{x}_1(w-\sigma), \; x_1(t-\tau)\overline{x}_2(w-\sigma),$$
$$x_2(t-\tau)\overline{x}_1(w-\sigma), \; x_2(t-\tau)\overline{x}_2(w-\sigma)] \tag{2-19}$$

the covariance vector is given by

$$\kappa_y(t,w) = \int_{-\infty}^{\infty} \int_{-\infty}^{\infty} E[M(t,\tau) \cdot \overline{N}(w,\sigma)] \; \tilde{X}(t-\tau,w-\sigma) \, d\sigma d\tau \tag{2-20}$$

This may be written as

$$\kappa_y(t,w) = \int_{-\infty}^{\infty} \int_{-\infty}^{\infty} K_{\underline{H}\underline{H}}(t,\tau,w,\sigma)\, \underline{X}(t-\tau,w-\sigma)\,d\sigma\,d\tau, \tag{2-21}$$

where

$$K_{\underline{H}\underline{H}}(t,\tau,w,\sigma) = E[M(t,\tau) \cdot \bar{N}(w,\sigma)] \tag{2-22}$$

is defined as the ***scattering matrix covariance matrix.***

If the entries of $H(t,\tau)$ and $H(w,\sigma)$ are uncorrelated for $\tau \neq \sigma$ - that is, when the return signals from different points on the target are uncorrelated - then

$$\kappa_y(t,w) = \int_{-\infty}^{\infty} E[M(t,\tau) \cdot \bar{N}(w,\tau)]\, \underline{X}(t-\tau,w-\tau)\,d\tau. \tag{2-23}$$

It is important to note that

$$M(t,\tau) \cdot \bar{N}(w,\sigma) = \begin{bmatrix} h_{11}\bar{h}_{11} & h_{11}\bar{h}_{12} & h_{12}\bar{h}_{11} & h_{12}\bar{h}_{12} \\ h_{11}\bar{h}_{21} & h_{11}\bar{h}_{22} & h_{12}\bar{h}_{21} & h_{12}\bar{h}_{22} \\ h_{21}\bar{h}_{11} & h_{21}\bar{h}_{12} & h_{22}\bar{h}_{11} & h_{22}\bar{h}_{12} \\ h_{21}\bar{h}_{21} & h_{21}\bar{h}_{22} & h_{22}\bar{h}_{21} & h_{22}\bar{h}_{22} \end{bmatrix} = \bar{N}(w,\sigma) \cdot M(t,\tau), \tag{2-24}$$

where the h_{ij} are functions of t and τ, while the $\bar{h}_{ij}$ are functions of w and σ.

2.3.4 Further Notes

It is important to note that in the dual channel description above (Equations (2-2) and (2-3)) a radar target is characterized by a linear system whose impulse response matrix is the target scattering matrix ($H(t,\tau)$ (Equation (2-1)). However in this case, the entries of $H(t,\tau)$ are random processes and, in general, are unknown. Thus from a system theoretic viewpoint, we have a linear random system and our problem is basically that of "identifying" the random entries $h_{ij}(t,\tau)$ of its impulse response matrix $H(t,\tau)$. To this end we have transformed Equation (2-2) into Equation (2-5) by introducing the scattering vector $S(t,\tau)$ from Equation (2-4) and the transmit matrix $\underline{X}(t-\tau)$ from Equation (2-6). This is justified by the fact that Equation (2-2) when written out in full becomes

$$\begin{bmatrix} y_1(t) \\ y_2(t) \end{bmatrix} = \int_{-\infty}^{\infty} \begin{bmatrix} h_{11}(t,\tau)\, x_1(t-\tau) + h_{12}(t,\tau)\, x_2(t-\tau) \\ h_{21}(t,\tau)\, x_1(t-\tau) + h_{22}(t,\tau)\, x_2(t-\tau) \end{bmatrix} d\tau \tag{2-25}$$

Then each of the scalar terms

$$\int_{-\infty}^{\infty} h_{ij}(t,\tau) \quad x_k \quad (t-\tau)\, d\tau \quad , \quad i, j, k, = 1, 2, \tag{2-26}$$

is actually the output of a linear scalar (i.e , single input–output) system whose impulse response function is the scalar random function $h_{ij}(t,\tau)$ and whose input is the scalar function $x_k(t-\tau)$. Since the system is linear, Equation (2-26) can also be regarded as the output corresponding to the input $h_{ij}(t,\tau)$ (in time and space) of the system whose impulse response is $x_k(t-\tau)$. Hence Equation (2-2) becomes Equation (2-5) in which the four scalar inputs $h_{ij}(t,\tau)$, i, j = 1, 2, are arranged into the 4 X 1 scattering vector $S(t,\tau)$. Hence, it is easy to see that Equation (2-5) is a linear transformation from a 4-dimensional space into a 2-dimensional space. Since the input vector $X(t-\tau)$ is a 2 X 1 vector, Equation (2-2) is just a linear transformation from a 2-dimensional space to a 2-dimensional space.

The advantages of Equation (2-5) are many fold First, the problem of identifying the matrix $H(t,\tau)$ now becomes that of identifying the vector $S(t,\tau)$ from the output data $Y(t)$. This allows one to use techniques of signal design, processing and simulation in radar problems. Secondly, in computing the output covariance matrix $K_y(t,w)$ in Equation (2-17), we have relied heavily on the covariance matrix $K_S(t,\tau,w,\sigma)$ in Equation (2-11) for the vector process $S(t,\tau)$. This in turn is expressible in terms of the two matrices $M(t,\tau)$ and $N(w,\sigma)$ of Equations (2-9) and (2-10) respectively. These matrices, as we have shown, are on the one hand directly related to the vector $S(t,\tau)$ and therefore allow one to compute $K_y(t,w)$ from simulated or experimental data, and also on the other hand lead to the type of "spectral polarization," of $K_S(t,\tau,w,\sigma)$ in Equation (2-16) and $K_H(t,\tau,w,\sigma)$ in Equation (2-22).

Finally, it is noted that for the case of an isotropic target, $h_{12} = h_{21}$, the matrices $M(t,\tau)$ and $N(t,\tau)$ are both symmetric and so is the matrix $K_H(\ )$, whereas $K_S(\ )$ and $K_y(\cdot)$ are always hermitian matrices.

The two methods discussed earlier are used in Sections 3.1.3 and 3.1.2 respectively. It is appropriate to comment on the fact that due to the nature of the Generalized Matrix Approach, the second method cannot be used, whereas the Generalized Vector Approach may use either methods. However, from the computational aspects, the second method was preferred.

2.4 COVARIANCE MATRICES OF POINT TARGET IN CHAFF

We now apply the results found above to the case of a point target. We have in this case

$$H(t,\tau) = \begin{bmatrix} h_{11}(t) & h_{12}(t) \\ h_{21}(t) & h_{22}(t) \end{bmatrix} \cdot \delta(\tau - \tau_0) = H(t) \cdot \delta(\tau - \tau_0) \tag{2-27}$$

where τ_0 is the two-way travel time to the point target.

It is seen from Equations (2-9) and (2-10) that

$$M(t,\tau) = \begin{bmatrix} h_{11}(t)I_2 & h_{12}(t)I_2 \\ h_{21}(t)I_2 & h_{22}(t)I_2 \end{bmatrix} \cdot \delta(\tau - \tau_0) = M(t) \cdot \delta(\tau - \tau_0) \tag{2-28}$$

and

$$N(t,\tau) = \begin{bmatrix} H(t) & 0_2 \\ 0_2 & H(t) \end{bmatrix} \cdot \delta(\tau - \tau_0) = N(t) \cdot \delta(\tau - \tau_0) \tag{2-29}$$

Therefore, from Equation (2-22)

$$K_H(t,\tau,w,\sigma) = E[M(t) \cdot \overline{N}(w)] \cdot \delta(\tau - \tau_0) \cdot \delta(\sigma - \tau_0). \tag{2-30}$$

and from Equation (2-16)

$$K_S(t,\tau,w,\sigma) = E[M(t) \cdot \underline{I} \cdot \overline{N}(w)] \cdot \delta(\tau - \tau_0) \cdot \delta(\sigma - \tau_0). \tag{2-31}$$

Then, using Equation (2-23) we find

$$K_y(t,w) = E[M(t) \cdot \overline{N}(w)] \cdot X(t - \tau_0, w - \tau_0). \tag{2-32}$$

Similarly, from Equation (2-17)

$$K_y(t,w) = \underline{\underline{X}}(t - \tau_0) \cdot E[M(t) \cdot \underline{I} \cdot \overline{N}(w)] \cdot \underline{\underline{X}}(w - \tau_0)^*. \tag{2-33}$$

Let $H_T(t,\tau) = H_T(t) \cdot \delta(\tau - \tau_0)$ be the scattering matrix of a point target ***surrounded*** by a chaff cloud – whose scattering matrix is denoted by $H_C(t,\tau)$. As in the above, let X(t) and Y(t) be the transmitted and received signals, respectively, then

$$Y(t) = H_T(t) \cdot X(t - \tau_0) + \int_{-\infty}^{\infty} H_C(t,\tau) \cdot X(t - \tau) \cdot d\tau$$

$$= Y_T(t) + Y_C(t)$$

Let $K_y(t,w)$ be the covariance matrix of $Y(t)$, we have

$$K_y(t,w) = E\{(Y_T(t) + Y_C(t))\ (Y_T(w)^* + Y_C(w)^*)\}.$$

Therefore, since Y_T and Y_C are uncorrelated

$$K_y(t,w) = E[Y_T(t)Y_T(w)^*] + E[Y_C(t)Y_C(w)^*].$$

$$= K_{y_T}(t,w) + K_{y_C}(t,w), \qquad (2\text{-}34)$$

where the point target covariance matrix $K_{y_T}(t,w)$ is computed from Equation (2-33), while the chaff cloud covariance matrix $K_{y_C}(t,w)$ can be derived from Equation (2-17).

It is also evident from Equation (2-34) that

$$\kappa_y(t,w) = \kappa_{y_T}(t,w) + \kappa_{y_C}(t,w) \qquad (2\text{-}35)$$

where $\kappa_{y_T}(t,w)$ is given by Equation (2-32) and $\kappa_{y_C}(t,w)$ can be computed from Equation (2-21).

As noted in the following sections, the received signal covariance functions become key elements in the design of the transmit waveform and associated receiver weighting for maximizing the output s/c ratio.

Section 3

OPTIMAL TRANSMIT WAVEFORM AND RECEIVER DEVELOPMENT

The previous section described the manner whereby radar targets and clutter can be characterized by scattering operators. Associated with these scattering operators are scattering vectors, which can be regarded as stochastic vector processes. With this description, the signals received from the target and clutter can be formulated as the outputs of a deterministic system whose inputs are the scattering vectors, see Figure 3-1. Since a major study task was to maximize the probability of target detection for a given false alarm rate, the more immediate problem becomes one of transmit waveform and associated receiver design to meet this objective. Given then the scattering vector descriptions of both target and clutter, it was necessary to find the optimal deterministic transmit waveform and optimum receiver weighting for maximizing the target return signal-to-chaff plus receiver noise ratio.

Five variants of the scattering theory approach were investigated. Two of these methods fall into the domain of finite dimensional discrete time and frequency space. These were more fully developed than the other methods in terms of obtaining both theoretical and simulation results for waveform/receiver design and associated detection performance. The state space and matched filter Fredholm Equation approaches were both mathematically formulated, but they were not simulated on a computer.

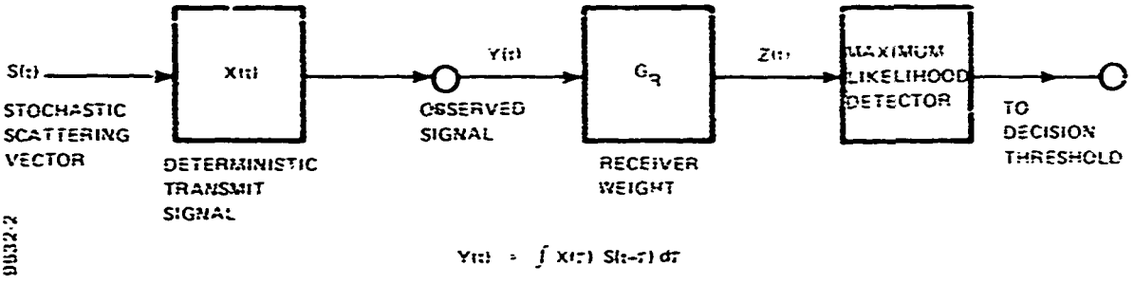

Figure 3-1. Simplified System Model

3.1 FINITE DIMENSIONAL SPACE

The two methods related to finite dimensional discrete-time and frequency space were developed. They are herein designated as the vector and matrix approaches. The matrix approach has the potential for utilizing all of the information available within the dimensional space constrained by both the transmit signal and target/chaff scattering properties. Assume, for example, that the target and chaff scattering vectors each consist of four variables (h_{11}, h_{12}, h_{21}, h_{22}), and that the transmit signal is composed of N pulses, each containing separable V and H polarized components. The four element scattering vector, in combination with the N dual polarized transmit pulses, establishes a 4N x 4N receiver weighting matrix for optimum processing of the return signal. As subsequently shown, the weighting matrix results from eigenvector solutions involving the target and chaff scattering vector covariance matrices. However, since the observable data consist of only 2N separable signal returns, the receiver weighting dimension must be reduced to a 2N x 4N matrix. The matrix elements then consist of the 2N eigenvectors associated with the 2N largest eigenvalues resulting from the scattering vector covariance matrix solutions. This resultant weighting matrix maximizes the signal-to-clutter ratio (s/c) under conditions shown in Section 3.1.2.

By contrast, the vector approach utilizes only the one eigenvector which is associated with the largest eigenvalue. Consequently, the receiver weight is then a 4N-element vector. Although the vector approach can be considered as a subset of the matrix implementation, it was developed from a somewhat different mathematical approach and provided valuable insight into subsequent development of the matrix method. Additionally, the vector approach is simpler to implement both from a software and hardware standpoint, which can prove to be of further benefit in the realization of actual systems, even though performance is not as good.

Associated with the vector and matrix approaches is the concept of the maximum likelihood receiver, from which the false alarm and target detection probabilities were derived. The likelihood implementation is, therefore, described in the following sections for completeness. It should be realized however, that the design of the transmit waveform and receiver weighting function need not depend upon the maximum likelihood concept.

3.1.1 Generalized Vector Approach

The vector approach is described below relative to the interaction of a coherent pulse train with a target characterized by a polarization scattering matrix possessing both temporal and range variations. The analysis presented here is general and can be applied to both the coherent pulse train and the single coded pulse waveform. In what follows, we assume that the radar system under consideration employs two orthogonal polarizations on transmit and receive.

The envelope of transmitted vector is

$$X(t) = \begin{pmatrix} x_1(t) \\ x_2(t) \end{pmatrix} \tag{3-1}$$

and the target scattering matrix is represented by

$$H_T(t,\tau) = \begin{bmatrix} h_{11}(t,\tau) & h_{12}(t,\tau) \\ h_{21}(t,\tau) & h_{22}(t,\tau) \end{bmatrix} \tag{3-2}$$

The target covariance matrix is a 4 x 4 matrix given by

$$K_{HT}(t-u;\tau) = (k_{ij}(t-u;\tau)) \; i = 1, \ldots, 4, \; j = 1, \ldots, 4. \tag{3-3}$$

where, referenced to equation (2-24):

$$k_{11}(t-u;\tau) = E[h_{11}(t,\tau)\,\bar{h}_{11}(u,\tau)]$$

$$k_{12}(t-u;\tau) = E[h_{11}(t,\tau)\,\bar{h}_{12}(u,\tau)]$$

$$k_{13}(t-u;\tau) = E[h_{12}(t,\tau)\,\bar{h}_{11}(u,\tau)], \text{ etc.}$$

and where $E[\cdot]$ = expectation operator. (Note that when the scatterer is isotropic (i.e., $h_{12} = h_{21}$) then K_H is symmetric.)

For a receiver weighting function

$$W(t) = \begin{pmatrix} w_1(t) \\ w_2(t) \end{pmatrix} \tag{3-4}$$

the video amplitude at the output of the receiver is given by

$$V(t) = \int_{-\infty}^{\infty} dt_1 \; W^*(t_1-t) \int_{-\infty}^{\infty} H_T(t_1,\tau)\,X(t_1-\tau)\,d\tau \tag{3-5}$$

From above we find that the average output power is proportional to

$$E[V(t)\,V^*(t)] = \int_{-\infty}^{\infty} dt_1 \int_{-\infty}^{\infty} dt_2 \int_{-\infty}^{\infty} d\tau_1 \int_{-\infty}^{\infty} d\tau_2 \; E[W^*(t_1-t)\,H_T(t_1,\tau_1)\,X(t_1-\tau_1)\,X^*(t_2-\tau_2)\,H_T^*(t_2,\tau_2)\,W(t_2-t)] \tag{3-6}$$

If we assume that the elements of $H_T(t_1, \tau_1)$ and $H_T(t_2, \tau_2)$ are uncorrelated for $\tau_1 \neq \tau_2$, then we can write (3-6) as

$$P(t) = E[V(t)\, V^*(t)] = \int_{-\infty}^{\infty} dt_1 \int_{-\infty}^{\infty} dt_2\, W^*(t_1-t)\, K_{yT}(t_1,t_2)\, W(t_2-t) \qquad (3\text{-}7)$$

where $K_y(t_1,t_2)$ is a 2 x 2 covariance matrix whose elements are given by (3-8) below as previously derived in Equation (2-20).

$$K_{yT}(t_1,t_2) = \begin{bmatrix} K_{yT11}(t_1,t_2) \\ K_{yT12}(t_1,t_2) \\ K_{yT21}(t_1,t_2) \\ K_{yT22}(t_1,t_2) \end{bmatrix} = \int_{-\infty}^{\infty} d\tau\, K_{H_T}(t_1-t_2;\tau) \begin{bmatrix} x_1(t_1-\tau)\ \bar{x}_1(t_2-\tau) \\ x_1(t_1-\tau)\ \bar{x}_2(t_2-\tau) \\ x_2(t_1-\tau)\ \bar{x}_1(t_2-\tau) \\ x_2(t_1-\tau)\ \bar{x}_2(t_2-\tau) \end{bmatrix} \qquad (3\text{-}8)$$

Introducing the discrete vector W, where N is the number of pulses

$$W^* = [W^*(1), W^*(2) \ldots W^*(N)] \qquad (3\text{-}9)$$

(the asterisk indicates complex conjugate transpose), we note that in discrete form P(0) obtained from Equation (3-7) for t = 0 is given by

$$P(0) = W^* K_{yT} W \qquad (3\text{-}10)$$

where K_{yT} is an N x N covariance matrix whose elements are the 2 x 2 matrices $K_y(i\Delta t, j\Delta t)$, where Δt is the interpulse period. Thus, using Equations (3-6) and (3-7), we can write the signal-to-chaff ratio as

$$s/c = \frac{(W^* H_T X)(X^* H_T^* W)}{W^* K_{yc} W} \qquad (3\text{-}11)$$

where K_{yc} is the N x N clutter covariance matrix defined in a similar manner as K_{yT} above.

$$\tilde{X} = [X^*(1), X^*(2), \ldots X^*(N)] \tag{3-12}$$

and

$$X(m) = \begin{pmatrix} x_1(m) \\ x_2(m) \end{pmatrix} \tag{3-13}$$

The expression in Equation (3-11) is a direct extension of the results of Rummler (1966), (1967), and DeLong and Hofstetter (1967) to the polarization sensitive targets. The vector $\tilde{W}$ that maximizes Equation (3-11) was shown by Rao (1973) to be

$$W = K_{yc}^{-1} H^* X^* \tag{3-14}$$

Note that K_{yc} is actually a function of X, i.e., $K_{yc} = K_{yc}(X)$.

The basic functions described above are indicated in Figure 3-2 for a train of three transmit pulses with dual polarization. As noted in Equation (3-14), the desired weighting

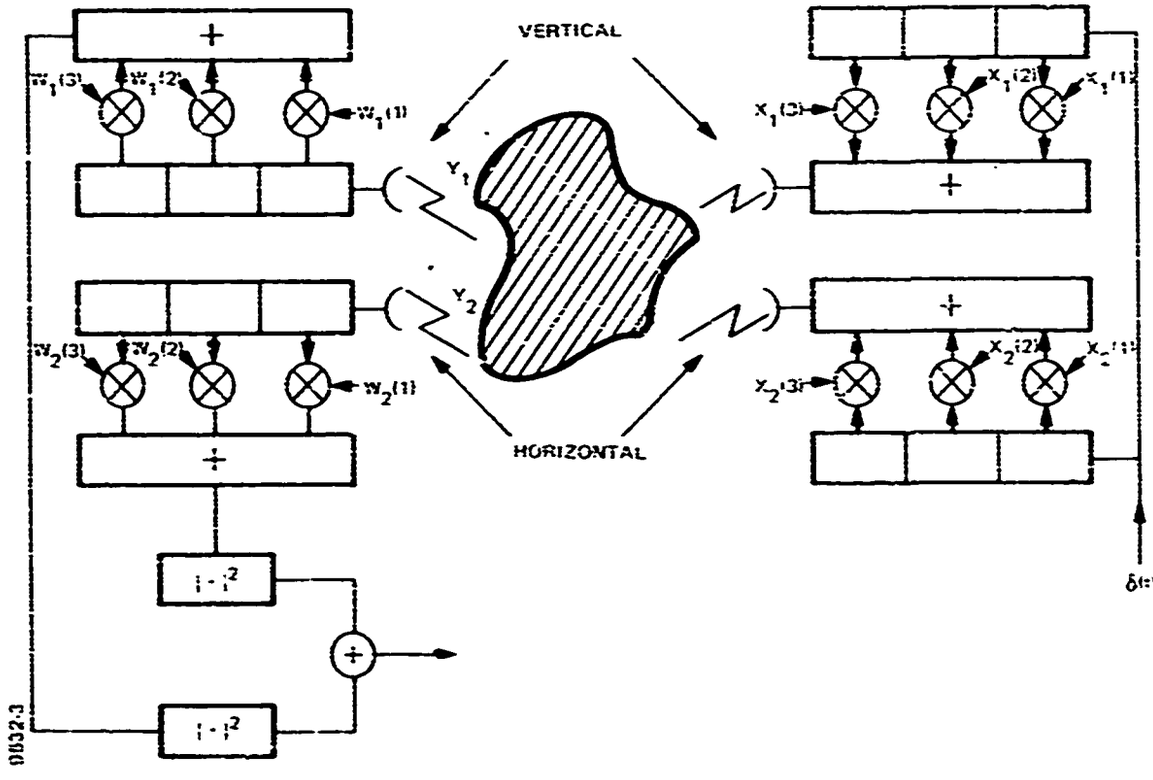

Figure 3-2. Schematic of Transmitter Receiver Configuration

vector is a function of the target and chaff scattering covariance matrices, and also of the transmit signal vector. Although the scattering properties are known stochastic functions, the weighting vector cannot be determined until the transmit waveform is specified. The vector approach as derived above, therefore, does not yield a direct solution for the optimal transmit waveform. An iterative procedure is possible, however, which does result in a quasi-optimum transmitter waveform design under certain conditions, as described below.

3.1.2 Vector Approach Waveform Design

The approach of Rummler (1966, 1967) is adapted herein to the formulation of an optimum set of transmitter/receiver operators for maximization of the s/c ratio for dual channel systems. The generalized solution for the receiver weighting vector W as given in Equation (3-14), will be applied to the case of a Doppler spread point target in Doppler spread clutter. For convenience, the notation denoting the time varying properties of the transmit vector and scattering functions will be omitted. The signal-to-chaff ratio of Equation (3-10) can be written for the above point target case as:

$$s/c = \frac{W^* K_{yT} W}{W^* K_{yc} W} \tag{3-15}$$

where K_{yT} and K_{yc} are the target and clutter covariance matrices, and where

$$K_{yT} = E[(HX)(HX)^*] = X\, E[HH^*]\, X^* = K_{HT} X \tag{3-16}$$

H is the previously defined 2 x 2 target scattering matrix. The parameter K_{yc} is defined similarly for clutter. It is again emphasized that both K_{yT} and K_{yc} are functions of the transmit signal, X. Given K_{yT} and K_{yc}, the problem becomes one of finding the value of W which maximizes the s/c ratio.

It is clear that s/c (kW) = s/c (W) where k is any arbitrary scalar constant. So we may assume, without loss of generality, that $W^* K_{yc} W = 1$. Hence, the original unconstrained optimization is equivalent to the following constrained optimization problem:

$$\begin{aligned} &\max \quad W^* K_{yT} W \\ &\text{subject to} \quad W^* K_{yc} W = 1 \end{aligned} \tag{3-17}$$

Applying Lagrange's multiplier rule (see Appendix C), we see that the optimum W and s/c must satisfy the following conditions:

$$\begin{aligned} &(K_{yT} - \lambda_{max} K_{yc})\, W = 0 \\ &(s/c)_{max} = \lambda_{max} \end{aligned} \tag{3-18}$$

where

$$\lambda_{max} = \text{maximum eigenvalue of } K_{yc}^{-1} K_{yT}$$

The optimum signal-to-chaff ratio is then the largest eigenvalue of $K_{yc}^{-1} K_{yT}$, and the optimum weighting vector is the eigenvector corresponding to this largest eigenvalue.

Note that the s/c ratio was maximized for a given transmit vector, which had to be chosen a priori. The choice would generally be made based upon experience dealing with specific target/clutter situations. According to Rummler, this initial choice could be the unweighted, uncoded vector. In any case, it may be possible to further improve the s/c through an iterative procedure devised by Rummler. This is based upon the fact that the s/c ratio is unchanged if the transmitted waveform and the receiver response are conjugated and interchanged. This is done by using the receiver weights from one iteration as the transmitted signal vector for the next iteration, for which the procedure will converge to a maximum s/c.

Although the solution converges to an optimum s/c ratio there is no guarantee that a better solution could not have been reached if the procedure had been started with a different initial waveform. Rummler has noted, however, that the s/c ratio convergence does not appear to be strongly dependent upon the choice of initial vector. Nevertheless, the vector to which the procedure converges is strongly dependent upon the initial choice.

This iterative procedure was developed for computer solution of transmit signal and receiver weighting configurations for optimization of the s/c ratio for both dual and single channel configurations. Results of this technique are reported upon in Section 5. A summary of the iterative procedure is given in Table 3-I.

TABLE 3-I. VECTOR METHOD WAVEFORM DESIGN

1) Maximize s/c ratio given scattering properties

$$s/c = \frac{W^* K_{yT}(X) W}{W^* K_{yc}(X) W}$$

2) For given transmit vector X, find receiver weight W to maximize s/c

3) Constrained optimization problem, eigenvalue solution of:

$$(K_{yT} - \lambda_{max} K_{yc}) W_{opt} = 0$$

where

$$\lambda_{max} = \text{maximum eigenvalue of } K_{yc}^{-1} K_{yT}$$

4) W_{opt} = eigenvector of λ_{max}

5) Iterate by interchanging X and W, obtain convergence to optimum s/c

One additional fact should be noted in regard to receiver noise. The effects of noise are taken into account by adding an identity I matrix to K_{yc}, where K_{yc} is appropriately scaled to reflect the received clutter-to-noise ratio (c/n).

3.1.3 Generalized Matrix Approach

In the analysis below, we consider the detection of a point Doppler-spread target in Doppler spread clutter, when the radar transmits a coherent pulse train composed of N equally spaced rectangular subpulses. It is also assumed that the radar is capable of modulating the transmitted polarization from pulse-to-pulse. A simplified block diagram of the system is shown in Figure 3-3. For convenience, the time notation will be omitted.

Given a transmitted sequence of N pulses, the transmit vector X will be a column vector shown as a (2N X 1) dimensional matrix. The transpose of X is represented by:

$$\tilde{X} = (X_{V1}, X_{H1}, \ldots, X_{VN}, X_{HN}) \tag{3-19}$$

where X_{V1} is the complex variable representating the amplitude and phase of the vertical component of the pulse-1 transmitted electric field, X_{H1} is the horizontal component, etc.

The scattering properties of the target and chaff are represented by their respective 2 x 2 scattering matrices, H_T and H_C. Given that

$$H_{T,C} = \begin{bmatrix} h_{11} & h_{12} \\ h_{21} & h_{22} \end{bmatrix}_{T,C} \tag{3-20}$$

and that the target (T) and clutter (C) scatterers are isotropic ($h_{12} = h_{21}$), then the elements of the scattering matrix can be rearranged for mathematical convenience as a scattering vector h, of dimension (3N X 1).

$$\tilde{h} = \left(h_{11}^{(1)}, h_{12}^{(1)}, h_{22}^{(1)}, \ldots, h_{11}^{(N)}, h_{12}^{(N)}, h_{22}^{(N)} \right) \tag{3-21}$$

where $h_{11}^{(1)}$ represents the vertical-to-vertical scattering property relative to pulse-1, etc. Note that the values of the elements vary with time for Doppler spread targets, such that in general $h^{(i)} \neq h^{(j)}$.

The signal received at the receiver antenna is denoted by the vector Y, as noted in Figure 3-3. For mathematical convenience, the transmit vector X is rearranged into a (2N X 3N) transmit matrix $\underline{\underline{X}}$, such that Y can be given by

$$Y = \underline{\underline{X}}\, h \tag{3-22}$$

where Y is a (2N X 1) vector with

$$\tilde{Y} = (y_{V1}, y_{H1}, \ldots, y_{VN}, y_{HN}) \tag{3-23}$$

The elements of Y represent the complex vertical and horizontal components of the received electric field vector. For Equation (3-22) to be dimensionally valid,

$$\underline{\underline{X}} = \begin{bmatrix} \begin{pmatrix} x_{V1} & x_{H1} & 0 \\ 0 & x_{V1} & x_{H1} \end{pmatrix} & & 0 \\ & \begin{pmatrix} x_{V2} & x_{H2} & 0 \\ 0 & x_{V2} & x_{H2} \end{pmatrix} & \\ 0 & & \begin{pmatrix} x_{VN} & x_{HN} & 0 \\ 0 & x_{VN} & x_{HN} \end{pmatrix} \end{bmatrix} \tag{3-24}$$

The above rearrangement of terms is a special case of Equation (2-6), where $h_{12} = h_{21}$, resulting in a dimension reduction of h.

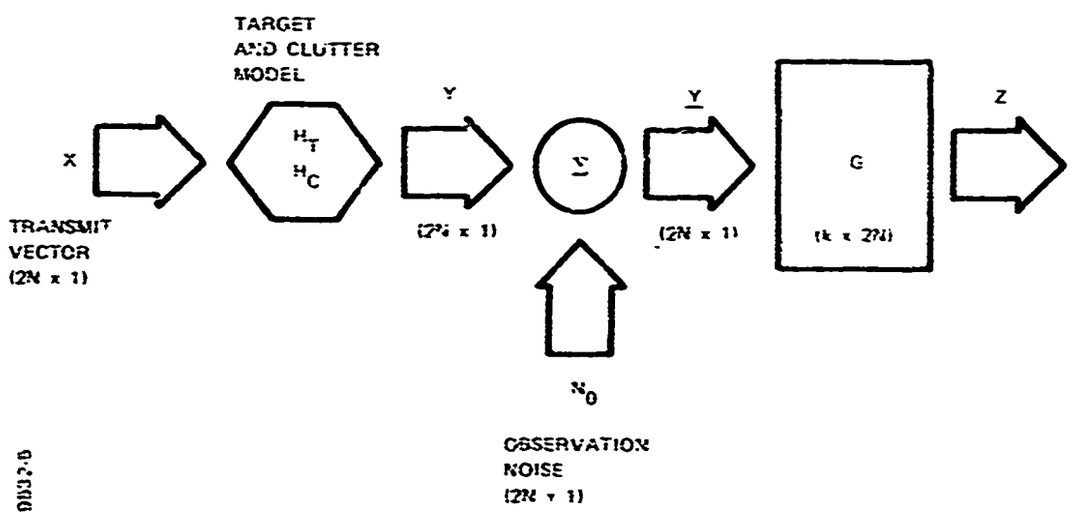

Figure 3-3. Simplified Block Diagram Matrix Method

Expression (3-24) shows the matrix $\underline{\underline{X}}$ as a (2N x 3N) arrangement of the elements of the transmit vector X. Observation noise N_0 is added to Y to produce the received (2N x 1) vector $\underline{Y}$. This realization of the vector $\underline{Y}$ is simply the result of the transmit signal X being reflected back to the radar by the target and chaff plus the additive receiver noise.

The preliminaries, to this point, of rearranging the mathematical form of the transmit signal and scattering properties into $\underline{\underline{X}}$ and h, was necessary to properly dimensionalize the matrix multiplication for

$$\underline{Y} = \underline{\underline{X}}\, h + N_0 \tag{3-25}$$

The effect of a linear receiver upon the signal vector Y, can then be expressed in terms of the matrix G, which operates on $\underline{Y}$ to give

$$Z = G\underline{Y} = G\,\underline{\underline{X}}\, h + GN_0 \tag{3-26}$$

The receiver output Z would then be subject to hypothesis testing for one of two conditions: the presence of target plus clutter or of clutter only. The implementation of this likelihood process will be deferred to Section 3.2. At this juncture, the major consideration is the design of $G\,\underline{\underline{X}}$ such that the s/c ratio at Z is maximized.

3.1.3.1 Matrix Transmit-Receive Design – Define a weighting matrix W, where

$$W = G\,\underline{\underline{X}} \tag{3-27}$$

The object then is to find the optimum W for maximizing the s/c ratio, given the statistics of the stochastic scattering vectors for both the target and clutter.

The target and clutter covariance matrices are given by

$$K_{yT} = E\,[h_T\, h_T^*] \tag{3-28a}$$

and

$$K_{yC} = E\,[h_C\, h_C^*] \tag{3-28b}$$

where

* represents the conjugate transpose.

Since K_{yT} and K_{yc} are positive definite hermitian matrices, they can be simultaneously diagonalized by a matrix ϕ (see Appendix D), where

$$\phi^* K_{yT} \phi = \Lambda$$

$$\phi^* K_{yc} \phi = I \tag{3-29}$$

The columns of ϕ are the generalized eigenvectors ϕ_i satisfying

$$K_{yT} \phi_i = \lambda_i K_{yc} \phi_i \tag{3-30}$$

where the λ_i are the eigenvalues of the matrix equation

$$K_{yT} - \lambda K_{yc} | = 0 \tag{3-31}$$

The joint diagonalization of K_{yT} and K_{yc} by this process, orthogonalizes the target and chaff covariance matrices through the matrix transformation ϕ. This in effect provides a maximum separation of the target and clutter vectors at the Z output, which is the desirable condition for hypothesis testing. Consequently, the matrix W can be chosen as the transformation matrix ϕ. There is, however, a dimensionality problem in that ϕ is a (3N x 3N) matrix, the result of the arrangement of the h. On the other hand, there are only 2N observations at Z as limited by the transmission of N dual channel pulses. Consequently, the dimension of the W matrix must be reduced (k x 3N), where $k \leq 2N$. The problem then arises as to the method of selecting k out of 3N eigenvectors for the matrix W, where

$$\tilde{W} = (W_1, W_2 \ldots . W_k) \tag{3-32}$$

and the W_i are (3N x 1) column vectors, representing the k eigenvectors of the transformation matrix ϕ, that correspond to the k largest eigenvalues of matrix equation (3-31).

The criterion for selecting the k-optimum eigenvectors is based upon the Chernoff bound, whereby the probability of error is minimized with respect to the hypothesis test on Z. Given hypothesis H_0 (clutter only) and H_1 (target plus clutter), it can be shown that the probability of error P_e is bounded between [Van Trees, 1971].

$$\tfrac{1}{2}\min\{p,q\}\, J^2 \leq P_e \leq \tfrac{1}{2} J \tag{3-33}$$

where p is the a priori probability that H_1 is true, q is the a priori probability that H_0 is true and J is the integral

$$J = \int_{\Omega} [p(Z/H_1)\, p(Z/H_0)]^{1/2}\, dz \tag{3-34}$$

For zero mean Gaussian densities (see Appendix E),

$$B = -\ln(J) = \ln\left\{\frac{|K_{Z1} + K_{Z0}|}{2^k |K_{Z1}|^{1/2} |K_{Z0}|^{1/2}}\right\} \tag{3-35}$$

where $B = -\ln(J)$ is known as the Bhattacharyya distance. Note that since $0 \leq J \leq 1$, the minimization of J is equivalent to the maximization of B. Therefore, we select the transformation matrix W so as to maximize the Bhattacharyya distance.

In Equation (3-35), K_{Z1} and K_{Z0} are the covariance matrices of Z under hypotheses H_1 and H_0 respectively. These quantities are:

$$K_{Z1} = W K_{yT} W^* + W K_{yc} W^*$$

$$K_{Z0} = W K_{yc} W^* \tag{3-36}$$

Substituting of the W matrix as resulting from the eigenvector solution of Equation (3-32) into the above for K_{Z1} and K_{Z0}, and then substituting of K_{Z1} and K_{Z0} into the Bhattacharyya distance B as given in Equation (3-35) yields

$$B = \tfrac{1}{2}\sum_{i=1}^{k} \ln\left[\frac{}{}(\lambda_i + 1) + \frac{i}{\lambda_i + 1} + 2\right] + k/2 \ln 4 \tag{3-37}$$

Note that due to the restriction on k, k must satisfy $k \leq 2N$. Then, maximization of B requires finding the appropriate k eigenvalues $\lambda_1, \ldots, \lambda_k$ out of 3N eigenvalues that satisfies

$$(\lambda_1 + 1 + \lambda_1 + 1^{-1}) > (\lambda_2 + 1 + \lambda_2 + 1^{-1}) > \ldots > (\lambda_k + 1 + \lambda_k + 1^{-1}) > \ldots > (\lambda_{3N} + 1 + \lambda_{3N} + 1^{-1})$$

Since $\quad (\lambda_i + 1 + \lambda_i + 1^{-1}) > (\lambda_j + 1 + \lambda_j + 1^{-1})$

implies $\quad \lambda_i > \lambda_j$ for all $\lambda_i, \lambda_j > 0$

the k eigenvalues that maximize B are then the k largest eigenvalues of the ordered set

$$(\lambda_{max} = \lambda_1) > \lambda_2 \ldots > \lambda_k > \ldots > \lambda_{3N} \tag{3-38}$$

It then follows that the k eigenvectors of W should be selected from those which correspond to the k largest eigenvalues of $K_{yT} - \lambda K_{yc} = 0$

3.1.3.2 **Transmit Waveform Determination** – Once the above optimum matrix W has been determined the receiver transformation matrix G and transmitter waveform matrix $\underline{\underline{X}}$ are selected by minimizing the Frobenius norm

$$\| G \underline{\underline{X}} - W \|_F \tag{3-39}$$

which is defined by

$$\| A \|_F = \left[\sum_{i,j} |a_{i,j}|^2 \right]^{1/2} \tag{3-40}$$

The choice of the Frobenius norm here is for mathematical convenience, since in finite dimensional spaces all norms are equivalent – as far as topological properties are concerned. For a given waveform matrix $\underline{\underline{X}}$, the minimizing G is given by

$$G = W \underline{\underline{X}}^* (\underline{\underline{X}} \underline{\underline{X}}^*)^{-1} \tag{3-41}$$

Substituting Equation (3-41) into the expression for the norm, yields

$$\| W (\underline{\underline{X}}^* (\underline{\underline{X}} \underline{\underline{X}}^*)^{-1} \underline{\underline{X}} - I) \|_F^2 \tag{3-42}$$

Optimum performance is obtained if Equation (3-42) is identically zero. The above discussion indicates that for a given matrix W the transmit matrix $\underline{\underline{X}}$ can in theory be computed by minimizing the Frobenius, norm. In reality, this direct method for solution of $\underline{\underline{X}}$ is extremely difficult. An alternative approach is to start with a large library of reasonable waveform structures, and search for the waveform which minimizes the norm. This was done during the study and will be reported in Sections 4 and 5.

Once $\underline{\underline{X}}$ is selected through this procedure, the receiver matrix G is computed from Equation (3-41). A summary of the matrix approach is given in Table 3-II.

TABLE 3-II. SUMMARY MATRIX WAVEFORM APPROACH

1) Solve for eigenvalues of $|K_{yT} - \lambda K_{yc}| = 0$
2) Select the $k \leq 2N$ largest eigenvalues
3) Form W matrix from the k eigenvectors of largest eigenvalues
4) Solve for transmit matrix by minimizing norm of
$$\| W (\underline{\underline{X}}^* (\underline{\underline{X}} \underline{\underline{X}}^*)^{-1} \underline{\underline{X}} - I) \|^2$$
5) Step 4 above can be satisfied by comparing a library of stored transmit vectors against W, and selecting the one resulting in the minimum error
6) Solve for receiver weight G using
$$G = W \underline{\underline{X}}^* (\underline{\underline{X}} \underline{\underline{X}}^*)^{-1}$$

3.1.4 Maximum Likelihood Detector

The matrix approach yields a transmit waveform with an associated receiver weight which maximizes the s/c ratio based upon the Bhattacharyya distance criterion for optimality. Up to this point of the design (output Z of Figure 3-3), the hypothesis test for the target or chaff decision process has not been a factor. For a surveillance radar application, one is interested in optimizing the probability of detecting a target in chaff for a given false alarm probability created by chaff plus receiver noise. Referring to Figure 3-3, the two conditions for hypothesis testing are

$$H_0: \quad \underline{Y} = \underline{Y}_C + \underline{N}_0$$

$$H_1: \quad \underline{Y} = \underline{Y}_T + \underline{Y}_C + \underline{N}_0 \tag{3-43}$$

Here H_0 represents the false alarm situation of chaff return plus noise, while H_1 represents the target return combined with the chaff and noise.

The above receiver inputs are linearly operated upon by the weighting matrix G to produce the observed receiver output Z. A decision must then be made as to whether Z satisfies hypothesis H_0 or H_1. The transmit vector X and receiver matrix G are now known design parameters. The statistics of the target and chaff scattering properties as well as the receiver noise are known stochastic processes; consequently, the signal distribution at Z is also known for each hypothesis. This then lends itself to a conventional maximum likelihood decision process for H_0 and H_1. The maximum likelihood receiver configuration can be found in standard texts [Van Trees, 1968], and will not be elaborated upon. There are, however, some design features peculiar to the matrix approach. These are discussed below with the aid of Figure 3-4, which is an extension of Figure 3-3.

At the threshold T, a binary decision is made for condition H_0 and H_1. Since it is desired to utilize a conventional receiver implementation such as, for instance, a square law detector, it is necessary to transform the output at Z to fulfill certain conditions. This is indicated by Figure 3-4 by the matrices Q and P which operate upon Z to produce the output signal r. This signal is then squared and summed to provide a signal u, upon which the threshold test is performed. The mathematics associated with the decision process involves knowledge of the probability density function of u, and this computation can be facilitated if the elements of the signal matrix at r are uncorrelated. This is accomplished by finding a transformation matrix Q which diagonalizes the covariance of signal Z; that is,

$$\underline{Z} = Q \cdot Z \tag{3-44}$$

where

$$E[\underline{Z} \cdot \underline{Z}^*] = \text{diagonal matrix.}$$

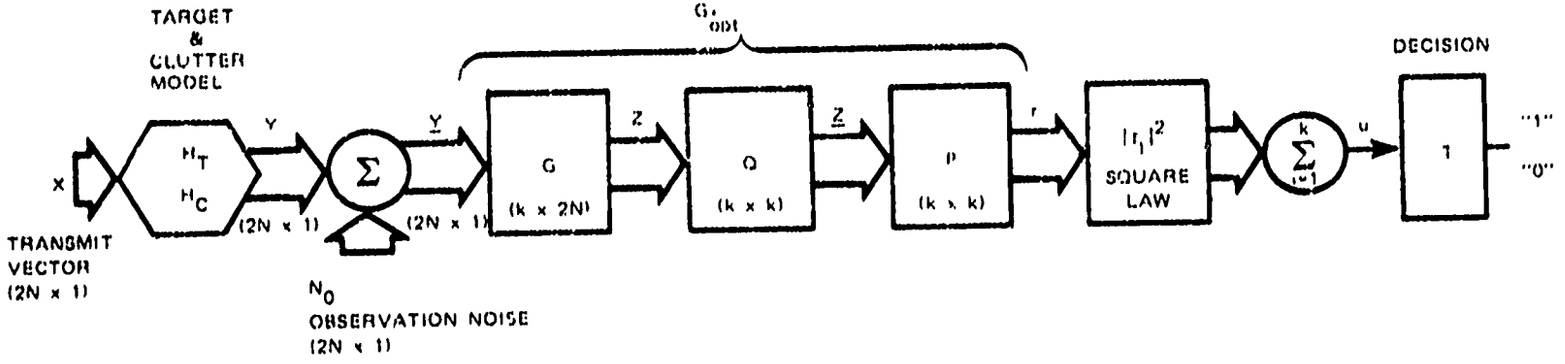

$$r = G_{opt} \cdot \underline{Y} = (P \cdot Q \cdot G) \cdot \underline{Y}$$

$$\underline{Y} = Y + N_0$$

$$Y = X + n$$

Figure 3-4. Matrix Maximum Likelihood Receiver

9532-7

It is noted that the covariance of Z may itself satisfy the orthogonality criterion. This would be true if in the matrix waveform design, the quantity $G\underline{\underline{X}}$ were identically equal to the matrix W. In general, however, the Frobenius norm $\| G\underline{\underline{X}} - W \|$ is satisfied by a least squares fit procedure, such that $G\underline{\underline{X}} \neq W$. In this case, Z must be orthogonalized by the transformation matrix Q. Additive receiver noise also requires imposition of the Q matrix.

The matrix P which operates on $\underline{Z}$ to produce r, is simply a scale factor to properly weight the elements of r prior to the square law operation. The final observed receiver output u, is then

$$u = r^* r = \sum_{i=1}^{k} |r_i|^2 \tag{3-45}$$

The likelihood ratio hypothesis test is dependent upon the probability density of u under the criteria H_0 and H_1. The probability of false alarm for a given threshold T, is then

$$P_{FA} = \int_T^\infty p(u|H_0)du \tag{3-46}$$

For a desired P_{FA}, the threshold T can be computed using the Newton-Raphson technique. Given T, the probability of detection then becomes

$$P_D = \int_T^\infty p(u|H_1)du \tag{3-47}$$

A target is declared if $u \geq T$. Note that the optimum receiver overall weighting function is now

$$G_{opt} = P \cdot Q \cdot G \tag{3-48}$$

Appendix B provides a detailed derivation of the foregoing procedure, assuming that Z is jointly Gaussian under both hypotheses H_0 and H_1. It should be noted that the maximum likelihood detector decision process can be applied to any of the waveform design techniques considered during this study.

3.1.5 Preliminary Design of the Processor

The processing algorithm is presented in a functional flow form in Figure 3-5. A sample vector (k x 1) is multiplied by a weighting matrix (k x k). The elements of both the sample vector and the weighting matrix are complex. This produces a (k x 1) result vector r with complex elements. The elements of the result vector r are squared and the squares are summed to form a scalar u which is then compared with a threshold T.

For the preliminary design, k is assumed equal to 6. Under this assumption, the sample vector will contain six complex (I,Q) samples: one sample from a channel with horizontal (H) polarization and one sample from a channel with vertical (V) polarization for each of three pulses. A pulse repetition time of three milliseconds is assumed. Further, the quantizer is assumed to quantize the I,Q quadrature components to 10-bits.

Under these assumptions, the processing load can be estimated as follows:

Processing Per Sample Vector

Matrix Multiplication:	144 real multiplys 132 adds/subtracts
Vector Squaring and Summing:	12 real multiplys 11 adds
Threshold Detection	1 subtract

These data may be summarized as follows: each three millisecond period, the processor is required to perform 156 multiplications and 144 add/subtracts for each sample vector processed. Input-output, bookkeeping, and other overhead operations are in addition to these requirements.

If these operations were to be performed in a general purpose 16-bit microprocessor or computer without any specialized multiplication hardware, a reasonable assumption would be one 16-bit by 16-bit multiplication each 16-clocks, and one add or subtract operation each clock. Using these assumptions the minimum processing load would be (156 x 16) + 144 = 2640 clocks. If in addition, we estimate four clocks of overhead for each element of the sample vector and of the weighting matrix, we require an additional 4 x (12 + 72) = 336 clocks for a total of 2976 clocks. This can be rounded up to 3,000 clocks.

Figure 3-5 contains a processing block diagram which contains a 16-bit microprocessor identified as the ITT Gilfillan Radar Processing Module (RPM). The RPM is capable of operating at a clock speed of 250 nanoseconds. A first estimate will be made assuming that the entire task were performed in the RPM. This requires 3000 x 0.250 = 750 microseconds during each three millisecond period for processing of the target in a single range bin.

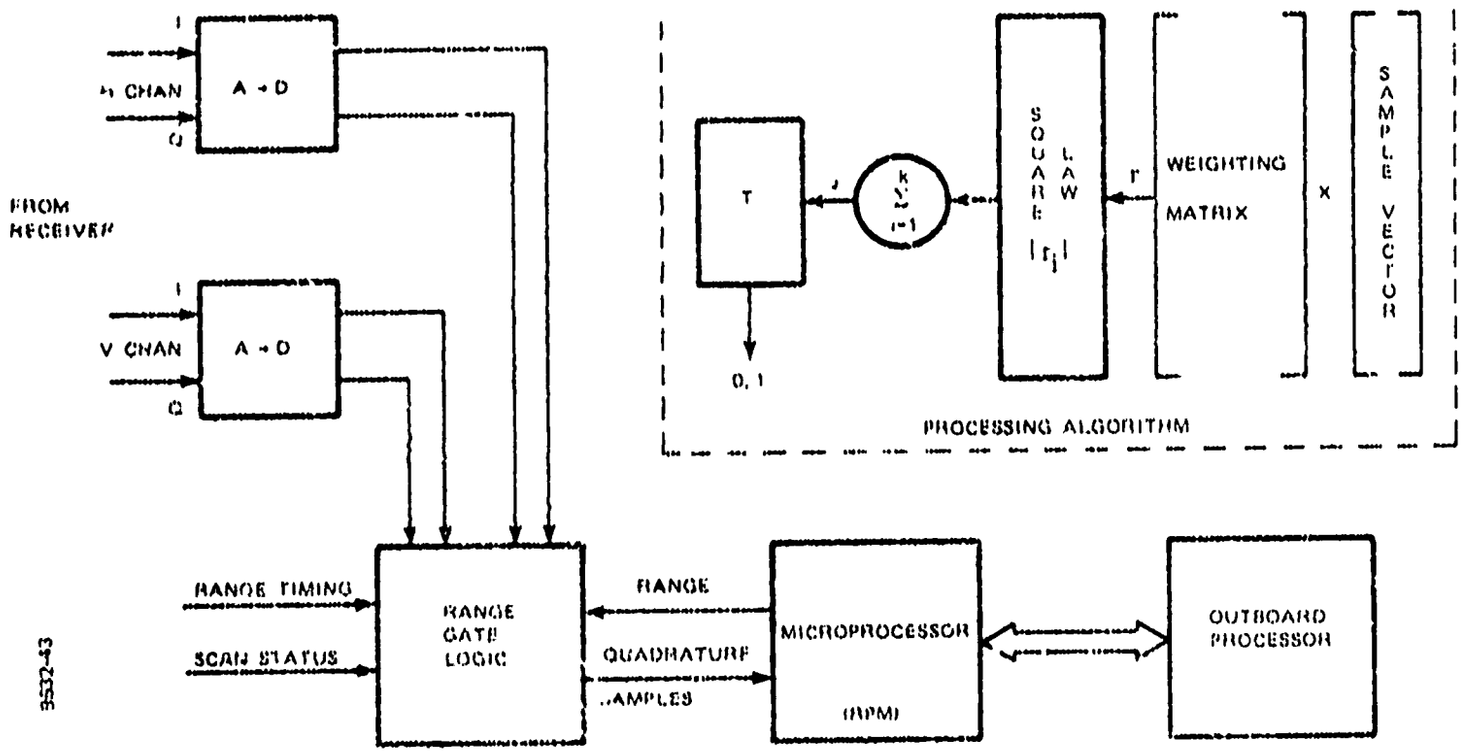

Figure 3-5. Processing Block Diagram

Figure 3-5 shows the use of a specialized programmable Outboard Processor designed to unload the RPM to improve processor efficiency. The detailed block diagram of the Outboard Processor is given in Figure 3-6 and represents an alternative to RPM only processing, noting that the RPM is still required for data management and other ranging functions. This processor is built around an available 12-bit by 12-bit LSI multiplier accumulator chip. This processor is designed to receive quadrature samples and matrix weights from the RPM in one set of memories while it is processing data from the other set of memories. This processor is designed to perform the matrix multiplication and vector squaring operations. Addition/subtractions into the accumulator are fully overlapped with multiplications. A total of 26 multiply and accumulates are required to produce the squares of the real and the complex parts of the elements of the result vector r, 13 for the real part and 13 for the imaginary part. This requires a total of 6 x 26 = 156 clocks for each sample vector processed. The elements of the matrix weights are changed only as required. In this configuration, assuming a 250 nanosecond clock, a matrix multiply and vector square operation can be done in 156 x 0.250 = 39 microseconds (much more efficient than the 750 microseconds associated with the RPM for this function).

With reference to Figure 3-5, the RPM designates the range at which samples are to be collected to the Range Gate Logic which strobes the outputs of the H channel and the V channel A/D converters and passes the samples to the RPM. The RPM passes the samples and the matrix weights to the outboard processor, which computes the squares of the elements of the result vector r and passes these squares back to the RPM where the squares are summed and thresholded.

The configuration of Figure 3-5 would be effective for implementing a track function in the radar, resident in the RPM. To apply the same processing to an acquisition function in the radar, additional processing capability would be required. Adaptation of the ITT Gilfillan developed Optimum Filter Transform (OFT) modular approach would provide the required additional processing capability (the OFT module implements a vector times a matrix multiplication and was developed for high performance Doppler processing in radar signal processing applications).

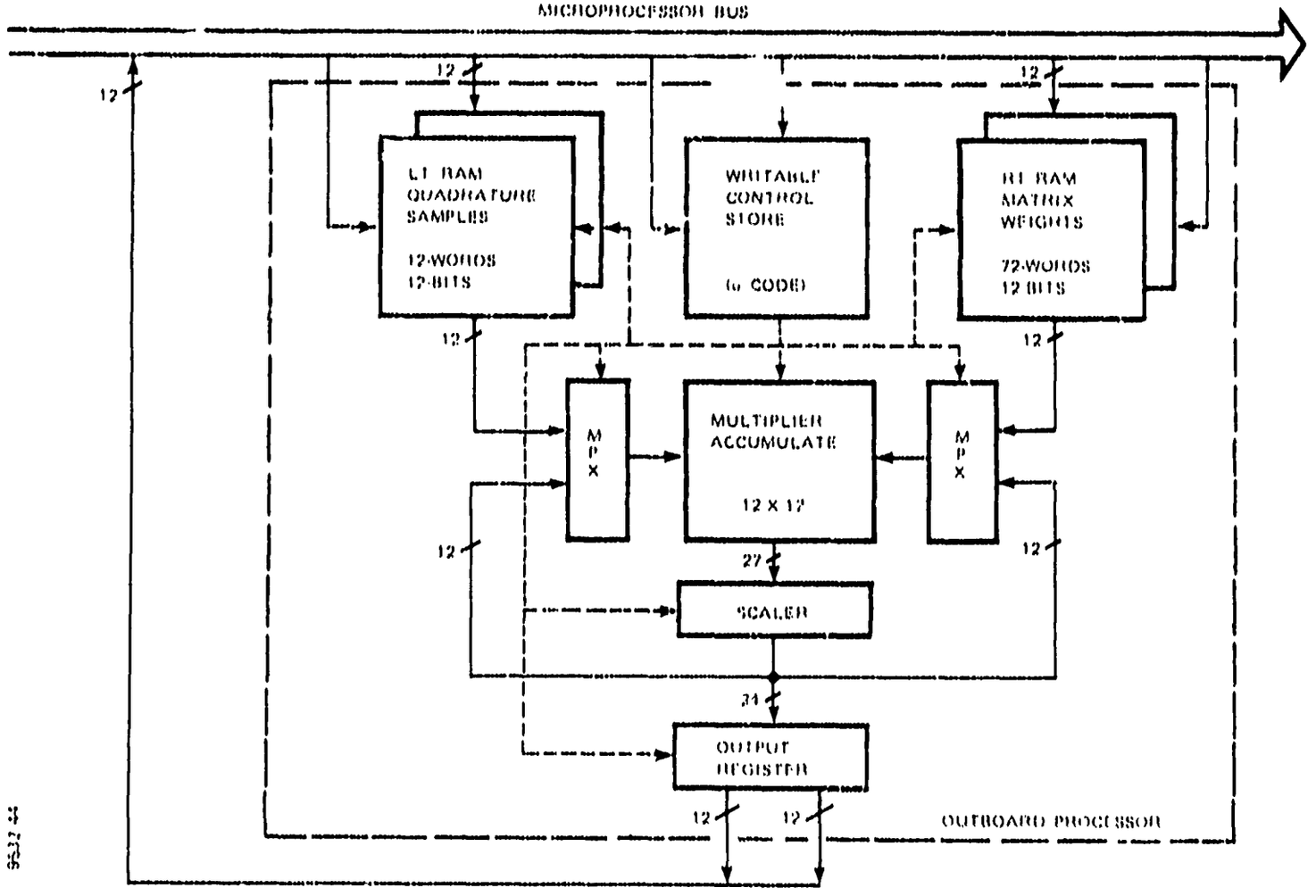

Figure 3-6. Outboard Processor Block Diagram

3.2 THE STATE SPACE APPROACH

This section is also devoted to modeling of radar targets and clutter and to the design of an optimum receiver for detecting a target in clutter. Here, as in previous sections, both target and chaff are taken to have a dual channel scattering operator description, but our approach will be that of the modern state space theory of systems.

From an external viewpoint, a system can be described by the family of all possible input-output pairs. This may be the most general description of a system but, unfortunately, it does not give a useful relationship between a given input of a system and its corresponding output. Because of this, we introduce the state space theory of systems.

The state of a system is the least amount of information which, together with the input, will uniquely determine the output. In what follows we shall be mostly concerned with ***discrete-time systems with a finite dimensional state space.*** Thus, let t be the time variable which takes the values 0, 1, 2, . . ., and let A, B, C be matrices of appropriate dimensions. Then a linear discrete-time system is described by the pair of equations

$$\left.\begin{aligned} s(t+1) &= A\,s(t) + B\,u(t) \\ q(t) &= C\,s(t) \end{aligned}\right\} \tag{3-49}$$

where s(t) is a vector called the state at time t, while u(t) and q(t) are the input vector and the output vector, respectively.

3.2.1 State Space Modeling of Radar Targets and Clutter

3.2.1.1 Point Target Model – The state space theory is not only developed for studying systems, but it is also intended for "generating" stochastic processes – by means of systems for applications, for instance, in communication and control systems. It is evident from Equation (3-49) that if the input u(t) is a stochastic process then so is q(t). Therefore if a stochastic process can be generated from a dynamic system with a state space description, then we have a ***state space model*** for the process

We now derive a state space model for a point target. Let $H_T(t, \tau)$ be the scattering matrix of the target, then

$$H_T(t, \tau) = H(t) \cdot \delta(\tau - \tau_0),\ H(t) = [h_{ij}(t)],\ i, j = 1, 2. \tag{3-50}$$

where $h_{ij}(t)$ are Gaussian processes. If x(t) is a transmitted signal – which is a 2 by 1 deterministic vector – and

$$\tilde{S}(t) = [\, h_{11}(t),\ h_{12}(t),\ h_{21}(t),\ h_{22}(t) \,] \tag{3-51}$$

is the transpose of the target scattering vector, then the corresponding received signal is

$$Y(t) = \underline{\underline{X}}(t - \tau_0) \cdot S(t) \tag{3-52}$$

where the 2 by 4 matrix $\underline{\underline{X}}(\cdot)$ is given by

$$\underline{\underline{X}}(t - \tau_0) = \begin{bmatrix} x_1(t - \tau_0) & x_2(t - \tau_0) & 0 & 0 \\ 0 & 0 & x_1(t - \tau_0) & x_2(t - \tau_0) \end{bmatrix} \tag{3-53}$$

which is deterministic. It follows from Equation (3-52) that the received signal vector $Y(t)$ can be regarded as the output of a linear time-varying dynamic system whose state vector is the scattering vector $S(t)$. Thus the problem of modeling the point target becomes that of modeling the vector process $S(t)$.

To model the process $S(t)$ we use an ***autoregressive model:*** that is, $S(t)$ is taken to be of the form:

$$S(t) = \sum_{n=1}^{N} A_n S(t - n) + u(t), \tag{3-54}$$

where the 4 x 4 constant matrices A_n are to be computed and the 4 x 1 vector $u(t)$ is a white noise process with zero mean. The N step autoregressive model Equation (3-54) is actually a form of a state space model and is equivalent to the pair of equations:

$$\begin{aligned} \vec{S}(t) &= A \cdot \vec{S}(t - 1) + \vec{U}(t), \\ S(t) &= C \cdot \vec{S}(t), \end{aligned} \tag{3-55}$$

where $\vec{S}(\cdot)$ and $\vec{U}(\cdot)$ are 4 x 1 vectors, while A and C are constant matrices of dimensions 4N x 4N, and 4 x 4N respectively.

The basic problem in representing $S(t)$ by an autoregressive model is to estimate the matrix coefficients $A_1, A_2, \ldots, A_N$, from the observations $S(1), S(2), \ldots, S(N)$. Let us now illustrate the estimation procedure for a one step autoregressive model. Thus let $S(t)$ be generated by the equation

$$S(t) = A_1 \cdot S(t - 1) + u(t), \tag{3-56}$$

where $A_1 = [a_{ij}]$, $i, j = 1, 2, 3, 4$, is to be estimated. For this we define

$$\tilde{\vec{a}} = [\, a_{11}, a_{12}, a_{13}, a_{14}, a_{21}, \ldots a_{24}, a_{31} \ldots a_{34}, a_{41} \ldots a_{44} \,]. \tag{3-57}$$

Then Equation (3-56) can be written as

$$S(t) = \phi(t-1) \cdot \vec{a} + u(t). \tag{3-58}$$

where the 4 x 16 matrix ϕ is made up of entries of the 4 x 1 vector $S(t-1)$. Now if the values $S(1)$ . . . $S(L)$ where $(L>5)$ are known, then we form the 4L x 1 vector

$$\tilde{S}(2, \ldots, L) = [\tilde{S}(2), \ldots \tilde{S}(L)] \tag{3-59}$$

and the 4L x 16 matrix

$$\underline{\underline{\phi}}(1, \ldots, L-1) = \begin{bmatrix} \phi(1) \\ \vdots \\ \phi(L-1) \end{bmatrix} \tag{3-60}$$

It then follows from Equations (3-58), (3-59) and (3-60) that

$$\tilde{S}(2, \ldots, L) = \underline{\underline{\phi}}(1, \ldots, L-1) \cdot \vec{a} + \tilde{U}(2, \ldots, L) \tag{3-61}$$

where

$$\tilde{U}(2, \ldots, L) = [\tilde{U}(2), \ldots \tilde{U}(L)]$$

To estimate the vector $\vec{a}$ – which in turn gives the estimate of the matrix A_1 – we use the least square criterion, i.e., we minimize the functional

$$\| S(2, \ldots, L) - \underline{\underline{\phi}}(1, \ldots, L-1) \cdot \vec{a} \|^2. \tag{3-62}$$

Then the least square estimate $\hat{\vec{a}}$ of $\vec{a}$ is given by

$$\hat{\vec{a}} = [\underline{\underline{\phi}}^*(1, \ldots, L-1) \cdot \underline{\underline{\phi}}(1, \ldots, L-1)]^{-1} \cdot \underline{\underline{\phi}}^*(1, \ldots, L-1) \cdot S(2, \ldots, L) \tag{3-63}$$

3.2.1.1.1 **Computation of Matrix Coefficients** – In the case of our problem, the observations are actually the transmitted signal data set $[X(1), \ldots, X(N)]$ and the received signal data set $[Y(1), \ldots, Y(N)]$. It is evident from Equation(3-52) that

$$S(t) = [\, \divideontimes (t - \tau_0)\,]^{-1} \cdot \underline{\underline{X}}(t - \tau_0) \cdot Y(t) \tag{3-64}$$

where

$$\divideontimes = \begin{bmatrix} x_1x_1 & x_1x_2 & 0 & 0 \\ x_2x_1 & x_2x_2 & 0 & 0 \\ & & x_1x_1 & x_1x_2 \\ 0 & 0 & x_2x_1 & x_2x_2 \end{bmatrix} = \underline{\underline{X}}^* \cdot \underline{\underline{X}} \tag{3-65}$$

Therefore the data set $[S(1), S(2), \ldots, S(N)]$ can be computed from Equation (3-64), using the transmitted and received data sets.

The matrix coefficients $A_1, A_2, \ldots, A_N$ can also be computed from the Yule-Walker equations

$$A_1 K_S(m-1) + A_2 K_S(m-2) + \ldots + A_N K_S(m-N) = K_S(m), \qquad (3\text{-}66)$$

$$\text{for } m = 1, 2, 3, \ldots, N.$$

Here $K_S(\cdot)$ is the covariance matrix of the process $S(t)$ which can be approximated by

$$K_S(\kappa) \approx \frac{1}{N} \sum_{n=1}^{N-\kappa} S(n+\kappa) \cdot S(n)^*, \text{ for } \kappa = 0, 1, 2, \ldots \qquad (3\text{-}67)$$

Equivalently, one can also compute $K_S(\cdot)$ from the received signal covariance matrix $K_y(\cdot)$, as discussed in Section 2.:

$$K_S(t-w) = [\underline{\underline{X}}(t-\tau_0)]^{-1} \cdot \underline{\underline{X}}(t-\tau_0)^* \; K_y(t-w) \cdot \underline{\underline{X}}(w-\tau_0) \cdot [\underline{\underline{X}}^*(w-\tau_0)]^{-1} \qquad (3\text{-}68)$$

3.2.1.2 Chaff Model – In this case we have the transmitted-received signal relationship

$$Y(t) = \int_{-\infty}^{\infty} X(t-\tau) \cdot S(t,\tau)\, d\tau, \qquad (3\text{-}69)$$

where, as in the above $X(\cdot)$ is the transmitted signal matrix and $S(\cdot)$ is the range-spread chaff scattering vector. The problem now becomes that of modeling the input $S(t,\tau)$ which is a stochastic process in t for each fixed τ – of a linear system, given the system weighting matrix $X(\cdot)$ and the output y. We shall now give an approximation procedure for this case.

Let $[\psi_n(\tau)]_{n=1}^{\infty}$ be a sequence of orthonormal 4 x 1 vectors over the interval $(-\infty, \infty)$, i.e.,

$$\int_{-\infty}^{\infty} [\psi_n(\tau), \psi_m(\tau)]\, d\tau = \delta_{n,m} = \begin{cases} 1 \text{ for } n = m \\ 0 \text{ for } n \neq m \end{cases}. \qquad (3\text{-}70)$$

where $[\ldots]$ denotes the inner product in C^4. Expanding the 4 x 1 vector $S(t,\tau)$ in terms of the sequence $[\psi_n(\tau)]$ we find

$$S(t,\tau) = \sum_{1}^{\infty} s_n(t) \cdot \psi_n(\tau) \qquad (3\text{-}71)$$

where the scalar functions $s_n(t)$ are random processes. Let $K_S(t, \tau; w, \sigma)$ be the covariance matrix of the process $S(t\ \tau)$.

$$K_S(t, \tau; w, \sigma) = \sum_n \sum_m A_{nm}(t, w) \cdot \psi_n(\tau) \cdot \psi_m(\sigma)^* \tag{3-72}$$

where

$$A_{nm}(t, w) = E[s_n(t) \cdot \bar{s}_m(w)]. \tag{3-73}$$

Therefore

$$A_{jk}(t, w) = \int_{-\infty}^{\infty} \int_{-\infty}^{\infty} \psi_j(\tau)^* \cdot K_S(t, \tau; w, \sigma) \cdot \psi_k(\sigma) \cdot d\sigma d\tau,$$

$$j, k = 1, 2, 3, \ldots \tag{3-74}$$

Having computed $A_{jk}(\ldots)$ from the covariance matrix $K_S(\ldots; \ldots)$ we can then model each of the processes $s_n(t)$ by the autoregressive scheme discussed above. Equivalently, we can model the vector process

$$\vec{s}_n(t) = [s_1(t)\ s_2(t) \ldots s_n(t)] \tag{3-75}$$

with

$$E[\vec{s}_n(t) \cdot \vec{s}_n(w)^*] = \text{Matrix}[A_{jk}(t, w)] \tag{3-76}$$

by the same procedure.

It is noted that the received signal $Y(t)$, in this case, admits the mean square approximation

$$Y_N(t) = \sum_1^N s_n(t) \cdot V_n(t) \tag{3-77}$$

where the 2×1 vectors $V_n(t)$ are given by

$$V_n(t) = \int_{-\infty}^{\infty} \underline{\underline{X}}(t - \tau) \cdot \psi_n(\tau) \cdot d\tau,\ n = 1, 2, 3, \ldots, N. \tag{3-78}$$

3.2.2 Optimum Receiver Design: The Case of a Point Target in a Cloud of Chaff Dipoles

Let Y(t) be the received signal from a point target in a cloud of chaff dipoles, then

$$Y(t) = Y_T(t) + Y_C(t), \tag{3-79}$$

where Y_T and Y_C are the received signals from the target and the chaff, respectively, and both Y_T and Y_C are Gaussian processes.

The binary detection problem is to find the optimum receiver for testing

H_0: Null Hypothesis (i.e., Zero Target Signal):

$$Y(t) = Y_C(t) + n(t), \text{ for all } t \text{ in } [T_1, T_2]; \tag{3-80}$$

H_1: Alternate Hypothesis:

$$Y(t) = Y_T(t) + Y_C(t) + n(t), \text{ for all } t \text{ in } [T_1, T_2]. \tag{3-81}$$

In the above, n(t) is an external additive, statistically independent 2 × 1 vector, white noise process. T_1 and T_2 are the initial and final observation times, and the interval $[T_1, T_2]$ is assumed to be long enough for complete observation of the received signal.

3.2.2.1 State Space Model for the Point Target – Without lost of generality, the point target is modeled by a "2-step" autoregressive scheme. Thus Equation (3-54) now becomes

$$S(t) = A_1 \cdot S(t-1) + A_2 \cdot S(t-2) + u(t) \tag{3-82}$$

where the 4 × 4 matrices A_1 and A_2 have been computed from the methods discussed above and u(t) is a statistically independent 4 × 1 vector white noise process. Set

$$\vec{S}(t) = \begin{bmatrix} S(t) \\ S(t-1) \end{bmatrix} \tag{3-83}$$

Then the state space model for the point target is

$$\vec{S}(t) = \begin{bmatrix} A_1 & A_2 \\ I_4 & 0_4 \end{bmatrix} \cdot \vec{S}(t-1) + \vec{u}(t) \tag{3-84}$$

$$Y_T(t) = X(t - \tau_0) \cdot [I_4 \;\; 0_4] \cdot \vec{S}(t)$$

where $\vec{u}(t) = \begin{bmatrix} u(t) \\ 0_{4,1} \end{bmatrix}$

and $0_{4,1}$ is a 4 × 1 zero vector.

3.2.2.2 **State Space Model for the Chaff Dipoles** – For the chaff dipoles, let us assume that

$$S_C(t, \tau) = s(t) \cdot N(\tau)^{1/2} \tag{3-85}$$

where,

$N(\tau)$ is a deterministic function of the average chaff cross section in range, and $s(t)$ is stochastic. It can then be shown from the discussion in Appendix A that

$$K_{S_C}(t - u, \tau) = \rho(t - u) \cdot N(\tau) \cdot \mu \tag{3-86}$$

and

$$K_S(t - u) = \rho(t - u) \cdot \mu, \tag{3-87}$$

where,

$$\rho(t) = [\exp(-j\bar{\omega}_d t - \frac{\sigma_d^2 t^2}{2})] \cdot [K_1 + K_2 \exp(-2\sigma_r^2 t^2) \cdot \cos 2\bar{\omega}_r t] \tag{3-88}$$

and

$$\mu = 0.9\lambda^2, \; K_1 = 1/5 \begin{pmatrix} 2/3 & 0 & 0 & 1/3 \\ 0 & 1/12 & 1/12 & 0 \\ 0 & 1/12 & 1/12 & 0 \\ 1/3 & 0 & 0 & 2/3 \end{pmatrix}, \; K_2 = 1/5 \begin{pmatrix} 1/3 & 0 & 0 & 1/6 \\ 0 & 1/4 & 1/4 & 0 \\ 0 & 1/4 & 1/4 & 0 \\ -1/6 & 0 & 0 & 1/3 \end{pmatrix} \tag{3-89}$$

It follows from the above that for the chaff dipoles we need only to model the process $s(t)$. Thus as in the case of the point target we take

$$s(t) = a_1 s(t - 1) + a_2 s(t - 2) + \mu^{1/2} \cdot v(t) \tag{3-90}$$

where a_1 and a_2 are 4 x 4 matrices, and $v(t)$ is a white noise zero mean process. Set

$$\vec{s}(t) = \begin{bmatrix} s(t) \\ s(t - 1) \end{bmatrix} \tag{3-91}$$

Then the state space model for the chaff dipoles is

$$\left.\begin{aligned} \vec{s}(t) &= \begin{bmatrix} a_1 & a_2 \\ I_4 & 0_4 \end{bmatrix} \cdot \vec{s}(t - 1) + \vec{v}(t) \\ Y_C(t) &= \int_{-\infty}^{\infty} \underline{\underline{X}}(t - \tau) \cdot N(\tau)^{1/2} \, d\tau \cdot [I_4 \; 0_4] \cdot \vec{s}(t) \end{aligned}\right\} \tag{3-92}$$

where the vector process $\vec{v}(t)$ is again white and with zero mean, and

$$\vec{v}(t) = \begin{bmatrix} \mu^{1/2} \cdot v(t) \\ 0_{4,1} \end{bmatrix}$$

The main information given for the design of the optimum receiver is the target received signal covariance matrix $K_{Y_T}(t, w)$, the chaff dipoles received signal covariance matrix $K_{Y_C}(t, w)$, and the white noise process $n(t)$ covariance matrix $K_n(t - w) = K \cdot \delta(t - w)$.

3.2.2.3 **Estimation of $y_T(t)$ under Hypothesis H_1** – In the state space target and chaff formulations, set

$$A_T = \begin{bmatrix} A_1 & A_2 \\ I_4 & 0_4 \end{bmatrix}, \text{ and } A_{Ch} = \begin{bmatrix} a_1 & a_2 \\ I_4 & 0_4 \end{bmatrix}. \tag{3-93}$$

Then define

$$Z(t) = \begin{bmatrix} \vec{S}(t) \\ \vec{s}(t) \end{bmatrix}, \text{ and } W(t) = \begin{bmatrix} \vec{u}(t) \\ \vec{v}(t) \end{bmatrix}. \tag{3-94}$$

We obtain – by combining Equations (3-80), (3-81), (3-93), and (3-92) – the following state space formulation for the received signal $Y(t)$ under hypothesis H_1:

$$Z(t) = \begin{bmatrix} A_T & 0_4 \\ 0_4 & A_{Ch} \end{bmatrix} \cdot Z(t - 1) + W(t) \tag{3-95}$$

$$Y(t) = C_1(t) \cdot Z(t) + n(t)$$

where

$$C_1(t) = [\underline{\underline{X}}(t - \tau), 0_{2,12}] + [0_{2,8}, \int_{-\infty}^{\infty} \underline{\underline{X}}(t - \tau) \cdot N(t)^{1/2} dt, 0_{2,4}] \tag{3-96}$$

$$= C_T(t) + C_C(t) \text{ (say)}$$

It then follows that the problem of estimating $Y_T(t)$ now becomes that of estimating the state vector $Z(t)$. This is discussed below.

3.2.2.4 **The Kalman Filter for Estimating Z(t)** -- The least square estimate $\hat{Z}(t)$ of $Z(t)$ – basing on the observations $Y(t), Y(t - 1), \ldots, Y(0)$ – is obtained by the discrete Kalman filter. The derivation of the Kalman filter is standard and will be omitted here. Figure 3-7 gives a block diagram of the filter.

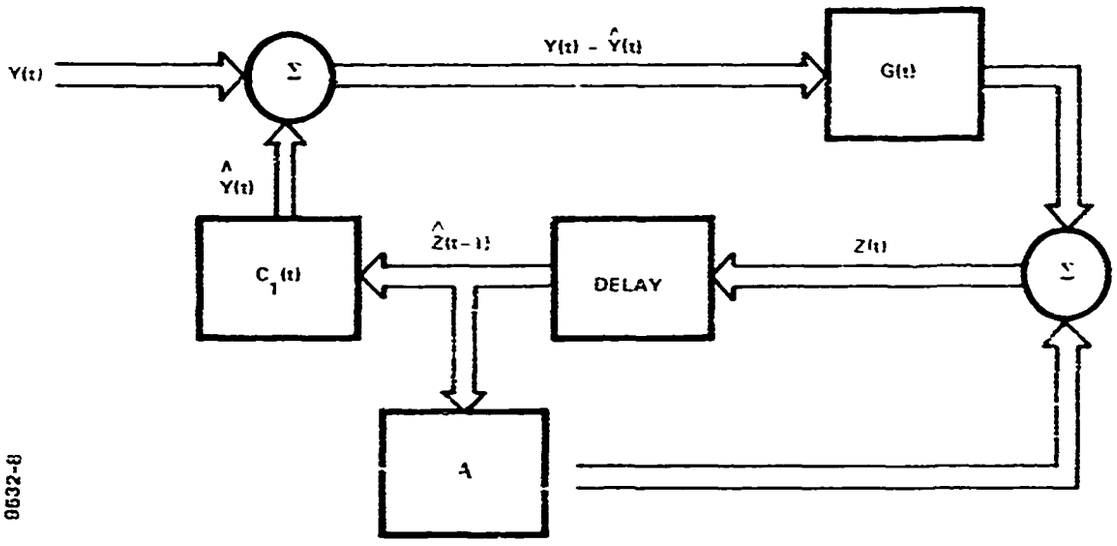

Figure 3-7. The Kalman Filter for Estimating Z

The basic equations for the realization of the Kalman filter are:

a) The estimate at time t of the state of Equation (3-95) is $\hat{Z}(t|t-1)$ -- the conditional mean -- and it satisfies the recursive equation:

$$\hat{Z}(t|t-i) = A \cdot \hat{Z}(t-1|t-2) + G(t)\,[Y(t) - C_1(t) \cdot \hat{Z}(t-1|t-2)]. \tag{3-97}$$

with the initial value $\hat{Z}(1|0)$ (say) given. The matrix G(t) is given by

$$G(t) = A \cdot P(t) \cdot C_1^*(t)\,[C_1(t) \cdot P(t) \cdot C_1^*(t) + K_\nu]^{-1}. \tag{3-98}$$

In the above

$$A = \begin{bmatrix} A_T & 0_4 \\ 0_4 & A_{Ch} \end{bmatrix} \text{ (Equation 3-95)} \tag{3-99}$$

and K_ν is the covariance matrix of the white noise process $\nu(t)$.

b) In Equation (3-98) the matrix P(t) is the covariance of the estimation error, and it is given by

$$P(t+1) = [A - G(t) \cdot C_1(t)]\, P(t)\, [A - G(t) \cdot C_1(t)]^{*} + K_w + G(t) \cdot K_v \cdot G^{*}(t) \qquad (3\text{-}100)$$

with the initial value P(0) taken to be the covariance matrix of the initial state Z(0).

3.2.2.5 **Estimation of $y_C(t)$ under Hypothesis H_0** – The chaff cloud received signal $Y_C(t)$ can of course be estimated by a Kalman filter as in the case of estimating the target received signal $Y_T(t)$. However, it is clear that once the state vector Z(t) has been estimated, the estimation of $Y_C(t)$ is readily given.

3.2.2.6 **The Optimum Receiver** – The optimum receiver is described in Figure 3-8. It compares $Y_T(t)$ under H_1 with $Y(t) - Y_C(t)$ – under H_0 against the decision threshold.

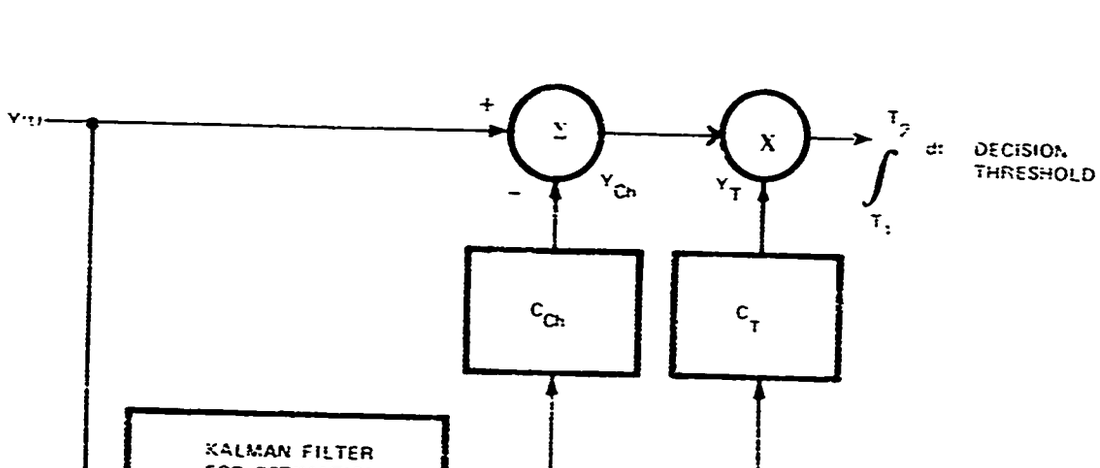

Figure 3-8. The Optimum Receiver

3.2.3 State Space Summary

The foregoing approach has provided a state space model for the design of an optimum receiver in terms of detecting a point target in clutter. The receiver implementation is given in the conventional Kalman filter realization, based upon knowledge of the target/clutter scattering properties and a given transmit waveform. Further study will be necessary to also utilize the state space model in the design of optimal transmit waveforms.

3.3 THE FREDHOLM INTEGRAL EQUATION APPROACH

We discuss in this section the design of yet another form of receiver for the binary detection problem of the previous section. It consists of:

a) An optimum linear filter E_0 which estimates the target received signal $Y_T(t)$ from an observation $Y(t)$ – assuming that hypothesis H_1 is true, and

b) A prewhitening filter Q_0 for the chaff cloud interference.

This receiver is shown in Figure 3-9, where the two filters E_0 and Q_0 are solutions of two matrix Fredholm Integral Equations.

We now illustrate this approach for the case of a point target in a cloud of chaff dipoles considered in the previous section.

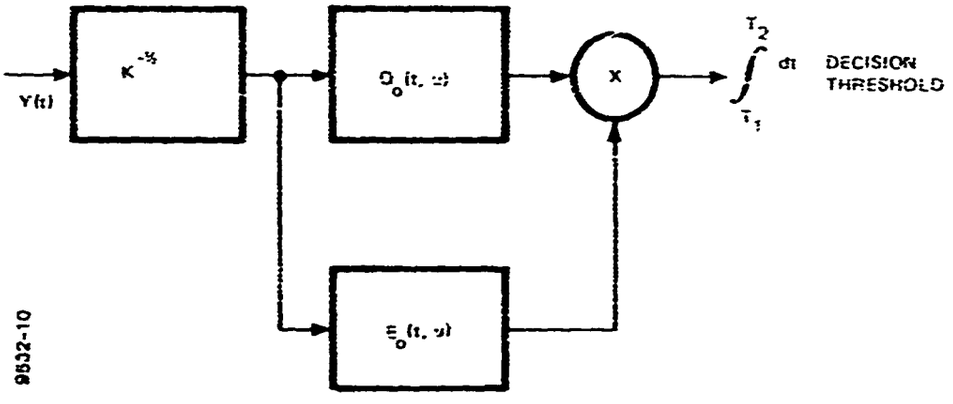

Figure 3-9. The Correlator–Detector Receiver

3.3.1 Integral Equation for the Filter Q_0

The dual channel filter Q_0 has the weighting matrix

$$Q_0(t, u) = K^{-1} [I_2 \cdot \delta (t - u) - D_0(t, u)], \tag{3-101}$$

where K – a 2 x 2 constant matrix – is the white noise process covariance matrix, and the 2 x 2 matrix $D_0(.,.)$ satisfies the following matrix Fredholm Integral Equation:

$$D_0(t, u) \cdot K + \int_{T_1}^{T_2} D_0(t, s) \cdot K_{y_C}(s, u) \cdot ds = K_{y_C}(t, u). \tag{3-102}$$

To solve for $D_0(.,.)$ from Equation (3-102) we first compute the chaff dipoles received signal covariance matrix $K_{y_C}(t, u)$.

We have – from Equation (3-86) of the previous section –

$$K_{S_C}(t - u, \tau) = \rho(t - u) \cdot N(\tau) \cdot \mu \tag{3-103}$$

then

$$K_{y_C}(t, u) = \int_{-\infty}^{\infty} K_{S_C}(t - u, \tau) \cdot \tilde{X}(t - \tau, u - \tau) \cdot d\tau \tag{3-104}$$

where we recall that $K_{y_C}(\cdot)$ is the 4 x 1 vector with entries of $\tilde{K}_{y_C}(\cdot)$, and

$$\tilde{X}(t - \tau, u - \tau) = [x_1(t - \tau)\, \bar{x}_1(u - \tau),\ x_1(t - \tau)\, \bar{x}_2(u - \tau),\ x_2(t - \tau)\, \bar{x}_1(u - \tau),\ x_2(t - \tau)\, \bar{x}_2(u - \tau)]. \tag{3-105}$$

Here x_1 and x_2 are entries of the transmitted signal. We have

$$K_{y_C}(t, u) = \rho(t - u) \cdot \int_{-\infty}^{\infty} \mu \cdot \tilde{X}(t - \tau, u - \tau) \cdot N(\tau) \cdot d\tau \tag{3-106}$$

$$= \rho(t - u) \cdot \mu \cdot G(t, u) \text{ (say)}$$

Now, let g_{ij}, i, j = 1, 2, be the entries of the 2 x 1 vector G, then

$$K_{y_C}(t, u) = \rho(t - u) \begin{bmatrix} 3g_{11}(t, u) + g_{22}(t, u) & g_{12}(t, u) + g_{21}(t, u) \\ g_{12}(t, u) + g_{21}(t, u) & g_{11}(t, u) + 3g_{22}(t, u) \end{bmatrix} \mu, \tag{3-107}$$

where $\mu = 0.9\lambda^2$

3.3.2 The System of Fredholm Integral Equations for $D_0(t, u) = [D_0^{ij}(t, u)]$

Substituting Equation (3-108) into Equation (3-104), we obtain the following system of integral equations:

$$\rho(t-u)\, G_{11}(t,u)\,\mu = D_0^{11}(t,u)k_{11} + D_0^{12}(t,u)k_{21} + \mu \int_{T_1}^{T_2} [D_0^{11}(t,s)\, G_{11}(s,u) + D_0^{12}(t,s)\, G_{12}(s,u)]\, \rho(s-u)\, \cdot ds \quad (3\text{-}108)$$

$$\rho(t-u)\, G_{12}(t,u)\,\mu = D_0^{11}(t,u)k_{12} + D_0^{12}(t,u)k_{22} + \mu \int_{T_1}^{T_2} [D_0^{11}(t,s)\, G_{12}(s,u) + D_0^{12}(t,s)\, G_{22}(s,u)]\, \rho(s-u)\, \cdot ds \quad (3\text{-}109)$$

$$\rho(t-u)\, G_{21}(t,u)\,\mu = D_0^{21}(t,u)k_{11} + D_0^{22}(t,u)k_{21} + \mu \int_{T_1}^{T_2} [D_0^{21}(t,s)\, G_{11}(s,u) + D_0^{22}(t,s)\, G_{21}(s,u)]\, \rho(s-u)\, \cdot ds \quad (3\text{-}110)$$

$$\rho(t-u)\, G_{22}(t,u)\,\mu = D_0^{21}(t,u)k_{12} + D_0^{22}(t,u)k_{22} + \mu \int_{T_1}^{T_2} [D_0^{21}(t,s)\, G_{12}(s,u) + D_0^{22}(t,s)\, G_{22}(s,u)]\, \rho(s-u)\, \cdot ds \quad (3\text{-}111)$$

where k_{ij}, $i, j = 1, 2$, are entries of the constant matrix K, and G_{ij}, $i, j = 1, 2$, are entries of the matrix on the right hand side of Equation (3-106).

3.3.3 Integral Equation for the Filter E_0

The optimum filter E_0 which gives the minimum variance estimate of the signal y_T – under H_1 – is given by the matrix integral equation

$$E_0(t,u) \cdot K + \int_{T_1}^{T_2} E_0(t,s)\, [K_{y_T}(s,u) + K_{y_C}(s,u)] \cdot ds = K_{y_T}(t,u) \quad (3\text{-}112)$$

Here $K_{y_T}(\cdot)$ is the target received signal covariance matrix – which can be computed by the results of Section 3.2. The above can be expanded into a system of integral equations, as was $D_0(t, u)$ for the chaff.

3.3.4 Approach to Solving Equations

The design of the Correlator-Detector-Receiver is complicated by the fact that it involves solutions of two matrix Fredholm Integral Equations. It is clear that the above integral equations can, in general, be quite difficult to solve "exactly". Their solutions depend on the functions G_{ij} which, in turn, are dependent on the transmitted signal x(t).

In most cases, these solutions can be approximated by appropriate orthonormal sequences of functions (a mean square approximation), where the choice of these functions depends on each particular case. In the case of the chaff cloud for instance, since the interval $[T_1, T_2]$ is taken to be finite, we assume that the functions $D_0^{ij}(t, u)$ can be expanded in a "double" orthonormal series of Legendre polynomials $P_i(t)\ P_j(u)$:

$$D_0^{ij}(t, u) = \sum_{0}^{N} \sum_{0}^{N} \eta_{kl}^{ij}\ P_k(t) \cdot P_l(u)$$

Substituting in the system of integral equations we then obtain a system of algebraic equations for the coefficients η_{kl}^{ij}. Similarly, one can approximate the integral equation for $E_0(t, u)$.

It is also noted that an expedient choice of the transmit signal can simplify the problem somewhat. Referring back to the system of equations for D_0, we have

$$g_{ij}(t) = \int_{-\infty}^{\infty} N(\tau) \cdot x_i(t - \tau)\ x_j(t - \tau)^*\ d\tau \quad i, j = 1, 2. \tag{3-113}$$

where $x_i(t)$, $i = 1, 2$, are the entries of the transmitted signal X(t). Since X(t) can be chosen, and due to the specific form of the function $N(\tau)$, in this case, we can take

$$x_1(t) = He_0(t) = 1, \text{ and } x_2(t) = He_1(t) = (\sqrt{c}/\sigma_r)t. \tag{3-114}$$

the first two Hermite Polynomials. Then it can be easily verified that

$$g_{ij}(t) = 0 \text{ for } i \neq j \quad , i, j = 1, 2. \tag{3-115}$$
$$\neq 0 \text{ for } i = j$$

The matrix G(t) therefore becomes a diagonal matrix, which will simplify the solution.

3.3.5 Fredholm Approach Summary

The above approach has been the least developed during the course of this study, ending essentially with the mathematical formulation of the problem. The difficulties envisioned in solving the sets of integral equations, would tend to favor the finite dimensional and state space approaches as the more preferred methods in obtaining solutions to waveform design and associated coherent receiver processing. Additional study would be required to verify this assumption.

3.4 STOKES FORMALISM

The final method reported upon for utilizing scattering properties of target and clutter, is the formulation of the system model in terms of Stokes parameters. This method is summarized briefly below. A much more detailed description of this approach can be found in Rosien et al [1979].

3.4.1 Stokes Model

The previous sections have described the general concepts of scattering theory in terms of the target scattering matrix, as given by:

$$H = \begin{bmatrix} h_{11} & h_{12} \\ h_{21} & h_{22} \end{bmatrix} \tag{3-116}$$

Kennaugh [1951] has shown that the average received power can be expressed as:

$$P = \tilde{Y}AX \tag{3-117}$$

where X and Y are four-dimensional vectors, whose elements are the Stokes parameters, which describe the transmitter and receiver antenna polarizations. The matrix A is 4 x 4 real symmetric, and is known as the average Stokes scattering operator. The elements of A are composed of the expectations of various combinations of the elements of the scattering matrix H (see Rosien [1979] for details).

If one is given the Stokes target scattering operator A, and a similar operator for clutter C, then the problem becomes one of maximizing

$$\frac{\tilde{Y}AX}{\tilde{Y}CX} = s/c \tag{3-118}$$

The solution to Equation (3-118) is detailed in Rosien [1979], and consists of a constrained maximization of the ratio of two bilinear forms. The output is the optimum pair of Stokes vectors for X and Y, which completely describes the transmit and receive antenna polarizations.

Results of this approach will be reported upon in Section 5.2.

Section 4

MODELING AND SIMULATION

This section contains a brief description of the target and chaff models utilized in the computer simulations which provided the performance results reported in Section 5. Both the target and chaff models have been developed in prior work, and considerable additional information can be found in Rosien [1979]. The major items of interest for this study, as reported below, are the method for computing the target scattering covariance matrix and development of the autoregressive chaff model for the computer simulation runs. Also included are brief descriptions of the various software packages utilized to generate the dual and single channel target detection performance results.

4.1 TARGET MODELS

4.1.1 Methodology

Since exact solutions to the electromagnetic response of complex radar targets, such as aircraft, are almost impossible to obtain, most studies on modeling of the cross section for such targets employ approximate techniques, which are valid and sufficient for the frequency range of interest and intended applications. We are primarily interested in the high frequency response of these targets (i.e., wavelengths smaller than the characteristic dimensions of most of the scatters on the targets). Therefore, we have assumed that the target response can be approximated by the algebraic sum of the responses of a collection of individual scatters which form the target. Furthermore, to reduce the computation labor we have approximated most of the scattering components of aircraft targets by simple geometric shapes for which there are either exact cross section expressions or approximate expressions derived using Physical Optics (PO) and/or Geometric Theory of Diffraction (GTD) techniques. Both of these methods are high frequency approximations and are adequate for modeling of the scattering characteristics of most scatters at radar frequencies.

4.1.2 Target: A Collection of Scatters

The simple geometric shapes which we use in modeling aircraft targets are ellipsoids, elliptical flat plates, cylinders and thin wires. In addition to these we represent, as discrete scatters surface discontinuities such as the wing fuselage joints or the engine fuselage joints. Table 4-I lists the various types of scatterers which we have modeled and the corresponding theory (PO or GTD) used in deriving the analytical representation. Figure 4-1 depicts the BQM-34A Drone model used in our simulation program. Table 4-II lists the individual scatterers and corresponding scattering models used in the BQM-34A Drone.

The mathematical model of each scatterer is embodied in the scattering matrix. It is represented in spherical coordinates in the scatterer principle axis system, which is selected such that a diagonal scattering matrix results. In mathematical form, we have

TABLE 4-I. SCATTERER TYPES USED FOR THE SIMULATION OF THE RADAR CROSS SECTIONS

Scatterer Type	Theory
Ellipsoid	PO
Elliptical Flat Plate	GTD
Hollow Elliptical Cylinder	GTD & PO
Cylinder	GTD & PO
Thin Wire	From Series Expansion
Joint Between Two Cylinders	GTD
Exhaust Duct	GTD
Cone-Cylinder	GTD
Doubly Reflected Ray From Two Ellipsoids	PO
Smooth Junction of Curved Sufraces (Slope Discontinuity)	GTD

9532-11

TABLE 4-II. SCATTERER TYPES USED IN MODELING THE BQM-34A DRONE

Scatterer	Model
Fuselage Sections 1 and 3	Ellipsoid
Fuselage Section 2	Cylinder
Wings, Tail, Stabilizers, and Vertical Fin	Elliptical Plate + Thin Wire
Wings, Tail, Stabilizer, and Vertical Fin Joints	Joints
Slope Discontinuity at Engine Interlace and Exhaust	Slope Discontinuity
Engine	Open Ended Cylinder
Engine Blades	Two Thin Wires
Double Reflections	Two Ellipsoids
Wing - Fuselage	
Stabilizers - Tail	

9532-12

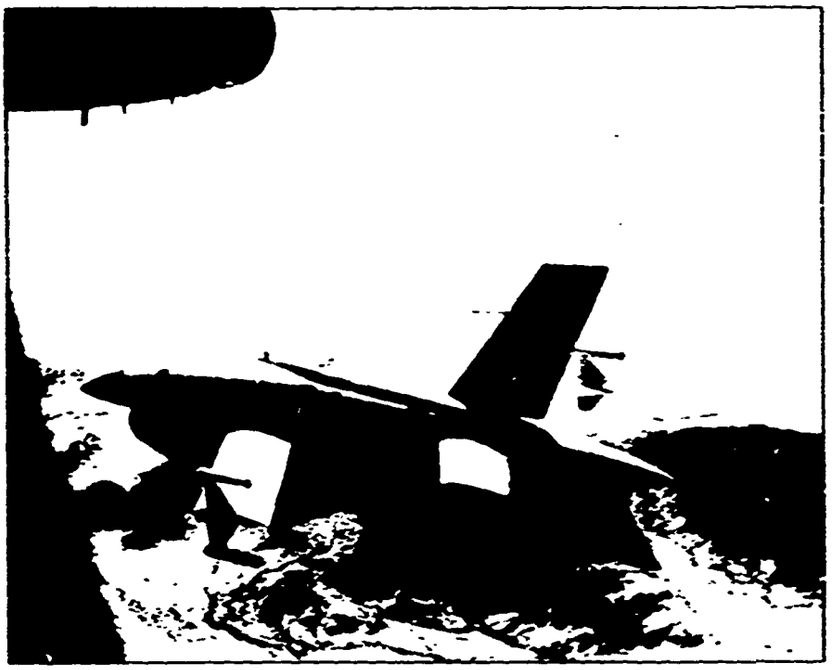

BQM-34A Firebee I Target Drone Dropping Away from the Launch Pylon of its Carrier Aircraft

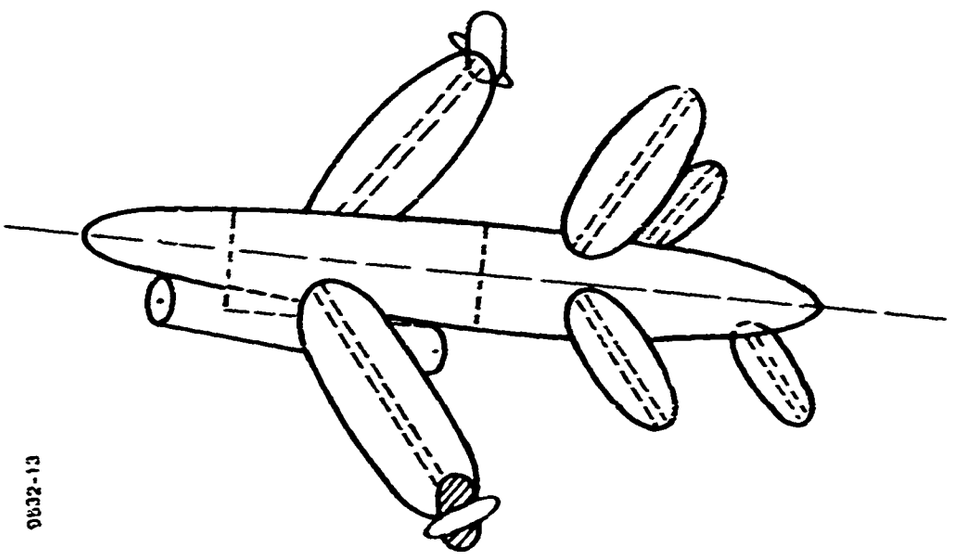

9632-13

Figure 4-1. Photo and Model of the BQM-34A Target Drone

$$S_i = \begin{bmatrix} 0 & 0 & 0 \\ 0 & S_{\theta i} & 0 \\ 0 & 0 & S_{\phi i} \end{bmatrix} e^{-j2k\rho_i} \qquad (4\text{-}1)$$

where S_i is the scattering matrix of the i^{th} scatterer in its own principle axis system. $S_{\theta i}$ and $S_{\phi i}$ are complex functions of the scatterer size and aspect angle in the orthogonal θ (vertical) and ϕ (horizontal) directions, and ρ_i is the one-way distance between a plane wave front passing through the reflection point and one passing through the center of the target coordinate system.

To compute the received signal, we transform the scattering matrix from the scatter principle axes system to radar coordinates. This includes several transforms as follows:

$$H_i = P'A'E'Q'S_i\ QBAP \qquad (4\text{-}2)$$

where H_i is the scattering matrix of the i^{th} scatterer in the antenna coordinate system. P is a transformation from spherical to Cartesian coordinates in the antenna frame. A is a transformation from the antenna frame to the target frame. B is a transformation from the target frame to the scatterer principle axis frame, and Q is a transformation from Cartesian to spherical coordinates in the scatterer frame.

In the case of a single pulse much longer than the target, the scattering matrix of the target may be approximated by the summation

$$H_T = \sum_i H_i \qquad (4\text{-}3)$$

The three element polarization signal vector backscattered from the target is then given by

$$E_b = H_T E_t \qquad (4\text{-}4)$$

where the subscript b refers to the backscattered target return in the antenna frame, and the subscript t refers to the transmit antenna polarization vector.

4.1.3 Radar Cross Section Validation

The target model of the BQM-34A drone was validated by comparing the simulated RCS plots for various transmit and receive polarizations with RATSCAT [1977] measurements. The drone model consists of approximately 30 individual scatterers, each of which includes both size parameters and a backscatter coefficient. The size parameters were selected to resemble the target configuration. Then from a knowledge of the characteristics of each scatterer model and through a trial and error process, the backscatter coefficients were adjusted in order to match the simulated RCS plots to those obtained from measurements. Sample results of the comparisons are shown in Figures 4-2, 4-3, and 4-4 for three different transmit and receive polarization settings. As can be seen, the simulation results match the measurements rather well in the areas of general curve shape, specular type returns, lobing structure, fluctuation, and relative scale (power levels).

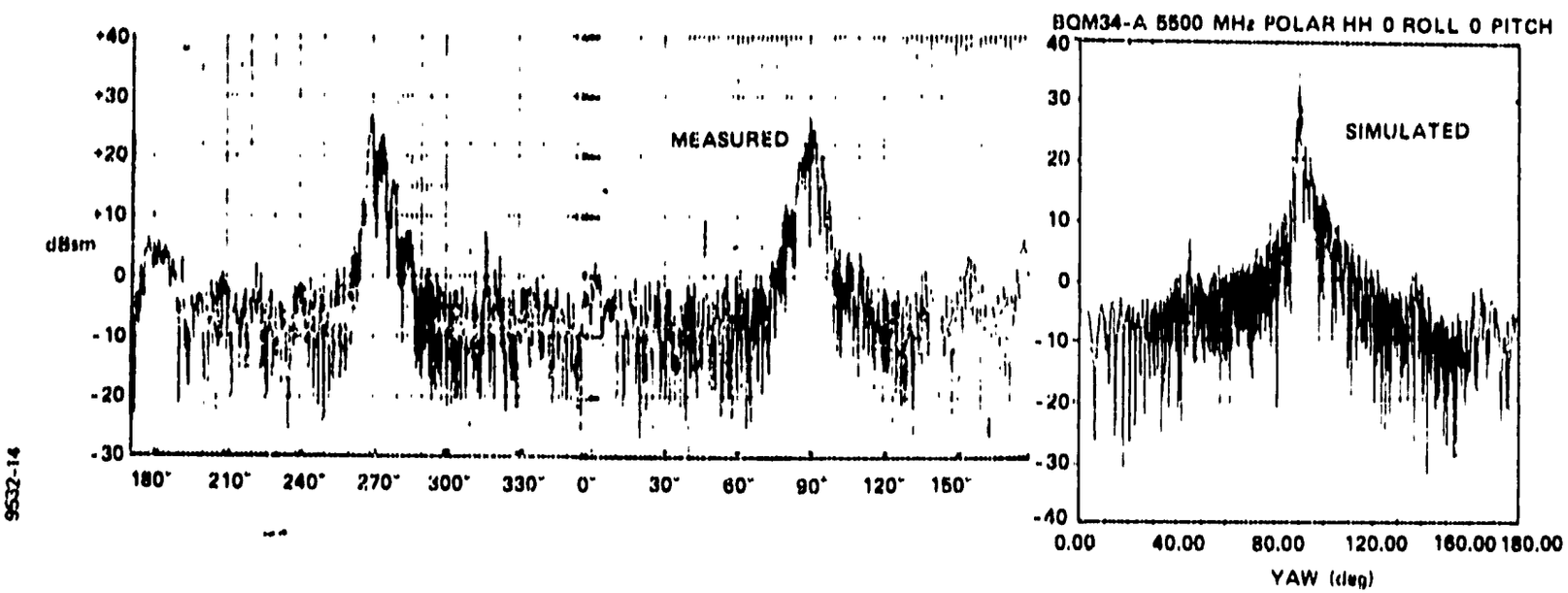

Figure 4-2. Measured and Simulated Cross Section of the BQM-34A Drone as a function of yaw angle at 5.500 MHz for horizontal transmit and receive polarizations

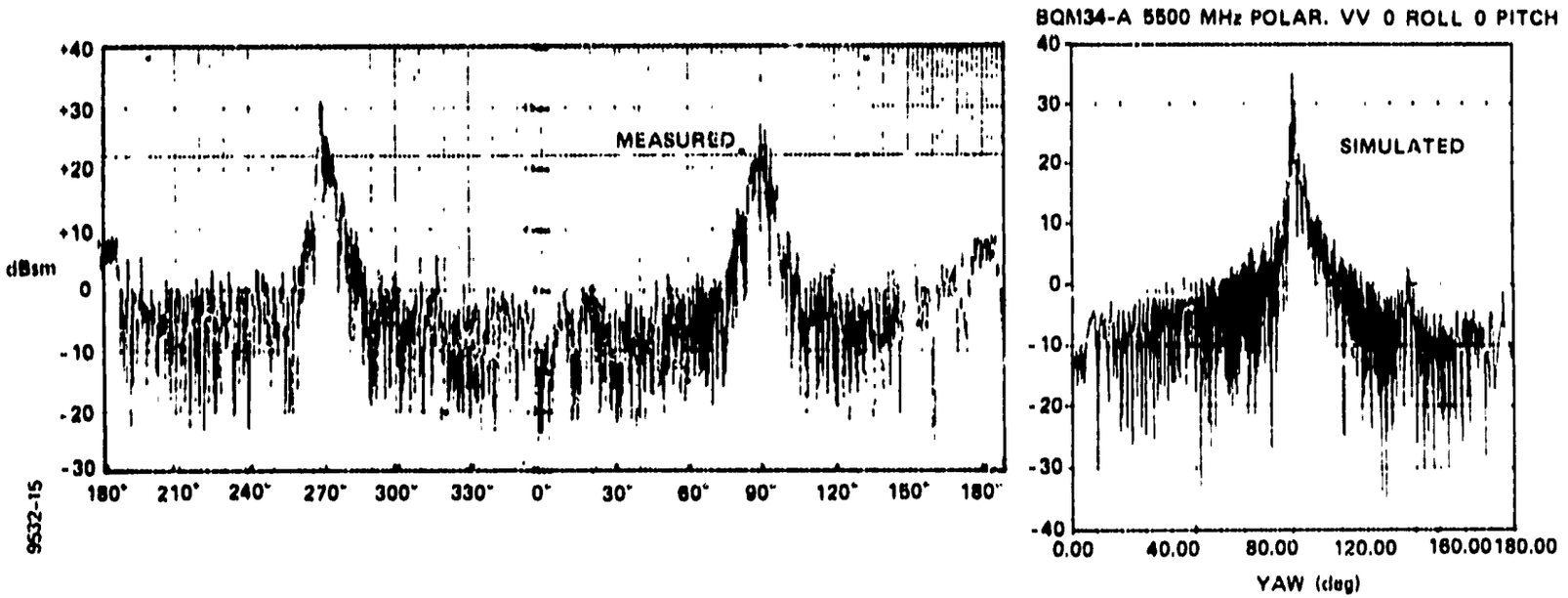

Figure 4.3. Measured and Simulated Cross Section of the BQM-34A Drone as a function of yaw angle at 5500 MHz for vertical transmit and receive polarizations.

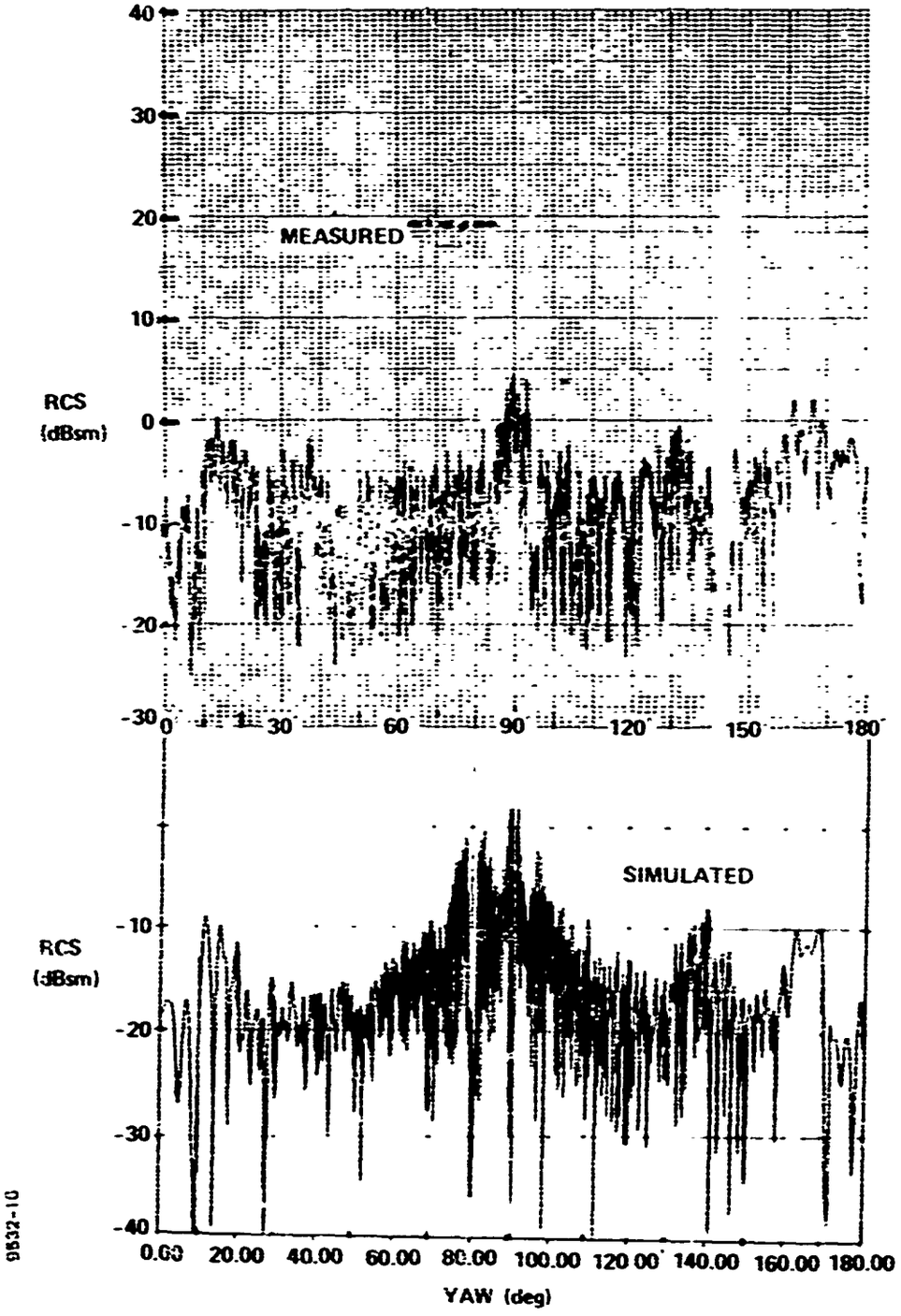

Figure 4-4. ***Measured and Simulated Cross Section of the BQM-34A Drone*** *as a function of yaw angle at 5500 MHz for vertical transmit and horizontal receive*

4.1.4 Covariance Matrix

The covariance matrix of the target was computed using 300 samples of RCS obtained from contiguous increments in aspect angle The angle stepping was performed in nested loops with yaw being stepped in the inner loop; roll in the intermediate loop; and pitch in the outer loop. Yaw was varied between 5 and 25 degrees with increments of 0.2 degree. Roll ranged from −30 to −28 degrees and was incremented in steps of 1 degree. Pitch was varied from 9 to 11 degrees in 1-degree steps. These aspect variations actually yield 900 samples, of which 300 were selected for covariance matrix computation. When the sample time was assumed to be 1 msec, 300 contiguous samples were used. When the sample time was assumed to be 3 msec, every third sample was used to compute the covariance matrix. (Note should be made that there are four sets of RCS samples of 900 numbers. Each set represents one of the elements of the scattering matrix (h_{11}, h_{12}, h_{21}, h_{22})). Plots of the correlation function derived from the simulated target model are shown in Figure 4-5 for both the amplitude and phase. Since $h_{21} = h_{12}$, h_{21} is not explicitly shown.

4.2 CHAFF

4.2.1 The Dipole Chaff Cloud Model

In this section a chaff cloud is modeled as a collection of rotating dipole scatterers. The model provides for simulation of the polarization and spectral characteristics of radar signals backscattered from a cloud of rotating dipoles which can have either completely random or any preferred orientation. A vector autoregressive process based upon the above model, is then used to obtain a Stochastic model for the simulation of the scattering matrix elements of the dipole cloud and signals scattered from the chaff.

4.2.2 Theoretical Covariance Matrix

A description of the theoretical aspects of the chaff covariance matrix is presented below (more detail is given in Appendix A). This covariance function can be written in terms of the spectral and polarization characteristics of the chaff cloud. These characteristics are dependent upon the geometrical configurations of the dipoles which constitute the cloud. As a consequence, the orientation of a typical dipole (as depicted in Figure 4-6) will be considered first in the development of the theoretical model.

To arrive at a description of the dipole orientation, we carry out a transformation consisting of three successive rotations defined by the Eulerian angles. Starting with the unprimed system, we rotate the double primed system by an angle ϕ counterclockwise about the z axis. The primed system is defined through a rotation by an angle θ in the counterclockwise direction around the x' axis. The dipole orientation is then found in the primed system, where the axis of rotation coincides with the x' axis and the dipole is in the (x', y') plane as defined by the angle ψ.

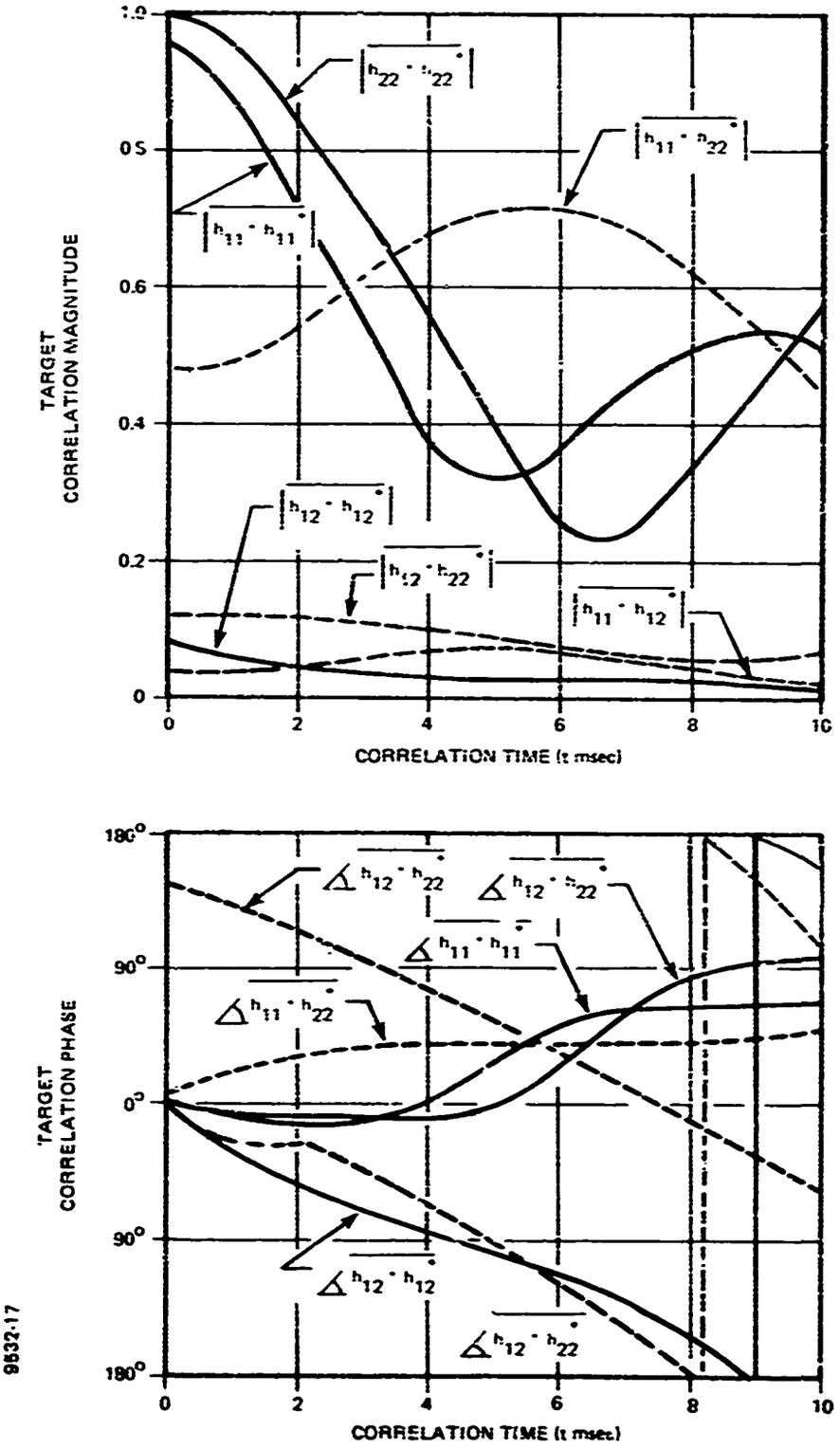

Figure 4-5. Simulated Target Correlation Function

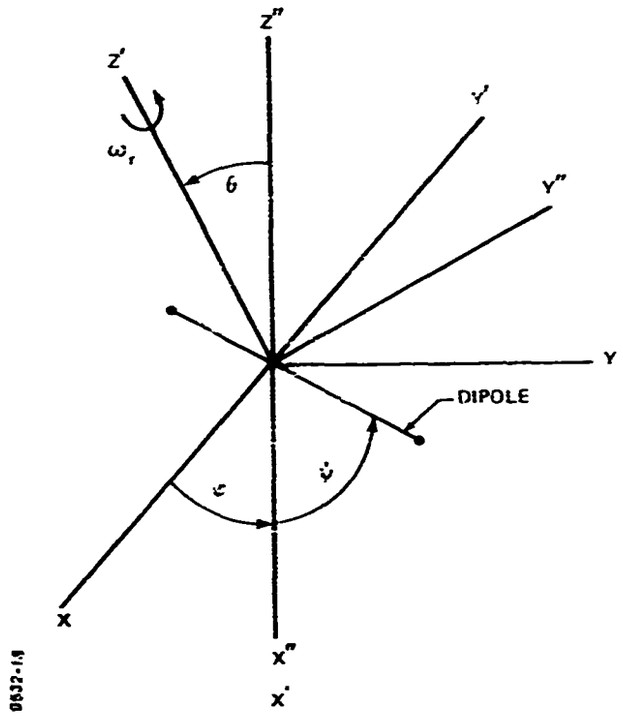

Figure 4-6. Dipole Orientation

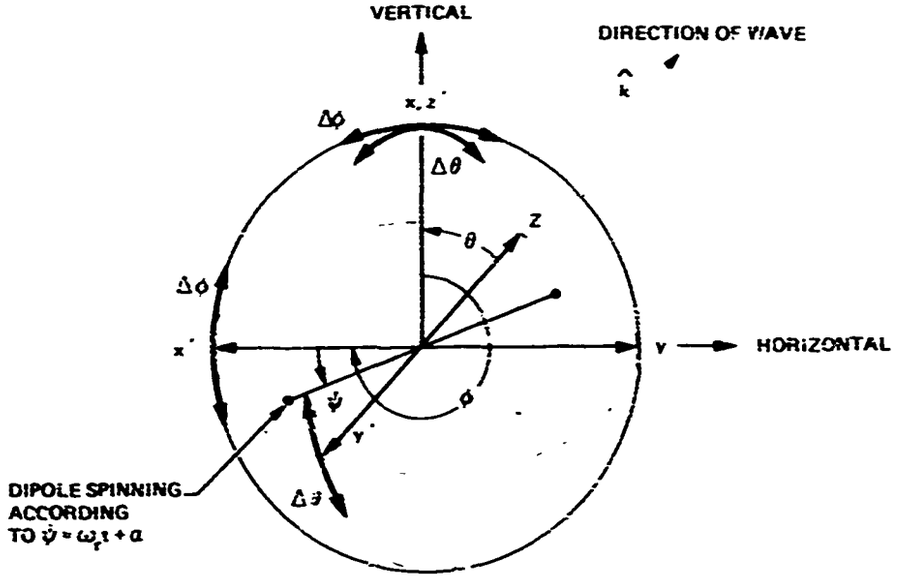

z' = AXIS OF DIPOLE ROTATION
ORIENTATION OF z' IS UNIFORMLY DISTRIBUTED $-180^\circ \leq \Delta\Phi \leq 180^\circ$, $-90^\circ \leq \Delta\theta \leq 90^\circ$
DIPOLES ROTATE IN (X', Y') PLANE

Figure 4-7. Dipole Geometry

In order to be consistent with our definition of the scattering matrix, we orient the unprimed system such that x is in the vertical direction and y is in the horizontal direction. The wave is assumed to travel along the z axis. The reoriented coordinate system is shown in Figure 4-7 where z is into the page. Notice also that the primed system is shown with the dipole rotating in the (x', y') plane. The primed system, as shown in Figure 4-7, is derived from Figure 4-6 by setting $\varphi = 270^\circ + \Delta\varphi = -90^\circ + \Delta\phi$, and $\theta = 90^\circ + \Delta\theta$. The angle ψ (a function of time) is given by $\psi = \omega_r t + \alpha$, where ω_r is the dipole rotation rate and α is the initial angle. As seen in the figure, the perturbations $\Delta\theta$ serve to orient the axis of rotation (z') and, subsequently, the plane of the rotating dipole relative to the x axis. Notice that with $\Delta\theta = 0$ the line of sight (z axis) remains in the plane of rotation. Only when $\Delta\theta \neq 0$ is the z axis not in the plane of rotation. The limits on the perturbations are as follows. $-90^\circ \leq \Delta\theta \leq 90^\circ$ and $-180^\circ \leq \Delta\phi \leq 180^\circ$. If the limits are reached, the dipole may have any orientation whatsoever.

If the dipole direction (denoted by the unit vector $\hat{d}$) is described in the (x', y') plane by the angle ψ, then we can find its orientation in the (x, y, z) coordinate system through the application of the inverse Eulerian transformation. The scattering matrix of such a dipole to an electromagnetic wave propagating along the z axis is given by (Borison [1967], Wang et al [1967])

$$H = \begin{bmatrix} h_{xx} & h_{xy} \\ h_{yx} & h_{yy} \end{bmatrix} = \sqrt{Q}\,\varphi \quad \lambda \hat{d}\hat{d}^* \tag{4-5}$$

where λ is the wavelength of the incident signal, $\hat{d}\hat{d}^*$ is defined as the outer product, and $h_{xy} = h_{yx}$. From this it is clear that h_{xx}, h_{xy}, h_{yx}, and h_{yy} are all functions of the variables θ, φ, and ψ, and λ, where $\psi = \omega_r t + \alpha$ is a function of the dipole rotation rate and time. The orientation of the dipole rotation plane described by θ and φ impact the polarization of the scattered wave, while the Doppler is dependent upon ψ and λ.

Before proceeding to determine the temporal and polarization characteristics of a collection of dipoles, let us define a new vector

$$\tilde{h}(t) = [h_{xx}(t), h_{xy}(t), h_{yy}(t)] \tag{4-6}$$

Then the covariance matrix of h(t) is given by

$$K_{HH}(\tau) = E[h(t)\, h^*(t - \tau)] \tag{4-7}$$

where the * denotes complex conjugate transpose.

When the angular rotation rate and the Doppler due to the drift velocity are each described by distribution functions which include means and standard deviations, then $K_{HH}(\tau)$ will be a function of $\bar{\omega}_r$, σ_r, $\bar{\omega}_d$, and σ_d, where the subscript r denotes rotation, the subscript d refers to Doppler, the bar means average, and σ is the standard deviation. If the dipoles are distributed over restricted regions of both θ and ϕ, $K_{HH}(\tau)$ will thus be a function

of these limits θ_1, θ_2, ϕ_1, and ϕ_2. As a result the covariance matrix includes spectral content due to the dipole activity and polarization characteristics due to the dipole distribution.

The covariance matrix can be written such that the spectral and polarization characteristics are separable functions (see Appendix A):

$$K_H(\tau) = M_d(\tau) \cdot \left\{ C + M_r(2\tau) \cdot D + \bar{M}_r(2\tau) \cdot \bar{D} \right\} \qquad (4\text{-}8)$$

where $M_d(\tau) = M_d(\tau, \bar{\omega}_d, \sigma_d)$ and $M_r(\tau) = M_r(\tau, \bar{\omega}_r, \sigma_r)$ are scalars, and where C and D are 3X3 matrix functions of θ_1, θ_2, ϕ_1, and ϕ_2. Notice that the spectral content for all of the elements in the covariance matrix stems from the same two sources, namely M_d and M_r. However, the elements may exhibit different correlation characteristics as a function of the matrices C and D. In effect, the correlation functions for all of the elements in $K_H(\tau)$ result from the summation of weighted time functions, where the weights differ for the various elements.

4.2.3 Stochastic Model Derived From Autoregressive Process

Given the theoretically derived matrix covariance function $K_H(\tau)$ of the chaff scattering matrix elements s_{ij}, the stochastic vector h(t) may be modeled by a three element complex vector autoregressive process excited with a zero mean complex vector white Gaussian noise source u(t) described as follows.

$$h(t) = \sum_{i=1}^{M} A_i \, h(t - i\Delta t) + u(t) \qquad (4\text{-}9)$$

where the A_i's are 3 x 3 complex matrix coefficients to be determined. The matrix coefficients A_i can be obtained by solving the matrix Yule-Walker equations

$$K_H(m\Delta t) = \sum_{i=1}^{M} A_i \, K_H\{(m - i)\Delta t\} \qquad m = 1, \ldots, M \qquad (4\text{-}10)$$

As the order of the autoregressive (AR) model increases by 1 from M to M+1, there are nine new matrix elements of A_{M+1} to be computed in addition to the 9 x M elements of A_1 through A_M that need to be recomputed.

It is noted, as stated previously, that the $K_H(\tau)$ in Equation (4-8) can be decomposed into three components as follows.

$$K_H(\tau) = (M_d(\tau) \cdot C) + (M_d(\tau) \cdot M_r(2\tau) \cdot D) + (M_d(\tau) \cdot \bar{M}_r(2\tau) \cdot \bar{D})$$

$$= K_{H1}(\tau) + K_{H2}(\tau) + K_{H3}(\tau) \qquad (4\text{-}11)$$

It can be shown that the covariance function of the sum of the outputs of three independent linear systems each being excited with a mutually independent zero mean white Gaussian noise source is equal to the sum of the autocovariance functions of the output of the three linear systems.

Hence, each of the covariance functions $K_{Hi}(\tau)$ (i=1,2,3) can be individually modeled with an autoregressive process.

Also, we note that $K_{H1}(\tau)$ is composed of a product of the time correlation function $M_d(\tau)$, which is a scalar, and the covariance matrix C of the scattering matrix elements h_{ij}. It then follows that the complex vector autoregressive process can be modeled with scalar coefficients $a_1 \ldots a_{M_a}$ that is

$$A_i = a_i I \qquad i=1, \ldots, M_a$$

and

$$h_1(t) = \sum_{i=1}^{M_a} A_i\, h_1(t - i\Delta t) + u_1(t) \tag{4-12}$$

$$K_{H1}(m\Delta t) = \sum_{i=1}^{M_a} a_i\, K_{H1}[(m - i)\Delta t] = C \cdot \sum_{i=1}^{M_a} a_i \cdot M_d[(m - i)\Delta t]$$

The same argument applies to $K_{H2}(\tau)$ and $K_{H3}(\tau)$.

Therefore,

$$h_2(t) = \sum_{i=1}^{M_b} b_i\, h_2(t - i\Delta t) + u_2(t) \tag{4-13}$$

$$K_{H2}(m\Delta t) = \sum_{i=1}^{M_b} b_i\, K_{H2}[(m - i)\Delta t]$$

$$= D \cdot \sum_{i=1}^{M_b} b_i \cdot M_d[(m - i)\Delta t] \cdot M_r[2(m - i)\Delta t]$$

and

$$h_3(t) = \sum_{i=1}^{M_c} c_i\, h_3(t - i\Delta t) + u_3(t) \tag{4-14}$$

$$K_{H3}(m\Delta t) = \sum_{i=1}^{M_c} c_i K_{H3}[(m - i)\Delta t]$$

$$= \bar{D} \cdot \sum_{i=1}^{M_c} c_i\, M_d[(m - i)\,\Delta t] \cdot \bar{M}_r[2(m - i)\Delta t]$$

Furthermore, since

$$D \cdot M_r(2\tau) + \bar{D} \cdot \bar{M}_r(2\tau) = 2\,\mathrm{Re}[D \cdot M_r(2\tau)]$$

it follows that c_i is the complex conjugate pair of b_i i.e., $c_i = \bar{b}_i$

and

$$h(\tau) = h_1(\tau) + h_2(\tau) + h_3(\tau) \tag{4-15}$$

The scalar coefficients a_i, b_i and c_i can be obtained by solving the Yule-Walker equations of the correlation functions $M_d(\tau)$, $M_d(\tau) \cdot M_r(2\tau)$ and $M_d(\tau) \cdot \bar{M}_r(2\tau)$ respectively.

From a closer examination into the properties of the correlation functions $M_d(\tau)$, $M_r(2\tau)$, $\bar{M}_r(2\tau)$ in Appendix A (Equations 10-14), it is noted that these functions are expressed in terms of exponential functions of complex exponents.

$$M_d(\tau) = \exp\left[-j\bar{\omega}_d\tau - \frac{\sigma_d^2}{2}\tau^2\right]$$

$$M_r(2\tau) = \exp\left[-j2\bar{\omega}_r\tau - 2\sigma_r^2\tau^2\right]$$

$$\bar{M}_r(2\tau) = \exp\left[j2\bar{\omega}_r\tau - 2\sigma_r^2\tau^2\right]$$

where $\bar{\omega}$ denotes the average value of ω, and σ^2 represents the variance of ω.

The real part of the exponents are all negative and thus an exponentially decorrelating function of time. The imaginary part $\bar{\omega}\tau$ is associated with the sinusoidal modulation of angular rate $\bar{\omega}$ (i.e., $m(\tau) = \exp(-j\bar{\omega}t)$, a line in the power spectral domain since this imaginary part of the exponent is a linear function of τ.

Under this special case, the real and imaginary parts of the exponent can be separated by associating the real part with the autoregressive process and the imaginary part with the sinusoidal modulation.

Realization of the autoregressive process for the general case of Equations (4-12), (4-13) and (4-14) yields complex valued coefficients. For the special case the coefficients are real.

For this special case we define the three autoregressive (AR) processes as $\hat{h}_1(t)$, $\hat{h}_2(t)$ and $\hat{h}_3(t)$ and the associated scalar coefficients $\hat{a}_i$, $\hat{b}_i$ and $\hat{c}_i$ which are real values.

Then we have

$$\hat{h}_1(t) = \sum_{i=1}^{M_a} \hat{a}_i \hat{h}_1(t - i\Delta t) + u_1(t) \tag{4-16}$$

$$\hat{K}_{H1}(m\Delta t) = \sum_{i=1}^{M_a} \hat{a}_i \hat{K}_{H1}[(m-i)\Delta t] = C \sum_{i=1}^{M_a} \hat{a}_i \cdot \exp\left[-\frac{\sigma_d^2}{2}(m-i)^2\Delta t^2\right]$$

$$\hat{h}_2(t) = \sum_{i=1}^{M_b} \hat{b}_i \hat{h}_2(t - i\Delta t) + u_2(t) \tag{4-17}$$

$$\hat{K}_{H2}(m\Delta t) = \sum_{i=1}^{M_b} \hat{b}_i \hat{K}_{H2}[(m-i)\Delta t]$$

$$= D \sum_{i=1}^{M_b} \hat{b}_i \exp\left[-\frac{\sigma_d^2 + 4\sigma_r^2}{2}(m-i)^2\Delta t^2\right]$$

$$\hat{h}_3(t) = \sum_{i=1}^{M_b} \hat{b}_i \hat{h}_3(t - i\Delta t) + u_3(t) \tag{4-18}$$

$$\hat{\kappa}_{H3}(m\Delta t) = \sum_{i=1}^{M_b} \hat{b}_i \hat{\kappa}_{H3}[(m - i)\Delta t]$$

$$= \bar{D} \sum_{i=1}^{M_b} \hat{b}_i \exp\left[-\frac{\sigma_d^2 + 4\sigma_r^2}{2}(m - i)^2\Delta t^2\right]$$

and

$$h(t) = e^{-j\omega_d t}[\hat{h}_1(t) + e^{-j\bar{\omega}_r t}\hat{h}_R(t) + e^{j\bar{\omega}_r t}\hat{h}_3(t)] \tag{4-19}$$

An efficient algorithm developed by Durbin [DURBIN, 1960] to compute the coefficients of the AR process, is used. This algorithm computes the coefficients in a recursive manner increasing the order of the AR process by one with each iteration until the desired mean squared error criterion of the fitness of the AR model to the theoretical convariance function is met. A discussion on the Durbin Recursive Algorithm is given by Appendix F.

Realization of the stochastic modeling of chaff is accomplished using the AR processor in the form of a digital filter with an appropriate number of delays T and an associated weighted feedback loop whose weights are the scalar coefficients. Two functional diagrams of the stochastic chaff model are given in Figures 4-8 and 4-9 for the general and special cases respectively.

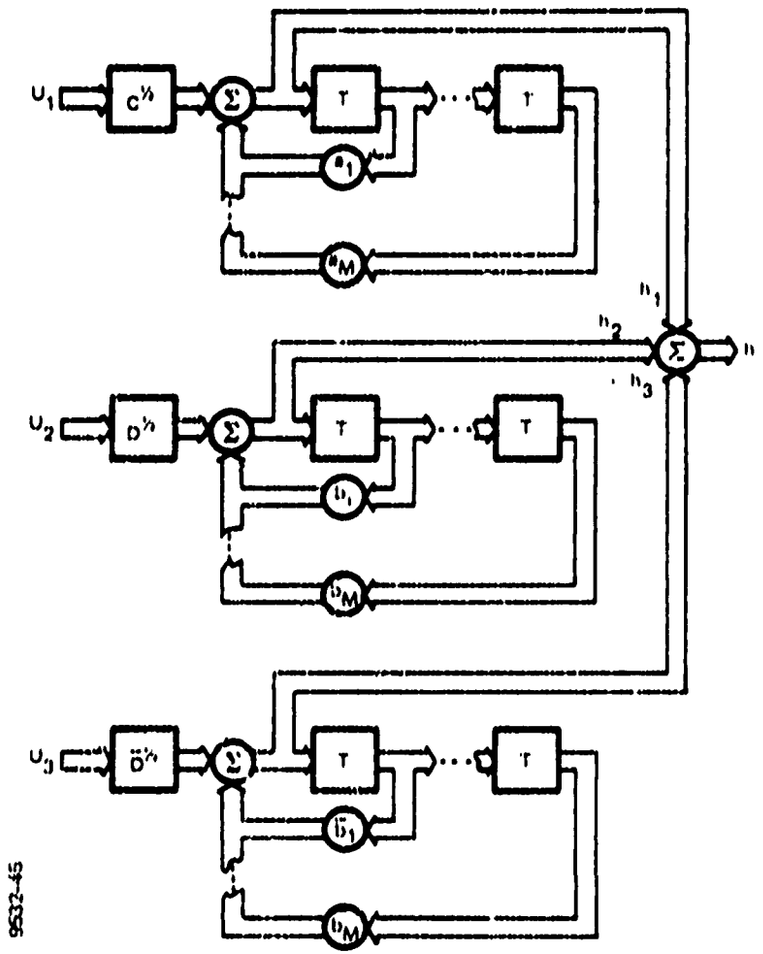

Figure 4-8. Matrix Autoregressive Model of Stochastic Process, General Case, Recursive Filter Representation

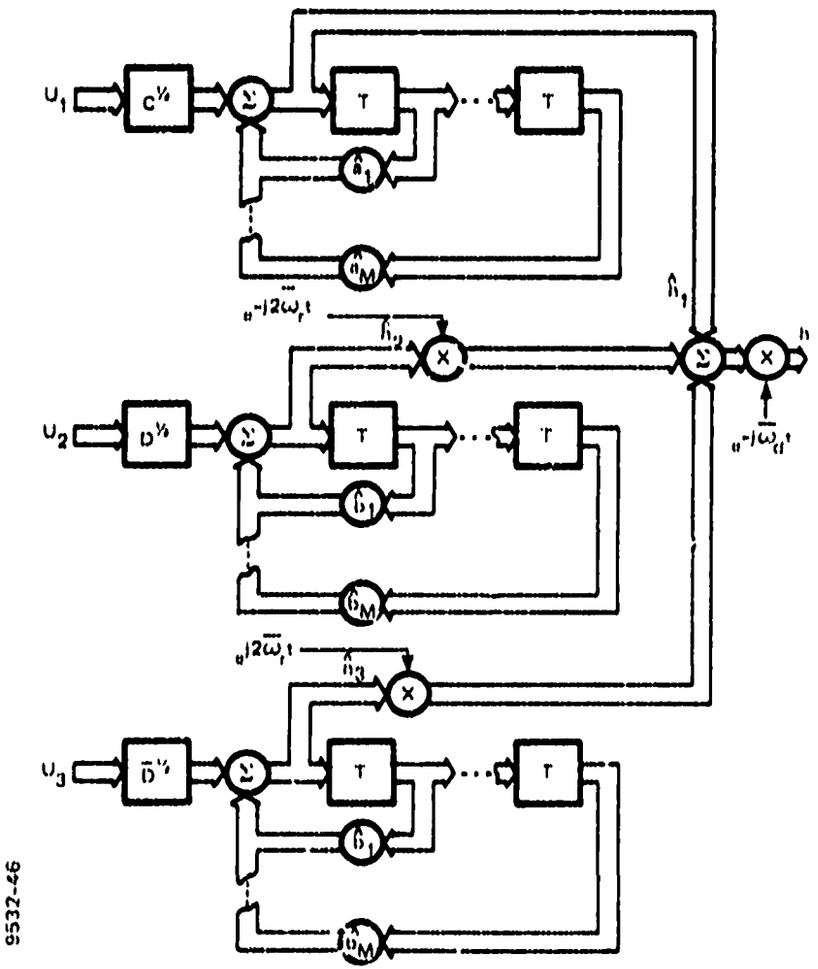

Figure 4-9. Matrix Autoregressive Modeling Stochastic Process, Special Case, Recursive Filter Representation

4.2.4 Covariance Matrix Validation

Correlation functions of the elements in the chaff scattering matrix are plotted in Figures 4-10 and 4-11. These functions were derived from the covariance matrix, which results from the scattering matrix. Figure 4-10 has plots of the theoretical correlation functions according to the results of Appendix A. Simulated correlation curves for a 7-point autoregressive fit of both amplitude and phase are found in Figure 4-11. As would be expected, the simulated curves differ slightly from the theoretical curves. However, the simulated curves would be expected to approach the theoretical curves if an infinite number of samples were used in the computation.

4.3 SIMULATION

4.3.1 Overview

The overall simulation is carried out in two major steps as indicated in Figure 4-12. The first step consists of simulating the target and chaff. Included in this function is the generation of sampled versions of scattering matrices for both target and chaff as would be sensed by the radar. The second major step is the simulation of the signal processing performed in the radar. This consists of computing the covariance matrices of the target and chaff from the sampled data and performing the optimization process to arrive at the weights (and waveform in the matrix weighting case) to be applied to the pulse train.

This simulation approach has the advantage that the target and chaff simulations need to be run only once for a given set of conditions. The results are stored on tape and can then be used as needed by the various processing routines.

4.3.2 Target

Simulation of the target consists of generating samples of the scattering matrix for a series of aspect angles representative of a target maneuver. Two basic modules are used in the simulation, each of which includes several subroutines. One is the geometry module; the other is the scattering matrix module. These modules and routines are shown in the target simulation block diagram of Figure 4-13.

Two loops are shown in the diagram, one is a loop on all of the scatterer's composing the target. The second loop controls the number of scattering matrix samples generated by the program.

The input to the program includes the range of aspect angles and angle increments to be used in computing the scattering matrix samples. The output consists of a vector sum of the individual scatterer scattering matrices. This sum includes both amplitude and phase from each of the scatterers for each of the elements in the scattering matrix. This is what produces the deep nulls in the rcs plots as a function of aspect angle.

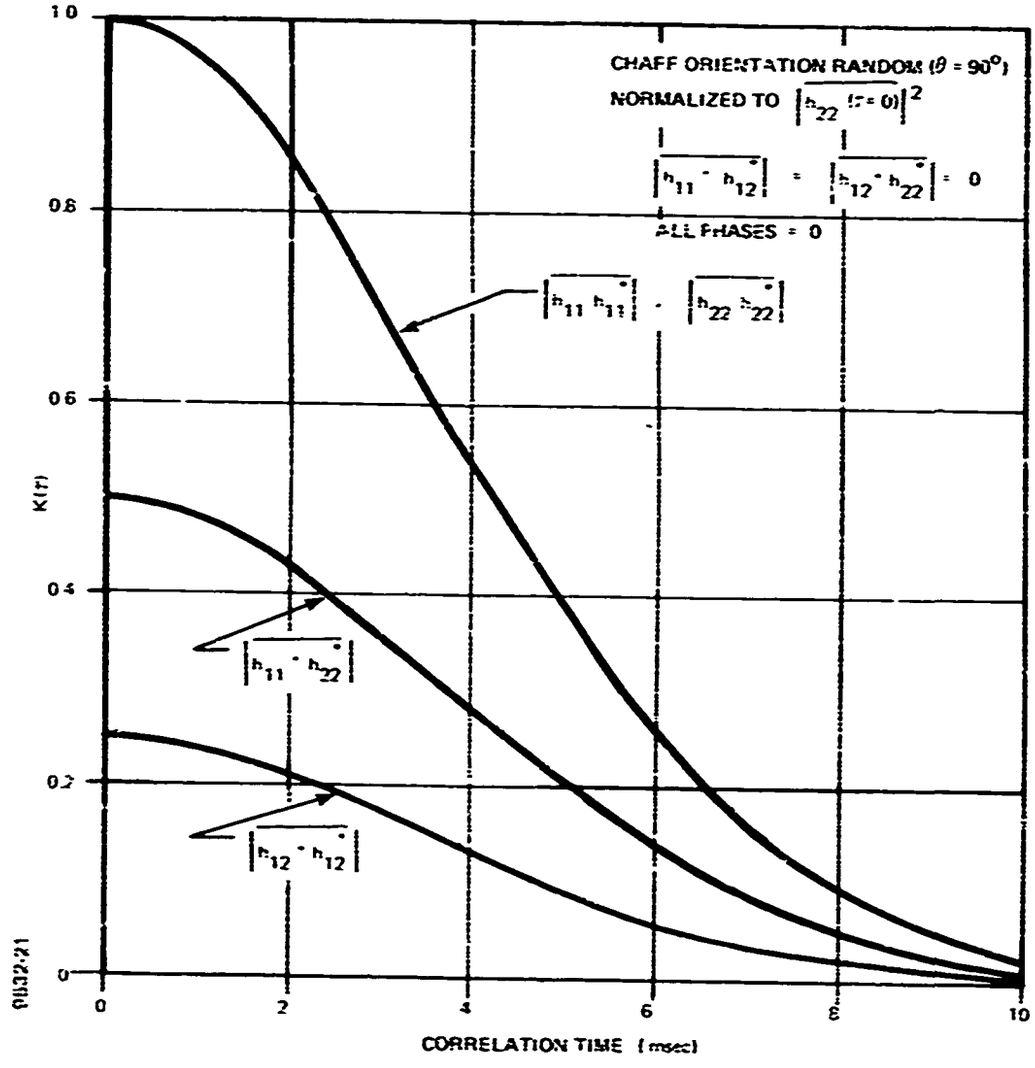

Figure 4-10. Theoretical Chaff Scattering Matrix Correlation Function

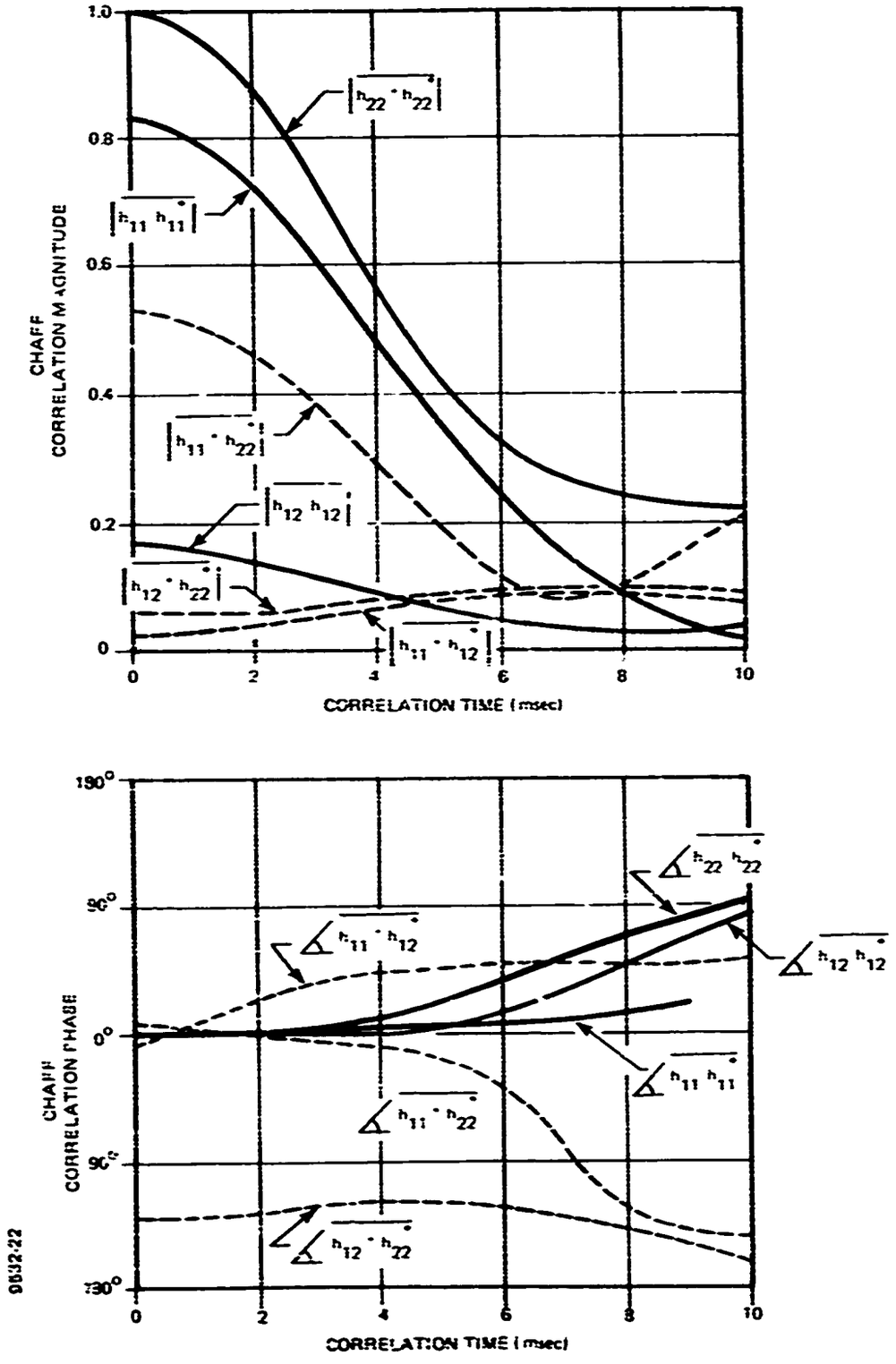

Figure 4-11. Simulated Chaff Model Autoregression Process

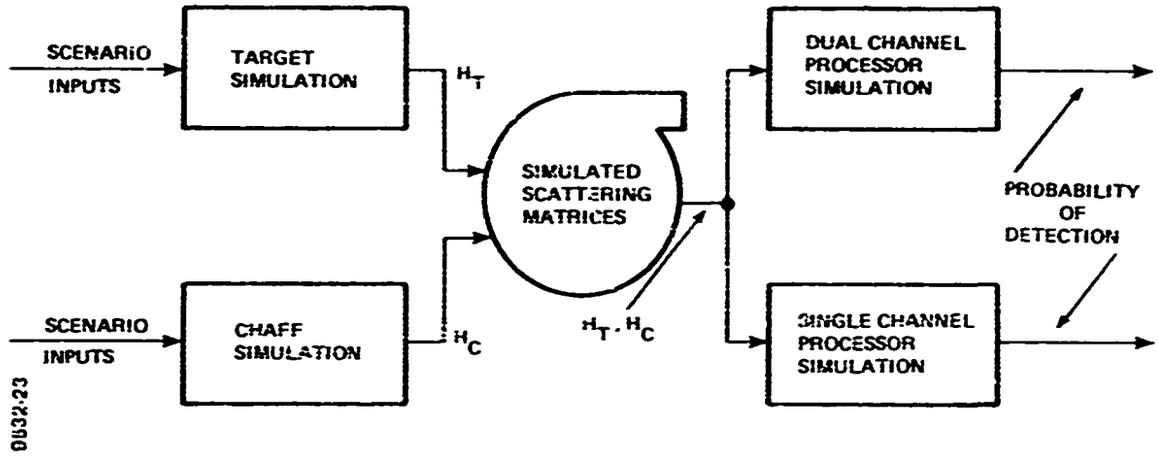

Figure 4-12. Overall Simulation Block Diagram

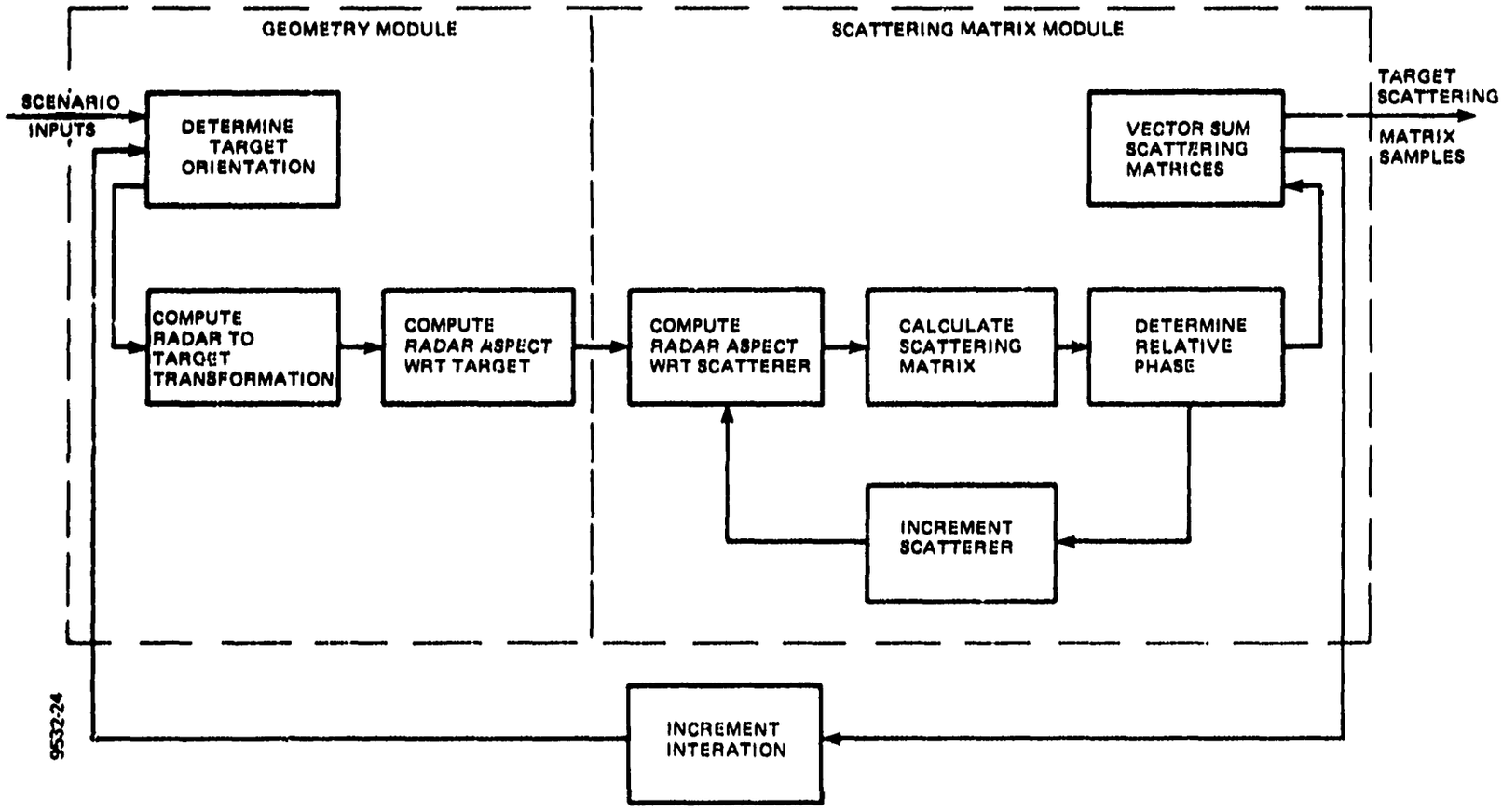

Figure 4-13. Target Simulation Block Diagram

4.3.3 Chaff

Chaff simulation consists of generating random samples of the scattering matrix from representative stochastic processes. A block diagram of the chaff simulation is shown in Figure 4-14. The program is divided into two basic areas. The first consists of a one-time computation of parameters and values needed for generation of the random samples. The second is the loop composed of the actual steps followed in the recursive generation of the stochastic process outputs.

Inputs to the program include parameters to the theoretical correlation model, angles describing the geometrical distribution of the dipoles, parameters affecting the power received by the radar, and the number (and size) of the time increments required. The outputs are samples of the elements in the scattering matrix as a function of the time increments.

4.3.4 Processing Algorithms

4.3.4.1 **Weighting Matrix** – A block diagram showing the main steps in the simulation of the weighting matrix followed by a maximum likelihood receiver is depicted in Figure 4-15. The inputs to this processor simulation are the target and chaff samples of the scattering matrices.

The first section of the program is devoted to computing the optimum transmit waveform and receive weighting/transform matrix. The weighting/transform matrix was computed according to the method discussed in Section 3. However, the transmit waveform is determined through a more direct approach. We assumed that an antenna in a practical system would be able to transmit polarization states defined by four bits of phase and four bits of amplitude information. This yields a total of 256 states, only 114 of which are nonredundant. Thus, the algorithm used in selecting the optimum waveform cycled through these 114 states for each pulse and chose the state which minimized the Frobenius norm as discussed in Section 3.

The second part of the program consists of a loop wherein the target and chaff samples are operated on by the optimum radar. This includes transmitting the optimum waveform, operating on the return with the weighting/transform matrix, and comparing the result with a threshold. The number of threshold crossings is then counted and used in determining the probability of detection.

4.3.4.2 **Weighting Vector** – A block diagram of the vector weighting method is shown in Figure 4-16. The simulation consists of two parts. The first includes a loop to iterate on the optimum weighting vector and then computes the signal-to-chaff ratio resulting from the application of this optimum vector. The second part computes the signal-to-chaff ratio for the simple matched filter case. Plots of the outputs provide comparison of the optimum vector approach to the conventional matched filter method.

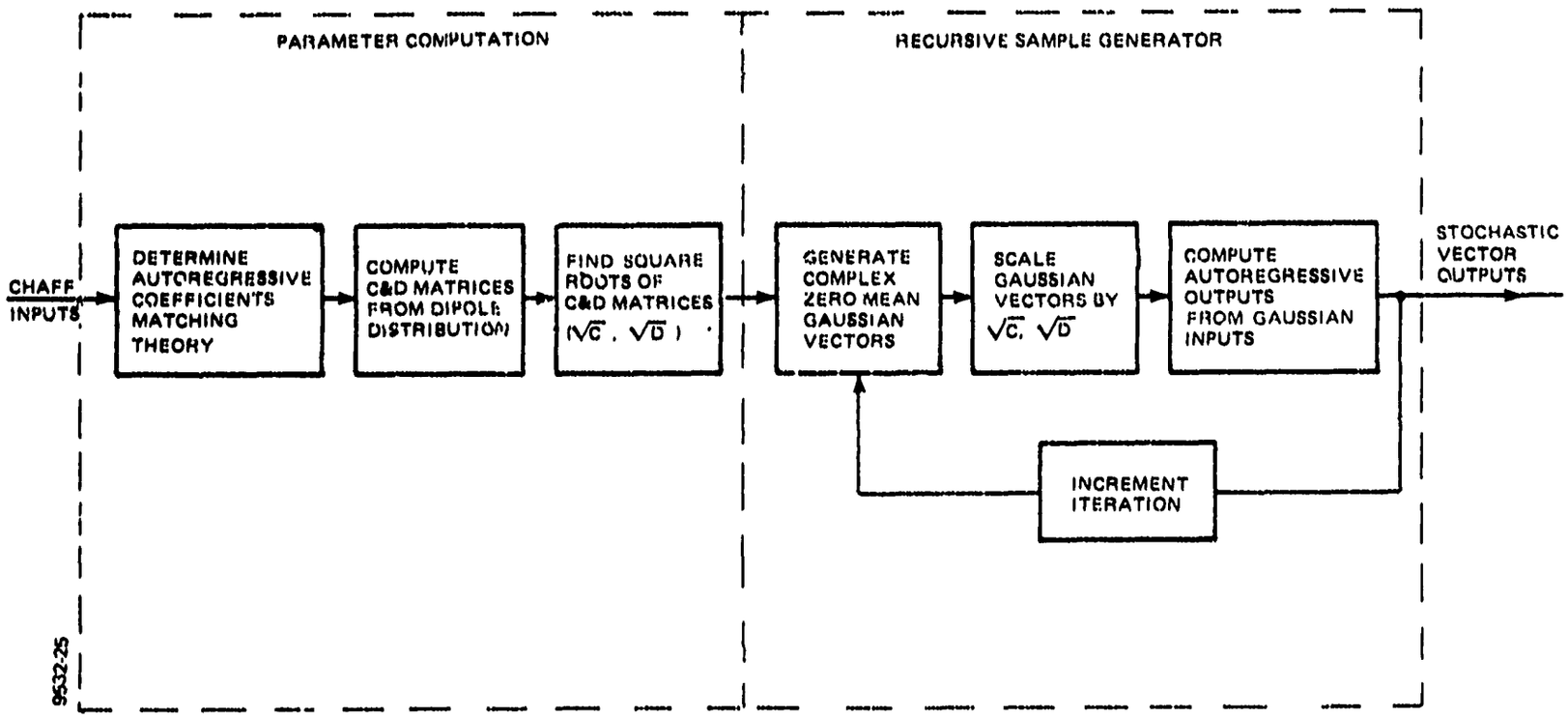

Figure 4-14. Chaff Simulation Block Diagram

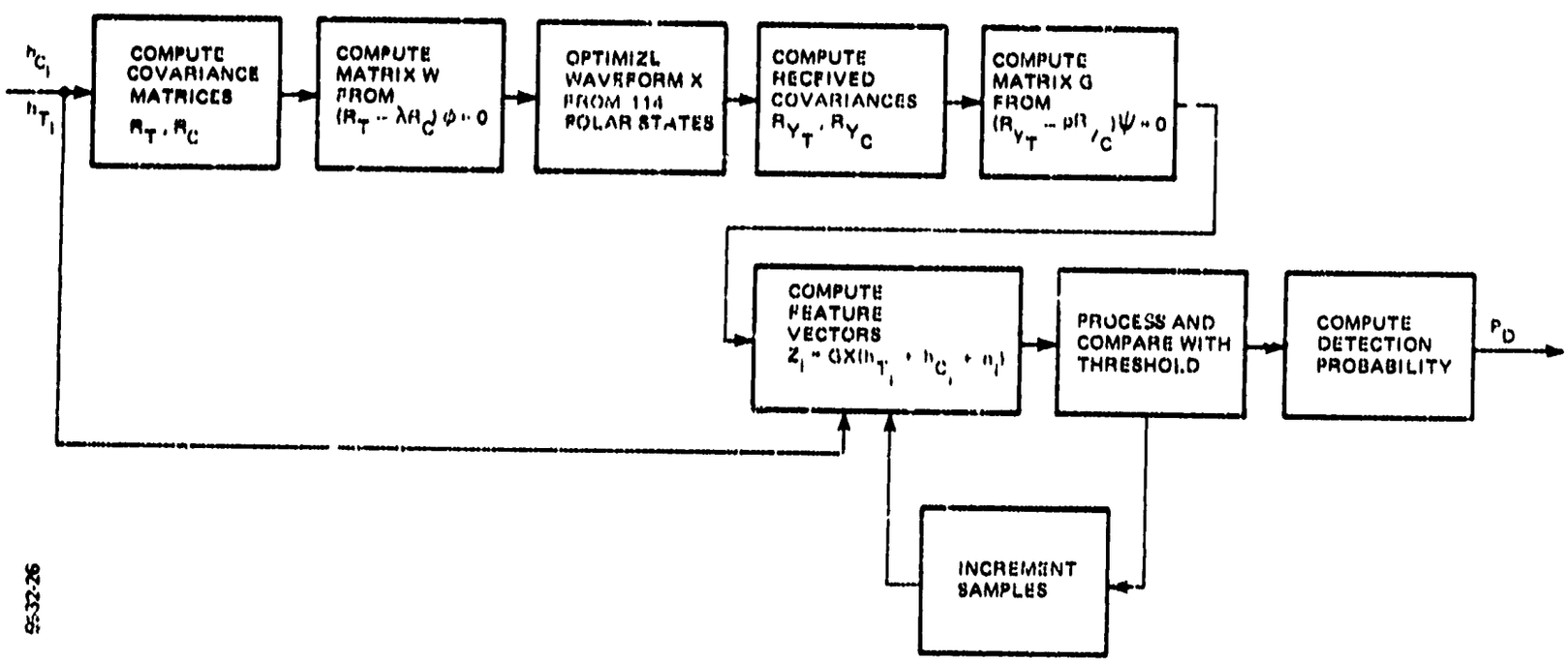

Figure 4-15. Block Diagram of Weighting Matrix Simulation

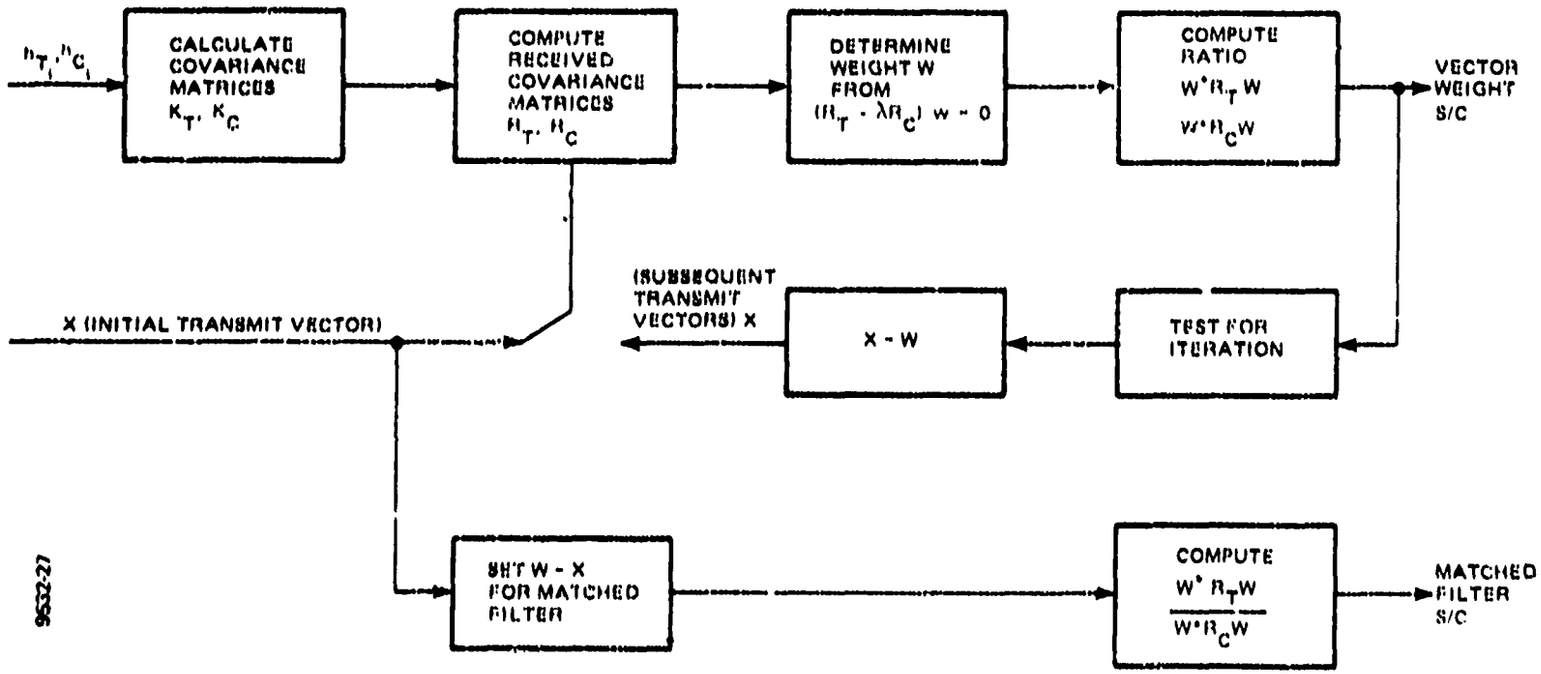

Figure 4-16. Block Diagram of Vector Weighting Simulation

4.3.4.3 Single Channel – A simple method was u ed in performing the simulation of the single channel system. The approach was to compute the target and chaff covariance matrices, introduce a waveform with equal pulses, account for matched filter weighting, and then to calculate the theoretical probability of detection based on the power computations for chaff plus noise vs target and chaff plus noise. A block diagram of the simulation flow is shown in Figure 4-17.

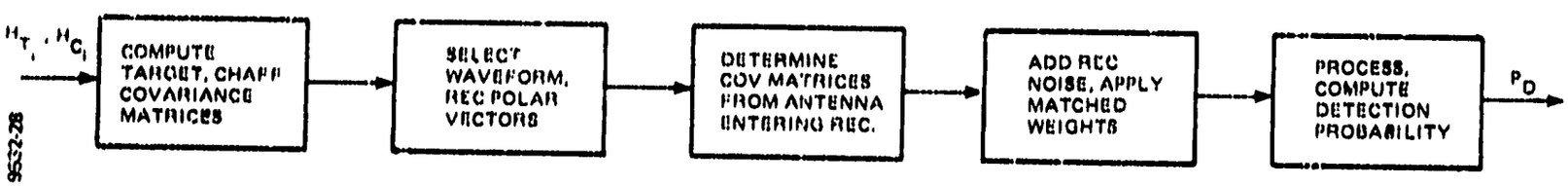

Figure 4.17. Block Diagram of Single Channel Simulation

Section 5

COMPUTER SIMULATION RESULTS

The purpose of the computer simulations was to evaluate the effectiveness of dual channel systems as compared to single channel systems. This was accomplished by exploiting the polarization properties of various target models relative to those of chaff, in terms of maximizing the receiver output signal-to-clutter ratio (s/c). The major figure-of-merit (FOM) considered was the probability of target detection for a given false alarm probability due to clutter plus receiver noise. Associated with each result is the other major study output which yields transmit waveform selection coupled with optimum receiver weighting.

The results reported include those of the matrix and vector approaches, as well as the Stokes formalism. The latter was noted as being obtained in a previous study [Rosien, 1979].

5.1 SIMULATION PARAMETERS

This section describes the various input/output parameters associated with obtaining results for the aforementioned three approaches, and discusses the types of conclusions one can draw from each.

5.1.1 Target and Chaff Models

The description of the generation and simulation of the target and chaff models, has been covered in Section 4. The scattering matrix correlation functions of the models utilized to obtain the reported upon dual and single channel results are compared for reference in Figure 5-1. The $|\overline{h_{\underline{\underline{2}}} h_{\underline{\underline{2}}}^*}|$ parameter is shown.

Three target models are noted: the standard Swerling I and two others designated as RT1 and RT3. The time base for the correlation functions is given in terms of an interpulse period ΔT, to conform with the use of transmit signals consisting of generalized pulse train formats. The SWI target model utilizes the same scattering matrix as the BQM-34A model, but has a constant correlation function (pulse-to-pulse correlation). The RT1 and RT3 target models are also those of the BQM-34A drone. This shorthand notation refers to interpulse sampling intervals of 1 msec and 3 msec respectively, where 3 msec represents a greater change in target aspect per ΔT. As a consequence, the RT1 model is more closely associated with the Swerling I, whereas RT3 would be more nearly like a Swerling II.

The chaff model closely matches the RT3 target in terms of its $h_{\underline{\underline{2}}}$ scattering matrix correlation function. It should be noted that the same chaff correlation property is used regardless of the value of the interpulse period. In this way one obtains a variation in the spectrum of the target relative to the chaff. For example, the RT3 target has essentially the same spectrum as does the chaff. By contrast, the chaff has a much broader spectrum than does the impulse associated with Swerling I. The RT1 target represents a choice between these two.

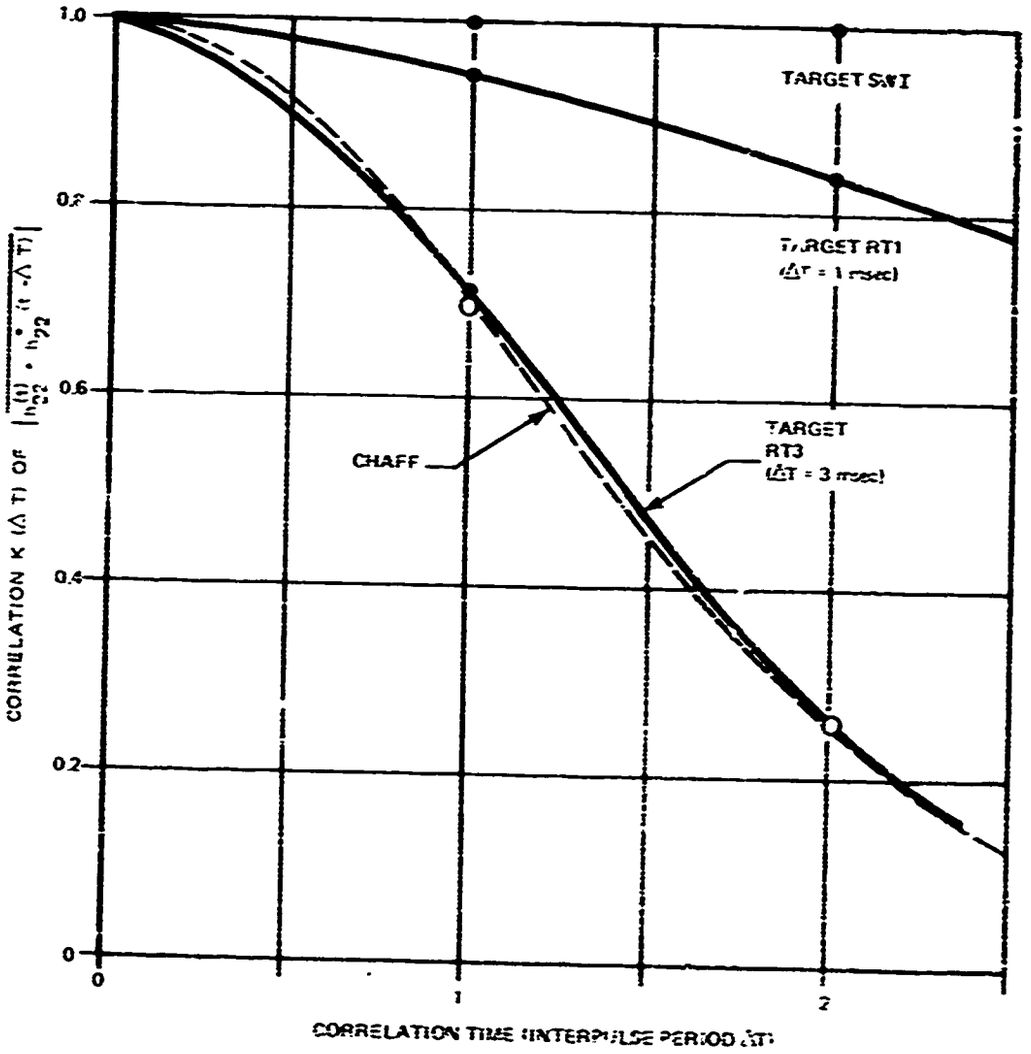

Figure 5-1. Target/Chaff Scattering Matrix Correlation Functions

5.1.2 Definition of s/c Ratio

Each of the approaches has a common reference for s/c ratio, a key parameter associated with probability of target detection. The ratio utilized is defined as the total available target power relative to the total available chaff power. The available power is given as:

$$P_a = |h_{11}|^2 + 2|h_{12}|^2 + |h_{22}|^2 \qquad (5\text{-}1)$$

where the H parameters are relative to either the target or chaff scattering properties.

Equation (5-1) represents all of the energy that can be scattered back from either target or chaff, when impinged upon by a dual channel transmit waveform. Receiver noise is taken into account by scaling P_a to a normalized noise vector. If, for example, the s/n ratio is designated as 20 dB, then P_a for the target would be 100 times greater than the input noise vector. Similarly, a s/n ratio of 17 dB results in a P_a for chaff which is 50 times the noise. This results in an available input s/c ratio of +3 dB, which is then the value plotted on the detection probability curves.

5.1.3 Qualitative Assessment

There are various differences noted in the computer simulations for the three approaches reported upon. The Stokes formalism compared dual and single channel results on the basis of single pulse probability of detection. As a consequence, the correlation properties of the target and chaff were not a factor, although the scattering matrices were key parameters in the optimization procedure. The Stokes output consisted of the optimum transmit and receiver antenna polarizations for maximizing the s/c ratio.

The vector method employed a transmit sequence of five pulses using the RTI target model. An iterative procedure was used to converge to the maximum s/c ratio. Comparisons were made for dual and single channel performance based upon relative s/c, but not to target detection. Other significant results consisted of the selected five-pulse transmit vector and associated dual channel receiver weighting function which maximized the s/c. As previously noted, these results depend upon the initial choice of the five-pulse waveform.

The matrix results were by far the most comprehensive, comparing performance for all three target models against both dual and single channel implementations. Results were derived for the probability of target detection figure-of-merit. Other outputs of interest were the optimum transmit vector selected from among a library of 114 waveforms utilizing a three-pulse sequence, and its associated 6 x 6 receiver weighting matrix.

Although the three approaches had differences associated with the choices of transmit vector pulse sequences, the results were consistent enough to be significant. All three exhibited the same basic result, in that the dual channel implementation does provide enhanced performance over conventional single channel configurations.

5.2 STOKES APPROACH RESULTS

The above was reported by Rosien, et al (1979). Figure 5-2 is excerpted from this report and is representative of the basic results obtained using the Stokes formalism.

The probability of target detection for single-pulse operation is shown for various s/c ratios (as defined previously). The false alarm probability was set to 10^{-6}, the chaff dipoles were uniformly distributed ±45 degrees from the horizontal, and the BQM-34A aspect angles are distributed as shown in the figure. Optimum dual channel performance is plotted relative to conventional single channel operation. Substantial improvement is noted when compared against single channel horizontal and circular polarized systems. Approximately 2 dB of improvement is seen versus the vertically polarized single channel system. The lesser improvement, in this case, is a result of the chaff model dipole distribution which favors the horizontal. The vertically polarized signal, therefore, results in substantially less chaff backscatter than does either the horizontally or circularly polarized waves. Since the target does not have a strong preferred polarization for its backscatter return, it becomes obvious that a vertically polarized system would be the choice for the single channel implementation, and a nearly vertically polarized system would also be implemented for dual channel operation.

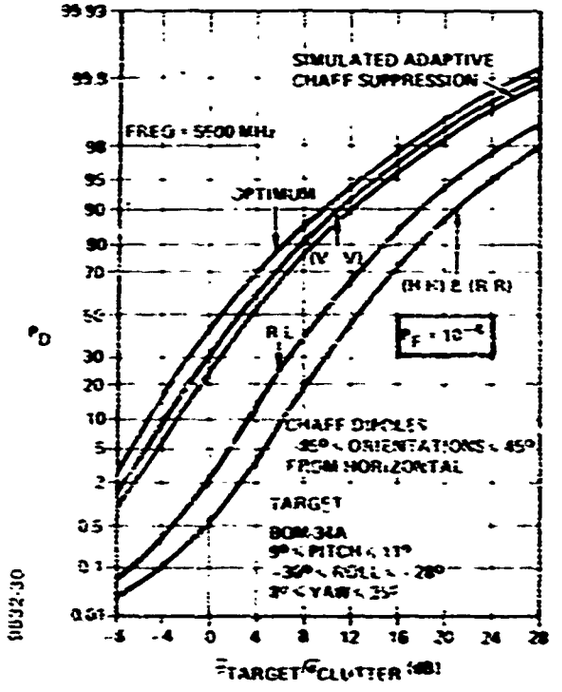

Figure 5-2. Single-Pulse Detection Probabilities for various (transmit-receive) polarizations

The major fact seen by these results, is that the Stokes method does yield better performance for dual channel operation, despite the obvious high level of performance exhibited by single channel vertical. It should also be noted that these results were for single pulse transmission, such that the spectral differences between the target and chaff could not be exploited in the signal processor.

5.3 VECTOR APPROACH RESULTS

The vector weighting results were based upon transmission of a five-pulse sequence. The figure-of-merit utilized was the relative improvement in s/c for various dual and single channel implementations, as a function of the chaff dipole distribution. No further effort was expended in this area, in view of the importance attached to the development of the more encompassing matrix approach.

Figure 5-3 depicts typical results for the RTI target in chaff. The s/c is shown relative to matched right circular single channel operation.* The dipole orientation angles refer to the distribution within the chaff cloud, where 90 degrees is for completely random

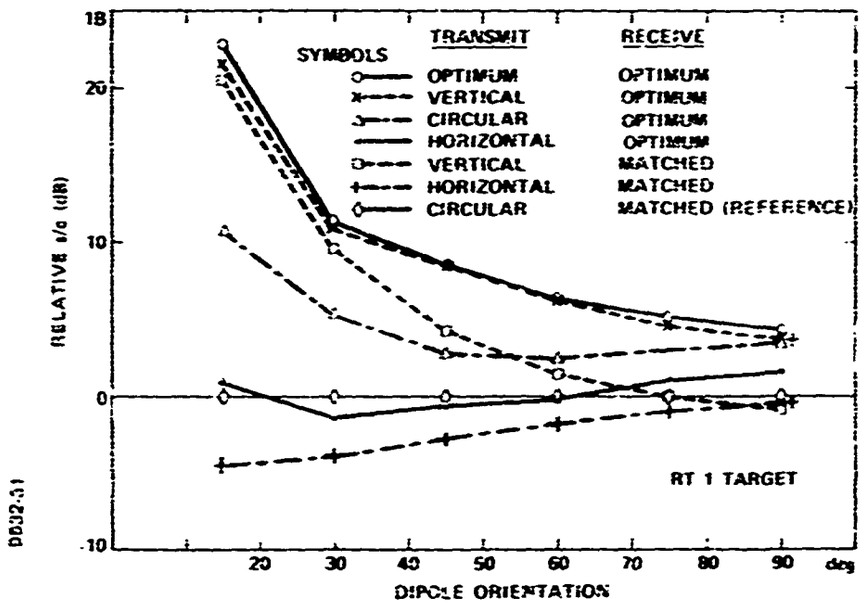

Figure 5-3. Signal-to-Clutter Improvement Ratio for Vector Weighting Method

* Matched filter is standard definition referred to maximizing received s/n ratio.

dipole distribution, and 15 degrees refers to nearly horizontal distribution. As noted in the figure, matched filter performance for single channel horizontal and circular polarizations is extremely poor. The matched vertical performance is good for dipole distributions which are nearly horizontal (less than 30 degrees). Beyond this, the matched vertical performance degrades rapidly, and, as would be expected, it converges to the circular and horizontal levels for the completely random chaff distribution at 90 degrees. This convergence at 90 degrees for matched filter operation was also evident in the Stokes results for single pulse transmission.

Figure 5-3 also indicates four variants of dual channel operation. The vertical transmit-optimum receive curve is for a dual channel receiver optimally weighted for transmission of a vertically polarized five pulse sequence. This in fact, is the result of the first iteration associated with the Rummler waveform convergence technique. Similar curves are shown for horizontal and circular polarized five pulse sequences. As expected from the predominantly horizontal chaff dipole distribution, the dual channel receiver weighted for vertical transmission provides the best overall performance. There is again convergence of results at 90 degrees.

The optimum curve is the result of utilizing the Rummler iterative technique, for which both the transmit vector and receiver weight are interchanged during each iteration. The iterative procedure was terminated when convergence in s/c ratio was achieved. Although the optimum curve is for full dual channel operation, it can be appreciated from prior results that the optimum performance is only slightly better than vertical transmit-optimum dual channel receive. This is a consequence of the optimum transmit waveform being nearly vertically polarized. A significant result of the iterative procedure was that the convergence in transmit waveform, was independent of the initial choice. The iterations were started with either vertical, circular, or horizontal five pulse sequences. In all cases, the optimum waveform converged to the identical nearly vertically polarized structure.

5.4 MATRIX APPROACH RESULTS

Computer runs were made for probability of target detection P_D as a function of the previously defined s/c ratio, at a false alarm probability of 10^{-4}. Performance levels for the three target model set of Figure 5-1 were computed for chaff dipole distributions corresponding to 15, 45, and 90 degrees. Comparisons were made between dual channel operation and matched filter single channel operation. The optimum transmit vector was chosen from a set of 114 three-pulse sequences. The associated dual channel receiver weight corresponds to a maximum likelihood detector, which is a function of the probability distributions related to the target, chaff, and receiver noise.

5.4.1 Dual Channel Results

Figure 5-4 is a comparison of dual channel performance between the three target set of RT1, RT3, and Swerling I. The limited range of s/c shown, was chosen to encompass the P_D region of interest for the more random dipole distributions; namely a P_D in the order of 0.5 for θ = 45°and 90°. At dipole distributions near the horizontal (θ = 15°), performance

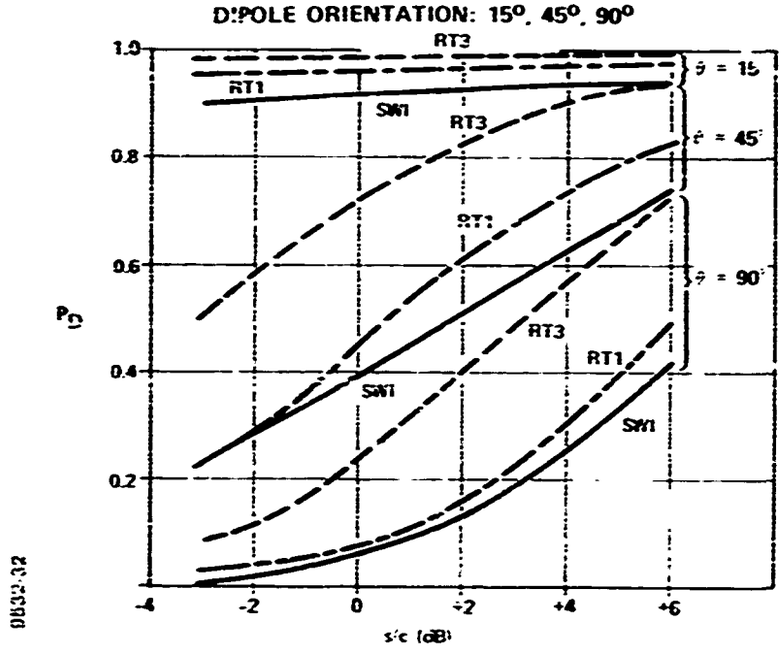

Figure 5-4. Comparison of Dual Channel Performance for RT3, RT1, SWI Targets

at these s/c ratios is very good for all three target representations. This would be expected at this dipole distribution, since operation with essentially vertically polarized transmit pulses yields minimal chaff backscatter (note similar good results at $\theta = 15°$ for vector and Stokes approaches to using vertical transmission).

As the dipole distribution becomes more random, performance degrades for these s/c ratios as noted in the figure. Performance for all target models at a P_D of 0.5, for example, is about 5–6 dB worse at $\theta = 90°$ than it is for $\theta = 45°$. The difference in detection performance at a P_D of 0.5 between $\theta = 15°$ and $\theta = 45°$ is not shown in Figure 5-4. The basic trend of the curves indicates a significantly greater difference than the 6 dB noted in the prior case. A rough estimate would place this differential in the order of 10–12 dB. It becomes rather obvious from these and prior results, that the structure of the chaff model emphasizing horizontal dipole orientation, strongly influences the ultimate choice of more nearly vertical transmit polarization vectors; and ultimately leads to poorer performance as the distribution becomes more random.

Regardless of the chaff distribution, however, target detection is best for the RT3 model, followed by RT1 and SW1, respectively. This trend would be expected, in general, in terms of target detection between SW1 and SWII models, noting that the RT3 model tends toward the uncorrelated pulse-to-pulse SWII. For a P_D of 0.5 and a P_{FA} of 10^{-4}, the SWII requires 1 dB less signal return than the SW1 in the case of a three-pulse sequence operating only against receiver noise. As noted in Figure 5-4, the RT3 target requires 5 dB less signal return than the SW1 when operating in the dual channel chaff plus noise environment at $\theta = 45°$. This added enhancement for the RT3 target can also be anticipated when utilizing the polarization discriminant. An analogy can be made if one examines the decorrelation of echoes from a complex target utilizing a polarization agile waveform as having effects similar to frequency agility [Nathanson, 1969] This decorrelation is desirable in a clutter and/or noise-only environment. Averaging of independent target samples will then essentially reduce the probability of a null in the target cross section at the aspect of interest. While this averaging process does not reduce the total clutter power, its variance will, however, be reduced. Since detectability is proportional to the ratio of target power to the variance of the total clutter plus noise power, target detection will be improved. This decorrelation of the target echo suggests a movement of the target model towards the more desirable SWII configuration.

Although complete target decorrelation is not anticipated for the three-pulse sequence utilized, it is noted that the RT3 target will have more degrees of freedom than the SW1 in terms of optimally combining the target echo returns relative to the chaff. It should be noted that the SW1 target will also become partially decorrelated, but not to the extent of either RT1 or RT3. This then results in the enhancement of RT3 relative to both RT1 and SW1, when the dual channel polarization returns are optimally combined.

5.4.2 Matrix Dual vs Single Channel Results

A comparison of the matrix dual channel implementation relative to conventional single channel matched filter systems is shown for the three target models in Figures 5-5 through 5-13 for chaff dipole distributions of 15, 45, and 90 degrees.

Figures 5-5, 5-6, and 5-7 show performance comparisons for the SW1, RT1 and RT3 targets respectively for $\theta = 15°$. The horizontal and right circular polarized systems perform very poorly in the matched single channel configurations, because of the horizontal distribution of the chaff dipoles. The matched vertical system performs very well over the range of s/c, as would be expected. In each case however, the dual channel implementation provides even better performance.

Figures 5-8, 5-9, and 5-10 show similar performance comparisons for $\theta = 45°$. Single channel horizontal and right circular systems still perform poorly, since the dipole distribution remains biased toward the horizontal plane. All three dual channel systems out perform the single channel vertical systems. At a P_D of 0.5, for example, SW1 operation is 2 dB better, RT1 is 4 dB better, while the RT3 target exhibits 9 dB better performance in the dual channel mode.

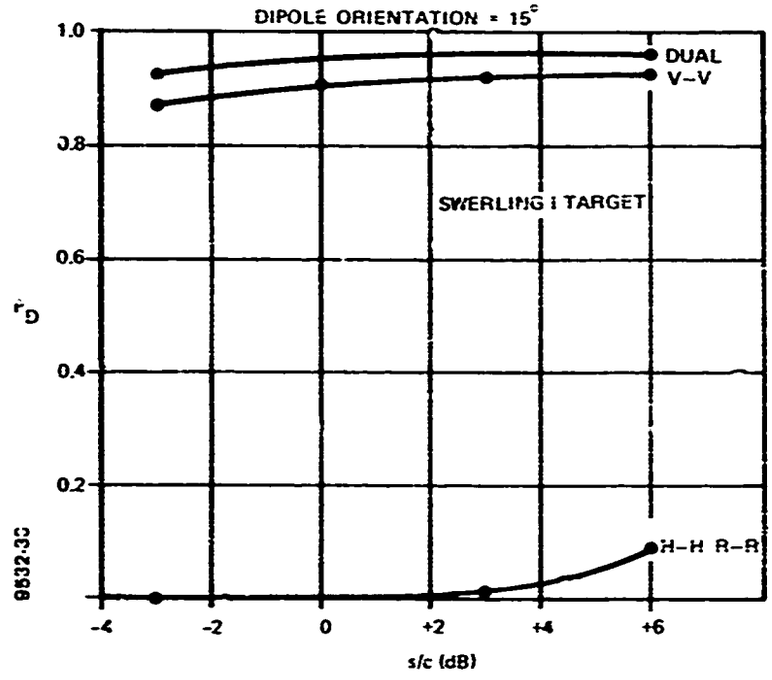

Figure 5-5. Dual vs Single Channel

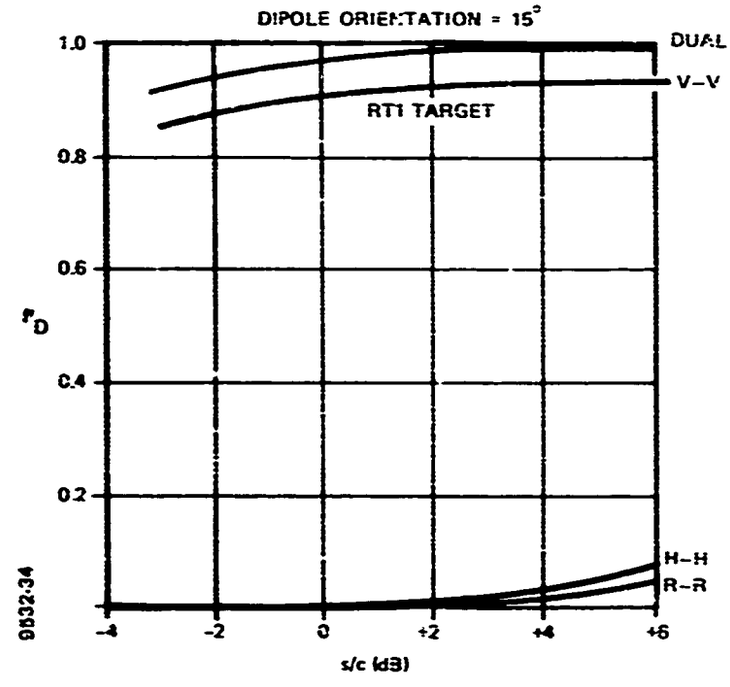

Figure 5-6. Dual vs Single Channel

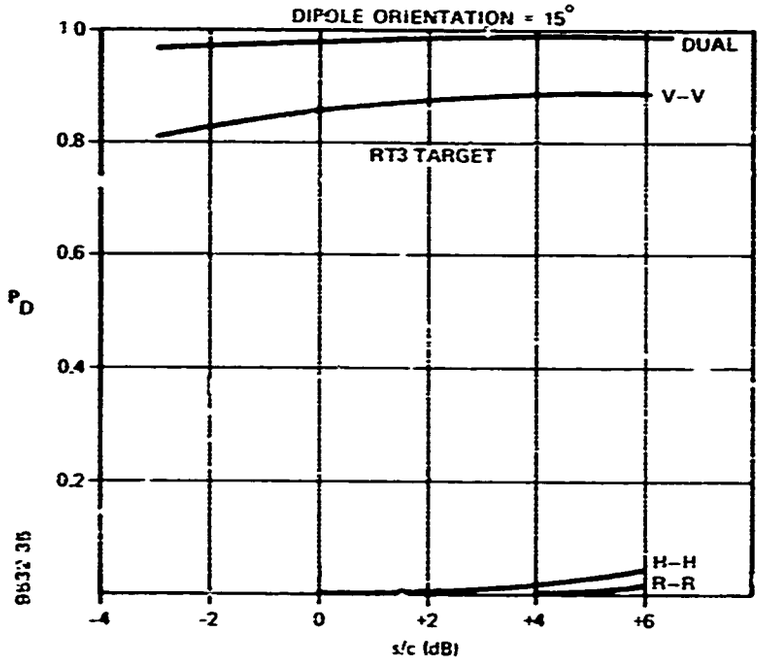

Figure 5-7. Dual vs Single Channel

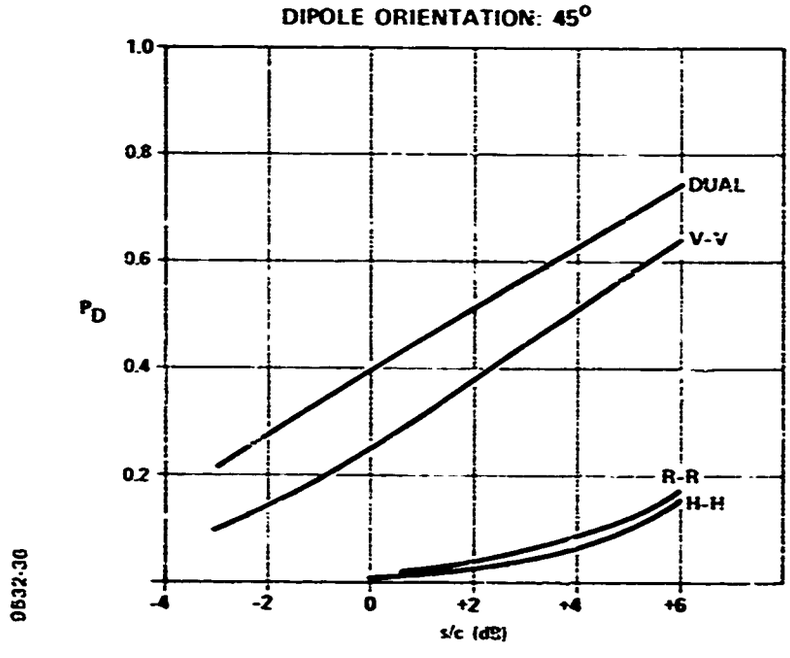

Figure 5-8. Dual vs Single Channel Swerling I Target

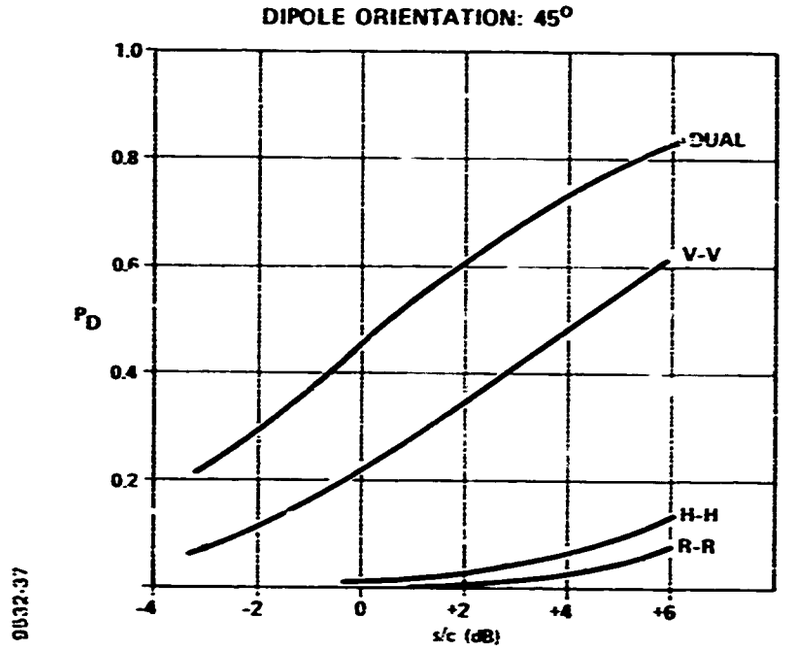

Figure 5-9. Dual vs Single Channel RT1 Target

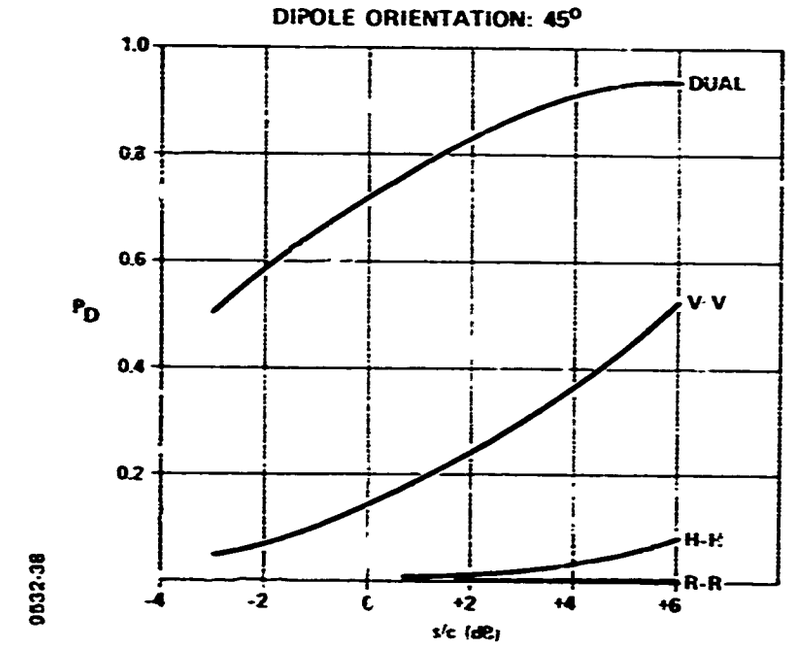

Figure 5-10. Dual vs Single Channel RT3 Target

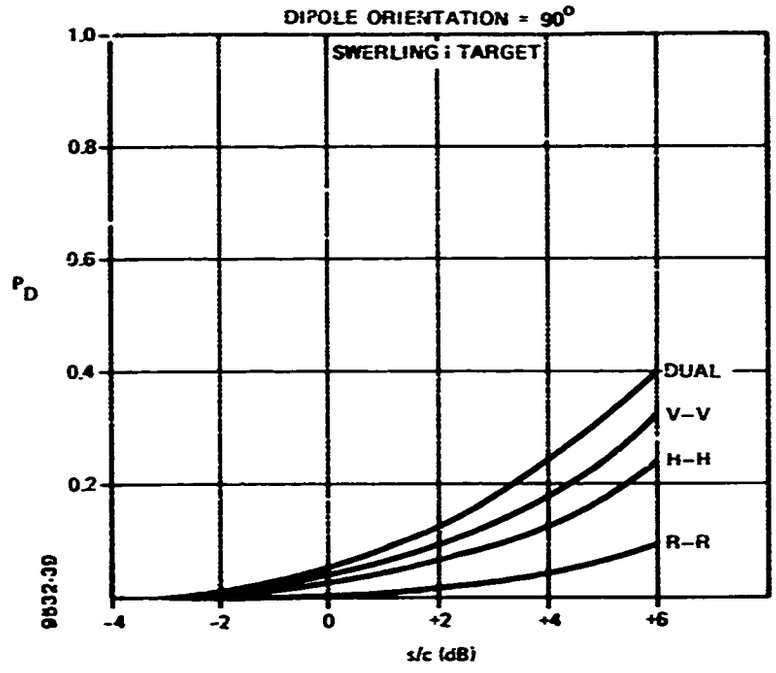

Figure 5-11. Dual vs Single Channel

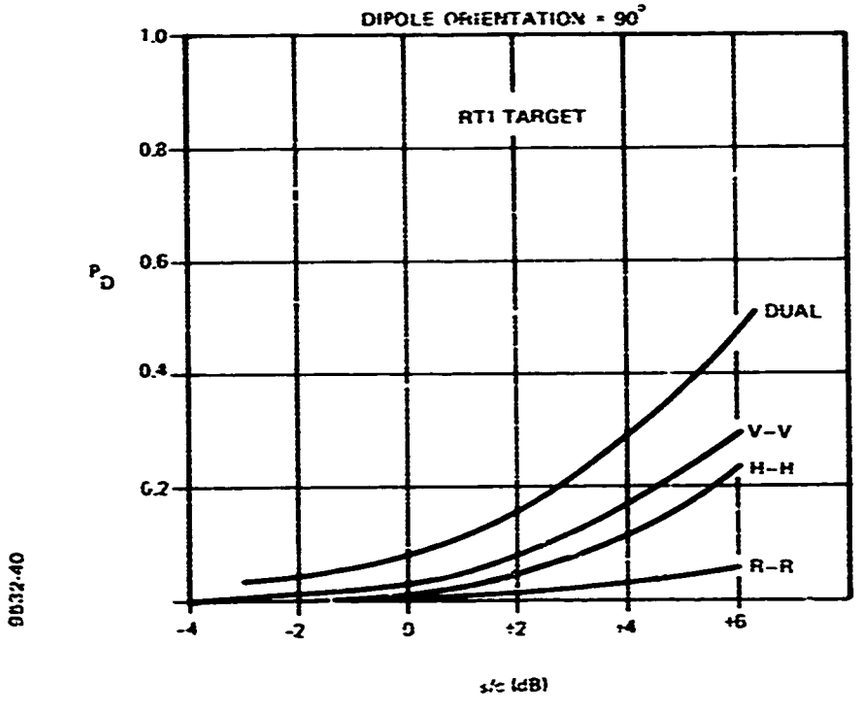

Figure 5-12. Dual vs Single Channel

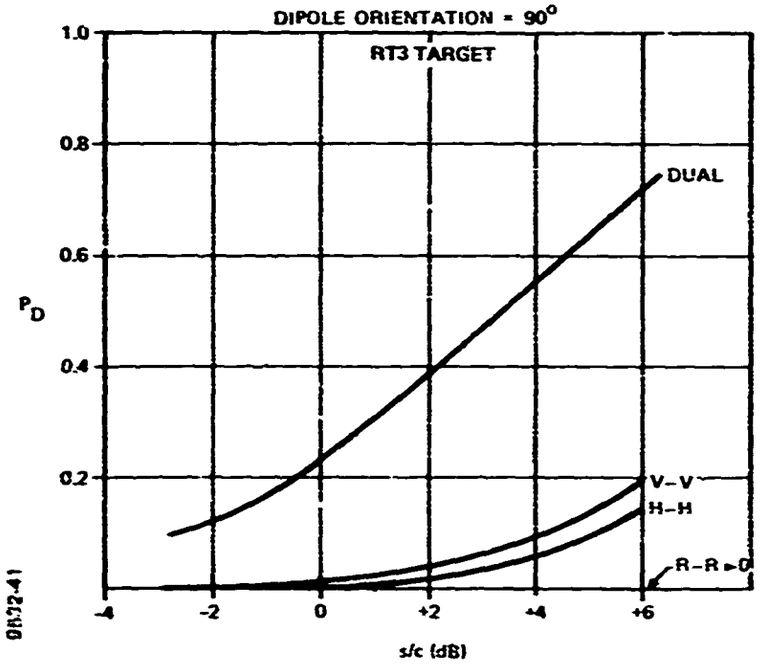

Figure 5-13. Dual vs Single Channel

Figures 5-11, 5-12, and 5-13 show similar results for $\theta = 90°$. With the dipoles now randomly distributed, the single channel matched horizontal and vertical systems tend toward the same performance levels. Here again, the dual channel performance remains superior although the dB differential relative to single channel vertical is less than for $\theta = 45°$. This is to be expected in view of the more random dipole distribution, which mitigates against the exploitation of the more deterministic chaff polarization at $\theta = 15°$ and $45°$.

In all cases of dipole distribution, it is noted that more effective dual channel to conventional single channel performance is possible for the RT3 target relative to either the RT1 or SW1 models. This again illustrates the advantages of a target model which is not as highly correlated on a pulse-to-pulse basis, particularly when exploiting the dual polarization scattering property.

5.4.3 Transmit Waveform Selection

The transmit waveform dual channel vector is selected by a minimization procedure relative to the Frobenius norm (see Section 3.1.2). The matrix method computation relied

upon a library of prestored polarization states and selected a 3-pulse sequence which most closely matched the norm. The library of available transmitter polarization states is illustrated in Figure 5-14.

This polar representation maps circular polarization at the origin, linear polarization along the circumference of a circle with radius = 1, and elliptical polarizations within a circle with radius < 1. The representation is such that the direction of a major axis of the ellipse for each polarization state is along the radius vector which goes through the point representing the state on the plot. Similarly, the direction of linear polarizations are along the radius vector. Furthermore, elliptical polarizations, whose sense of rotation is right handed, are mapped on the right-half plane of the polar plot, and left-handed polarizations are mapped on the left-half plane of the plot. The ellipticity is given by 1-r, where r is the radius of the circle. In this way, all of the information relating to the polarization state becomes readily available. The symbols (A) in Figure 5-14 indicate the library of prestored polarization states available for selection.

Two typical waveform choices are shown in Figure 5-14 for the SWI and RT3 targets, at a dipole distribution corresponding to $\theta = 45°$. The RT3 sequence consists of three pulses all linearly polarized, and lying from 11 to 22 degrees from the vertical. The first pulse is at 22 degrees, and the next two pulses are at 11 degrees (note small double circle in figure). The SWI set consists of a first pulse linearly polarized at 22 degrees from the vertical, a second pulse with a left-handed ellipticity of 0.56 and the major axis aligned 21 degrees from the vertical, and a linearly polarized third pulse 11 degrees from the vertical. As expected, the preferred dual channel polarizations do lie more nearly vertical. The SWI transmit vector has more ellipticity which denotes a trend towards more decorrelation of the SWI model through the polarization discriminist.

5.4.4 Receiver Matrix

The receiver weighting matrix is computed from knowledge of the transmit waveform and the likelihood function related to the target, clutter, and noise probability distributions. For the 3-pulse sequence, the optimum receiver matrix G_{opt} would be a 6 x 6. The SWI target is a special case because of the invariance of its pulse-to-pulse scattering matrix correlation function, which yields only three eigenvalues in the maximization procedure. Consequently, G_{opt} for SWI is a 3 x 6 matrix. A typical example of G_{opt} for SWI is shown below for a s/c ratio of +3 dB, and a dipole θ of 45°

Note the elements of G are written in polar form

$$G_{opt} = \begin{bmatrix} (0.32, -7°) & (0.17, -32°) & (0.1, -33°) & (0.14, -60°) & (0.24, -5°) & (0.1, -45°) \\ (0.07, 67°) & (0.11, -76°) & (0.05, 51°) & (0.21, -69°) & (0.03, -36°) & (0.04, 33°) \\ (0.003, -72°) & (0.12, -11°) & (0.05, -40°) & (0.03, -88°) & (0.02, -31°) & (-14, -5°) \end{bmatrix}$$

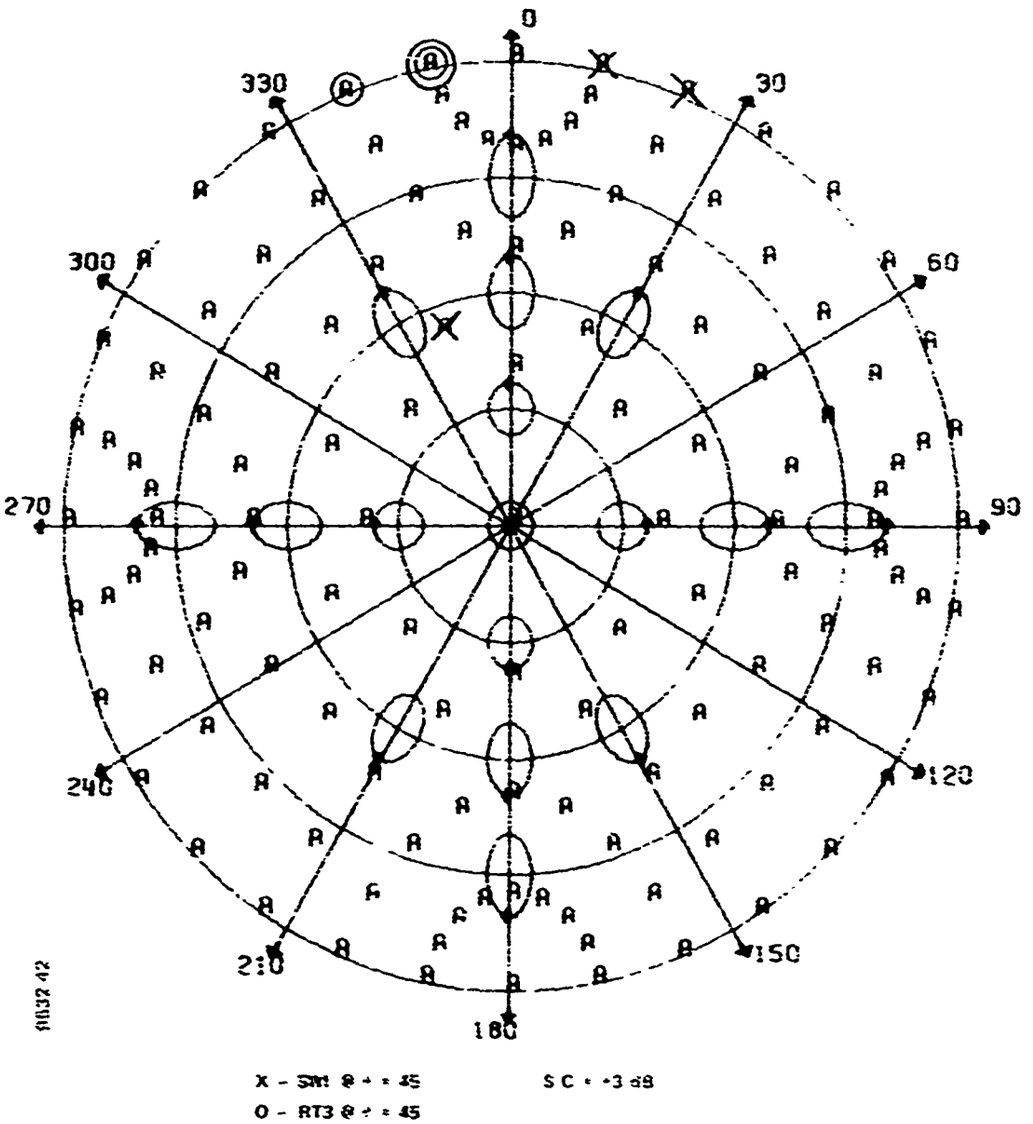

Figure 5-14. Transmitter Antenna Polarization States

Section 6

CONCLUSIONS AND RECOMMENDATIONS

The primary objectives of the study were met in the following specific areas:

a) An analytical and systematic approach was developed for dual channel optimum processing applicable to the radar scattering matrix of targets and clutter.

b) The matrix approach was utilized to develop an optimal transmit waveform and optimum receiver which maximizes the signal-to-clutter ratio for enhancement of target detection at a given probability of false alarm.

c) A statistical model was generated for the polarization scattering matrix of the BQM-34A target drone, and for a dipole chaff cloud. The properties incorporated in both models focused upon the temporal/range behavior of their scattering matrix elements. Two forms of the chaff model were developed; a theoretical representation composed of general mathematical expressions, and a stochastic model derived from an autoregressive process fit to the theoretical model.

d) The above models were utilized in computer simulations to compare target detection performance in chaff for dual channel system configurations against conventional single channel systems.

Five analytical approaches were considered for polarization processing implementation:

1) Matrix,
2) Vector,
3) State-space,
4) Fredholm,
5) Stokes.

Of the above, the matrix and vector approaches fall under the heading of finite dimensional space techniques. The matrix method was the most fully developed and as such yielded the most promise in terms of meeting the study objectives for dual channel waveform and receiver design. It utilizes all of the information available in the target/clutter measurement space, and results in a method of waveform selection based upon the scattering matrices of the target and clutter. Once the waveform has been chosen, a maximum likelihood criterion is utilized for target detection at a desired false alarm rate.

The vector method can be considered a special case of the matrix approach, in that only a part of the available information is processed from the measurement space. Although this yields better results than conventional single channel systems and is simpler to implement than a matrix receiver, its performance relative to the matrix receiver is obviously not as good.

Considerable effort was devoted to the development of a Kalman filter realization of a state-space model utilizing the target and clutter scattering properties. This approach was

carried to the point of an optimum receiver design, given the transmit waveform and the relevant scattering matrices. This effort exemplified the most consistently unified approach towards utilizing both the temporal and range behavior of the scattering matrix elements. Further work is required, however, in developing this approach for waveform design.

An approach using Fredholm integral equations was formulated to the extent of enumerating the system of equations involved with the target/clutter scattering elements. A generalized method of solution was presented. No further effort was expanded beyond this point, although a preliminary conclusion would indicate that the complexity involved, relative to the other techniques, might not warrant additional work.

The Stokes approach was formulated and investigated in a prior study. These results were reported upon for completeness and indicated the capability to design an optimum transmit-receive antenna polarization pair for maximizing the signal-to-clutter ratio for use with noncoherent processing.

Computer derived results were presented for the matrix, vector, and Stokes approaches. It was shown that for either single pulse or coherent pulse train processing, exploitation of the polarization discriminant in a dual channel configuration was clearly superior to conventional single channel matched filter performance. The matrix results also considered the differences in dual channel performance for three variants of the BQM-34A drone point target model in chaff. These included a pulse-to-pulse correlated Swerling I model and two less correlated versions tending toward Swerling II. Correlation of the chaff scattering matrix was set identical to the least correlated target model, RT3.

Probability of target detection was used as a figure-of-merit for a false alarm probability of 10^{-4}. Best performance was obtained for the least correlated target model, with worst performance for the Swerling I (a typical 6 dB differential for a P_D of 0.5). This is consistent with standard results for Swerling II relative to Swerling I targets. The pulse-to-pulse decorrelation, inherent in the RT3 target scattering property, provides for more degrees of freedom in terms of optimizing the receiver matrix combination associated with the individual pulse returns. This results in the noted better performance relative to SWI. It should be noted however, that performance of the Swerling I target was also enhanced by dual channel polarization processing relative to single channel matched filter detection.

The major conclusions reached from the foregoing results can be restated as follows:

a) Exploitation of polarization scattering properties will enhance the detection of targets in chaff relative to conventional single channel systems.

b) Analytical and systematic approaches have been presented to develop optimal transmit waveforms and associated receiver designs for maximizing the probability of target detection for a given false alarm rate.

c) The availability of previously developed polarization sensitive models of targets and chaff, provides a powerful tool in the systematic evaluation of the above techniques.

The following study tasks are recommended to further evaluate the practicality of multichannel polarization processing:

a) Expansion of the state-space approach to include waveform design as a possible adjunct to or replacement and generalization of the matrix method.

b) Reconfigure the target and chaff models to include realistic target trajectories and chaff mean velocities, to combine 'MTI processing' in conjunction with the polarization discriminant for dual channel waveform and receiver design evaluation. Use of longer pulse trains would be investigated for this implementation

c) Develop and/or utilize other clutter models to evaluate performance in different interfering environments. Ellipticity associated with rain drops, for example, would be a reasonable contrast to the dipole structure of the chaff model.

d) Develop a strategy for detection of targets in clutter, without prior knowledge of target scattering matrix. Use typical surveillance radar requirements. Evaluate performance of various approaches; for example, use waveform to minimize clutter backscatter or maximize s/c ratio for 'average' target.

e) Preliminary design of dual channel system utilizing methods developed during study. Provide qualitative cost assessment against single channel system.

f) Develop an approach using the range spread properties of the scattering matrix in conjunction with its polarization and temporal behavior, to design the waveform and receiver for optimizing target detection in clutter.

REFERENCES

Beguin, D.E., Bosc, H.J., and Colin, J.M., "Rain Echo Elimination," Laboratorie Central de Telecommunication, U.S. Patent Number pending.

Borison, S.L., "Bistatic Cross Section of a Randomly Oriented Dipole," IEEE Trans on Antennas, Vol AP-15, pp 320-321, 1967.

Daley, J.C., et al, "NRL Terrain Clutter Study Phase II," NRL Report 67-49, October 21, 1968.

DeLong, D.F. Jr., and Hofstetter, E.M. (1967), "On the Design of Optimum Radar Waveforms for Clutter Rejection," IEEE Trans on Information Theory, Vol IT-13, pp 454-463.

Durbin, J., "The Fitting of Time-Series Models," Rev. Inst. Statist., Vol 28, pp 233-243, 1960.

Ewell, G.W., Alexander, N.T. and Tomberlin, E.L., "Investigation of the Effects of Polarization Agility on Monopulse Radar Angle Tracking," Project A-1225, Engineering Experiment Station, Georgia Institute of Technology, 1971.

Friedman, B., "Principles and Techniques of Applied Mathematics," John Wiley & Sons, Inc., 1957.

Helstrom, C.W., "Statistical Theory of Signal Detection," 2nd Ed., 1968, Pergamon Press, N.Y.

Kennaugh, E.M., "Effects on the Type of Polarization on Echo Characteristics," Final Engineering Report, Antenna Lab, Ohio State University, Vol I, AF Contract 28 (099)-90, June 1951, AMC 3.51, Griffiss AFB, N.Y.

Nathanson, F.E., "Adaptive Circular Polarization," IEEE International Radar Conference, Washington, D.C., 1975.

Nathanson, F.E., "Radar Design Principles," McGraw-Hill, Inc., 1969

Poelman, A.J., "Reconsideration of the Target Detection Criterion Based on Adaptive Polarizations," 1976 AGARD Symposium.

"Radar Signature Measurements of the BQM-34A and BQM-34F Target Drones," RATSCAT 6585th Test Group, AFSWC-TR-74-01, January 1974.

Rao, C.R., "Linear Statistical Inference and its Application," J. Wiley, N.Y.

Rosien, R. et al, "Implementation Techniques for Polarization Control for ECCM," RADC-TR-79-4, February 1979, B035618L.

Rummler, W.D. (1966), "Clutter Suppression by Complex Weighting of Coherent Pulse Trains," IEEE Trans. on AES, Vol 2, pp 689-699.

Rummler, W.D. (1967), "A Technique for Improving the Clutter Performance of Coherent Pulse Train Signals," IEEE Trans. on AES, Vol 3, pp 898-906.

Van Trees, H.L., "Detection, Estimation, and Modulation Theory, Part I," John Wiley & Sons, Inc., 1968.

Van Trees, H.L., "Detection, Estimation, and Modulation Theory, Part III," John Wiley & Sons, Inc., 1971.

Wong, J.L., Reed, I.S. and Kaprielian, Z A., "A Model for the Radar Echo from a Random Collection of Rotating Dipole Scatterers," IEEE Trans on AES, Vol 3, pp 171-178, 1967.

Appendix A

A MODEL FOR THE SIMULATION OF THE SPECTRAL AND POLARIZATION CHARACTERISTICS OF CHAFF

by

GEORGE A. IOANNIDIS

ITT Gilfillan
Van Nuys, California 91409

Abstract

A vector autoregressive process is used to obtain a Stochastic model for the simulation of both the spectral and polarization characteristics of a chaff cloud consisting of a collection of rotating dipoles, which may have either completely random or preferred orientations.

INTRODUCTION

Recently there has been considerable interest in the use of polarization diversity to improve signal detection in the presence of background clutter.[1,2,3] In the design of such polarization agile radar systems, one must consider both the autocorrelation and cross correlation functions of the backscattered signals for two orthogonal polarizations.[3]

What follows is a model for a random collection of rotating dipole scatterers. This model is a generalization of a model by Wong et al,[4] and allows the simulation of both the polarization and temporal characteristics of radar signals backscattered from a collection of rotating dipoles, which have either completely random or preferred orientations. This model makes use of a vector auto-regressive process for the simulation of the scattering matrix elements of a dipole cloud and can be used for the statistical simulation of signals scattered from chaff.

THE SCATTERING MATRIX OF A ROTATING DIPOLE

When a dipole is rotating about the s-axis of an orthogonal coordinate system, (s, u, v) as shown in Figure A-1, the direction of its dipole moment is given by

$$\hat{d} = \hat{u} \cos \psi + \hat{v} \sin \psi \tag{1}$$

where ψ is the angle of the dipole with the $\hat{u}$-axis given by

$$\psi = w_r t + \alpha. \tag{2}$$

w_r is the dipole rotation rate in rad/sec

and α is a constant phone angle.

If the polar angles of the above s-axis, relative to a Cartesian frame (x, y, z), are θ and ϕ, as shown in Figure A-1, and if the u-axis is chosen to lay in the x-y plane, then by a coordinate rotation from the (s, u, v) to the (x, y, z) system we obtain that

$$\begin{aligned} \hat{d} = & -\hat{x} (\sin \phi \cos \psi + \cos \theta \cos \phi \sin \psi) \\ & + \hat{y} (\cos \phi \cos \psi - \cos \theta \sin \phi \sin \psi) \\ & + \hat{z} \sin \theta \sin \psi. \end{aligned} \tag{3}$$

When an electro magnetic wave is propagating along the z axis, the scattering matrix of the above dipole is given by (Borison[5], Wong et al[4])

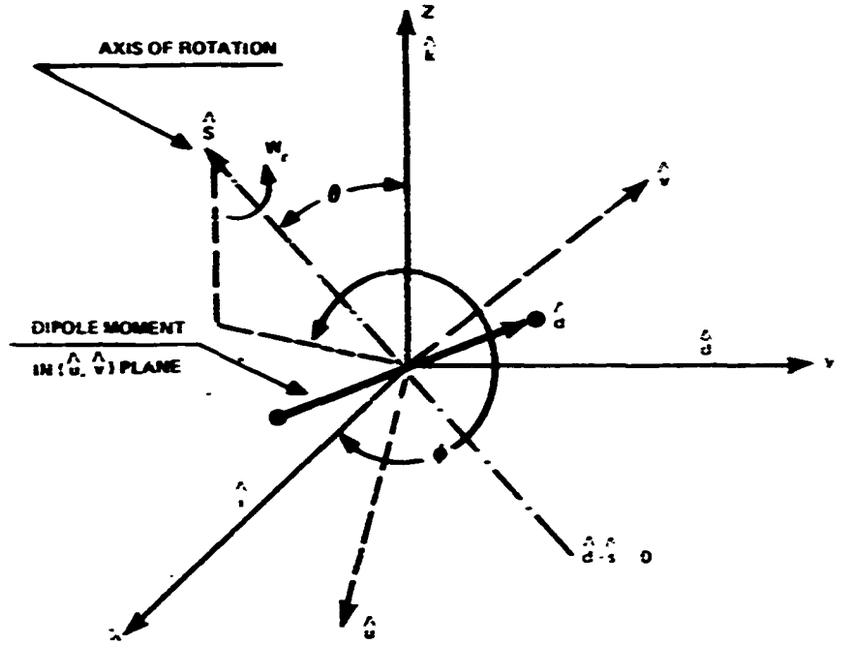

$$\hat{d} = u\cos\dot{\psi} + v\sin\dot{\psi}$$

$$\dot{\psi} = W_r t + \alpha$$

$$\hat{d} = \hat{i}(\sin\theta\cos\dot{\psi} + \cos\theta\cos\phi\sin\dot{\psi}) + \hat{j}(\cos\phi\cos\dot{\psi} - \cos\theta\sin\phi\sin\dot{\psi}) + \hat{k}(\sin\theta\sin\dot{\psi})$$

8112-15

Figure A-1. Rotating Dipole

$$H = \begin{pmatrix} h_{xx} & h_{xy} \\ h_{yx} & h_{yy} \end{pmatrix} = \sqrt{0.9}\,\lambda\,\hat{d}\,\hat{d}' \tag{4}$$

where (λ is the radar wavelength).

From Equations (3) and (4) we find that the elements of the scattering matrix H can be expressed as

$$h_{xx} = \sqrt{0.9}\,\lambda\,[C_1 + D_1\,e^{j2\psi} + D_1^{*}\,e^{-j2\psi}] \tag{5}$$

$$h_{yx} = h_{xy} = \sqrt{0.9}\,\lambda\,[C_2 + D_2\,e^{j2\psi} + D_2^{*}\,e^{-j2\psi}] \tag{6}$$

and

$$h_{yy} = \sqrt{0.9}\,\lambda\,[C_3 + D_3\,e^{j2\psi} + D_3^{*}\,e^{-j2\psi}] \tag{7}$$

where the superscript * denotes complex conjugate.

$$C_1 = \frac{1}{2}\,[\sin^2\phi + \cos^2\phi\,\cos^2\theta]$$

$$D_1 = \frac{1}{4}\,[\sin^2\phi - \cos^2\phi\,\cos^2\theta) - j\,\sin^2\phi\,\cos\theta]\ .$$

$$C_2 = -\frac{1}{2}\,\sin\phi\,\cos\phi\,\sin^2\theta\ .$$

$$D_2 = -\frac{1}{2}\,[\sin\phi\,\cos\phi + \sin\phi\,\cos\phi\,\cos^2\theta - j\,\cos(2\phi)\,\cos\theta]\ .$$

$$C_3 = \frac{1}{2}\,[\cos^2\phi + \sin^2\phi\,\cos^2\theta]\ .$$

$$D_3 = \frac{1}{2}\,[(\cos^2\phi - \sin^2\phi\,\cos^2\theta) + j\,\sin(2\phi)\,\cos\theta]$$

STATISTICS OF h_{xx}, h_{yy} FOR A RANDOM COLLECTION OF ROTATING DIPOLES

A study of the temporal and polarization response of a random collection of rotating dipoles requires estimates of autocorrelations and cross correlation functions for the elements of the scattering matrix H of Equation (4), such as

$$E[h_{xx}(t)\, h_{xx}^{*}(t-\tau)] \ , \ E[h_{xx}(t)\, h_{yy}^{*}(t-\tau)] \ ,$$

$$E[h_{xx}(t)\, h_{xy}^{*}(t-\tau)] \ , \ E[h_{yy}(t)\, h_{xy}^{*}(t-\tau)] \ , \text{ etc} \ .$$

where the expectation is over time and all possible orientations for the axes of rotation of the dipoles.

These relations can be expressed in a compact form by use of the covariance matrix

$$K_{H}(\tau) = E[\bar{h}(t)\, \bar{h}^{*}(t-\tau)] \tag{8}$$

of a vector $\bar{h}(t)$, defined as,

$$\bar{h}(t) = \begin{bmatrix} h_{xx}(t) \\ h_{xy}(t) \\ h_{yy}(t) \end{bmatrix} \tag{9}$$

If the distribution function for the angular rotation rate is $p_{w_r}(w_r)$ and for the Doppler shift due to the drift velocity is $p_{w_d}(w_d)$, then, using the results of Wong, et al.[4] and substituting from Equations (2), (5), (6) and (7) into Equations (8) and (9), we obtain that $K_H(\tau)$ can be expressed as

$$K_{H}(\tau) = M_{d}(\tau)\, [\bar{C} + 2\mathrm{Re}\, (M_{w_r}(2\tau) \cdot \bar{D})] \tag{10}$$

where the matrix $\bar{C}$ is given by

$$\bar{C} = \begin{pmatrix} E[C_1 C_1^{*}] & E[C_1 C_2^{*}] & E[C_1 C_3^{*}] \\ E[C_2 C_1^{*}] & E[C_2 C_2^{*}] & E[C_2 C_3^{*}] \\ E[C_3 C_1^{*}] & E[C_3 C_2^{*}] & E[C_3 C_3^{*}] \end{pmatrix} \tag{11}$$

the matrix $\tilde{D}$ is given by

$$\tilde{D} = \begin{pmatrix} E|D_1|^2 & E(D_1 D_2^*) & E(D_1 D_3^*) \\ E(D_2 D_1^*) & E|D_2|^2 & E(D_2 D_3^*) \\ E(D_3 D_1^*) & E(D_2 D_3^*) & E|D_3|^2 \end{pmatrix} \tag{12}$$

$M_d(\tau)$ and $M_{w_r}(\tau)$ are the characteristic functions

$$M_d(\tau) = E\left[e^{jw_d\tau}\right]$$

$$M_{w_r}(\tau) = E\left[e^{jw_r\tau}\right]$$

and $E(C_i C_j^*)$, $E|D_i D_j^*|$ are spherical random averages of the orientation of the rotation axes (Figure A-1) given by

$$E\left\{\begin{matrix}(C_i C_j^*) \\ (D_i D_j^*)\end{matrix}\right\} = \frac{1}{\Omega}\int_{\phi_1}^{\phi_2} d\phi \int_{\theta_1}^{\theta_2} \left\{\begin{matrix}C_i C_j^* \\ D_i D_j^*\end{matrix}\right\} \sin\theta \, d\theta \tag{13}$$

and

$$\Omega = \int_{\phi_1}^{\phi_2} d\phi \int_{\theta_1}^{\theta_2} \sin\theta \, d\theta = (\phi_2 - \phi_1)(\cos\theta_1 - \cos\theta_2)$$

$$0 \le \phi_1 \le \phi_2 \le 2\pi \ , \ 0 \le \theta_1 \le \theta_2 \le \pi$$

When the dipoles have all possible orientations and the variables w_d and w_r are normal with densities $N(\bar{w}_d, \sigma_d^2)$ and $N(\bar{w}_r, \sigma_r^2)$, respectively, we obtain that the covariance matrix $K_{II}(\tau)$ is given by

$$K_H(\tau) = \exp\left[-j\bar{w}_d\tau - \frac{\sigma_d^2\tau^2}{2}\right]\frac{1}{5}\begin{pmatrix}\frac{2}{3} & 0 & \frac{1}{2}\\ 0 & \frac{1}{12} & 0\\ \frac{1}{2} & 0 & \frac{2}{3}\end{pmatrix} + \exp\left[-j\bar{w}_d\tau - \frac{\sigma_d^2+4\omega_r^2}{2}\right]\cos(2\bar{w}_r\tau)\frac{1}{5}\begin{pmatrix}\frac{2}{3} & 0 & -\frac{1}{6}\\ 0 & \frac{1}{4} & 0\\ -\frac{1}{6} & 0 & \frac{1}{3}\end{pmatrix} \quad (14)$$

STOCHASTIC MODELING OF THE SCATTERING MATRIX ELEMENTS OF CHAFF

If we assume that the vector $\tilde{h}(t)$ of Equation (8) is a sample from a Gaussian vector process, then use of a vector autoregressive process yields a relatively simple linear model that has $\tilde{h}(t)$ as its output. In general, a vector autoregressive process requires the use of matrix coefficients[6]. However, because of the structure of the covariance function of $\tilde{h}(t)$, given by Equation (10), the stochastic vector $\tilde{h}(t)$ can be modeled as the sum of three vector autoregressive processes $\tilde{h}_1(t)$ $\tilde{h}_2(t)$ and $\tilde{h}_3(t)$ with scalar coefficients as

$$\tilde{h}(n\Delta t) = \left\{\tilde{h}_1(n\Delta t) + \tilde{h}_2(n\Delta t)\exp(-j2\bar{w}_r\Delta t n) + \tilde{h}_3(n\Delta t)\exp(+j2\bar{w}_r\Delta t n)\right\}\exp(-j\bar{w}_d\Delta t n) \quad (15)$$

where

$$\tilde{h}_1(n\Delta t) = \sum_{i=1}^{M_1} a_i\,\tilde{h}_1\left[(n-i)\Delta t\right] + X_n$$

$$\tilde{h}_2(n\Delta t) = \sum_{i=1}^{M_2} b_i\,\tilde{h}_2\left[(n-i)\Delta t\right] + Y_n$$

$$\tilde{h}_3(n\Delta t) = \sum_{i=1}^{M_3} b_i\,\tilde{h}_3\left[(n-i)\Delta t\right] + Z_n$$

and the a_i's and b_i's are scalar constants obtained from the Yule-Walker Equations (6)

$$\sum_{i=1}^{M_1} a_i R_1\left[(k-i)\Delta t\right] = R_1(k\Delta t), \quad k = 1, \ldots, M_1,$$

and

$$\sum_{i=1}^{M_2} b_i R_2\left[(k-i)\Delta t\right] = R_2(k\Delta t) \ , \ k = 1 \ , \ \ldots \ M_2$$

which can be solved by a fast recursive procedure developed by Durbin[7].

The orders of autoregression M_1 and M_2 depend on the sampling interval Δt and the desired accuracy in approximating the correlation functions $R_1(k\Delta t)$ and $R_2(k\Delta t)$, where

$$R_1(k\Delta t) = M_d(k\Delta t) \text{ evaluated for } \bar{w}_d = 0$$

and

$$R_2(k\Delta t) = M_d(k\Delta t) \cdot M_{w_r}(2k\Delta t) \text{ evaluated for } \bar{w}_d = 0 \text{ and } \bar{w}_r = 0.$$

The vectors X_n , Y_n and Z_n are independent noise vectors with autocovariance matrices

$$E\{X_i X_j^*\} = \delta_{ij}\tilde{C}$$

$$E\{Y_i Y_j^T\} = \delta_{ij}\tilde{D}$$

and

$$E\{Z_i Z_j^*\} = \delta_{ij}\tilde{\tilde{D}}$$

where the bar denotes complex conjugate.

In numerical simulations these vectors can be generated from

$$X_i = \tilde{C}_0 U_i$$

$$Y_i = \tilde{D}_0 V_i$$

and

$$Z_i = \tilde{\tilde{D}}_0 W_i$$

where

$$\tilde{C}_0 \tilde{C}_0^* = \tilde{C}$$

$$\tilde{D}_0 \tilde{D}_0^* = \tilde{D}$$

The asterisk denotes complex conjugate transpose and the vector U_i V_i and W_i are three-dimensional complex white noise vectors with Gaussian uncorrelated components. In many cases the covariance matrix $\tilde{D}$ is real or $\tilde{w}_r = 0$. If either of these conditions is true then one can show that $\tilde{h}(n\Delta t)$ can be expressed as the sum of only two autoregressions, which reduces the computations needed for simulation of the elements of the scattering matrix.

NUMERICAL RESULTS

As an example of the results obtained by use of the above model, we show in Figure A-2, a polar plot of the polarization states of waves backscattered from a random dipole cloud for three different transmitter antenna polarizations vertical, horizontal and circular. Data for these plots were obtained from the above model for dipoles oriented primarily within 30 degrees from the horizontal. The polar representation (r, ϕ) of the polarization states in these figures is such that the length of the radius vector is $r = 1 - e$, where e is the ellipticity, i.e., circular polarization is mapped at the origin, linear polarization along the circumference of a circle with radius = 1, and elliptical polarizations within a circle of radius = 1. The polar angle ϕ is such, that direction of the major axis of the ellipse for each polarization state is along the radius vector which goes through the point representing the state of the plot. Similarly, the direction of linear polarizations are along the radius vector. Furthermore, elliptical polarizations whose sense of rotation is right-handed, are mapped on the right-half plane of the polar plot. Thus, the above graphic representation is capable of representing all polarization states and, in effect, maps the surface of the Poincaré polarization sphere onto a circle. The only polarization state which is ambiguous in this representation is circular polarization. Both right-handed and left-handed circular polarizations are mapped on the same point at the origin of the coordinate system at the center of the polarization circle. For elliptical polarizations whose major axis is along the vertical, we have arbitrarily chosen to map left-handed polarizations onto the lower half of the vertical axis, and right-handed polarizations onto the upper half of the vertical axis. Furthermore, the size of the letter used for indicating the polarization of the received wave is varied in accordance with the total signal power in the wave, i.e., maximum power that can be extracted from the wave by a matched antenna.

FORMULAS FOR THE EXPECTATIONS $E(C_i C_j^*)$ AND $E(D_i D_j^*)$

$$\Omega = (\phi_2 - \phi_1)(\cos\theta_1 - \cos\theta_2)$$

$$I(\theta_1, \theta_2) = \frac{5}{8}(\cos\theta_1 - \cos\theta_2) - \frac{5}{48}(\cos 3\theta_1 - \cos 3\theta_2) + \frac{1}{80}(\cos 5\theta_1 - \cos 5\theta_2)$$

$$G(\theta_1, \theta_2) = -\frac{\cos^3\theta_2 - \cos^3\theta_1}{3} - (\cos\theta_2 - \cos\theta_1)$$

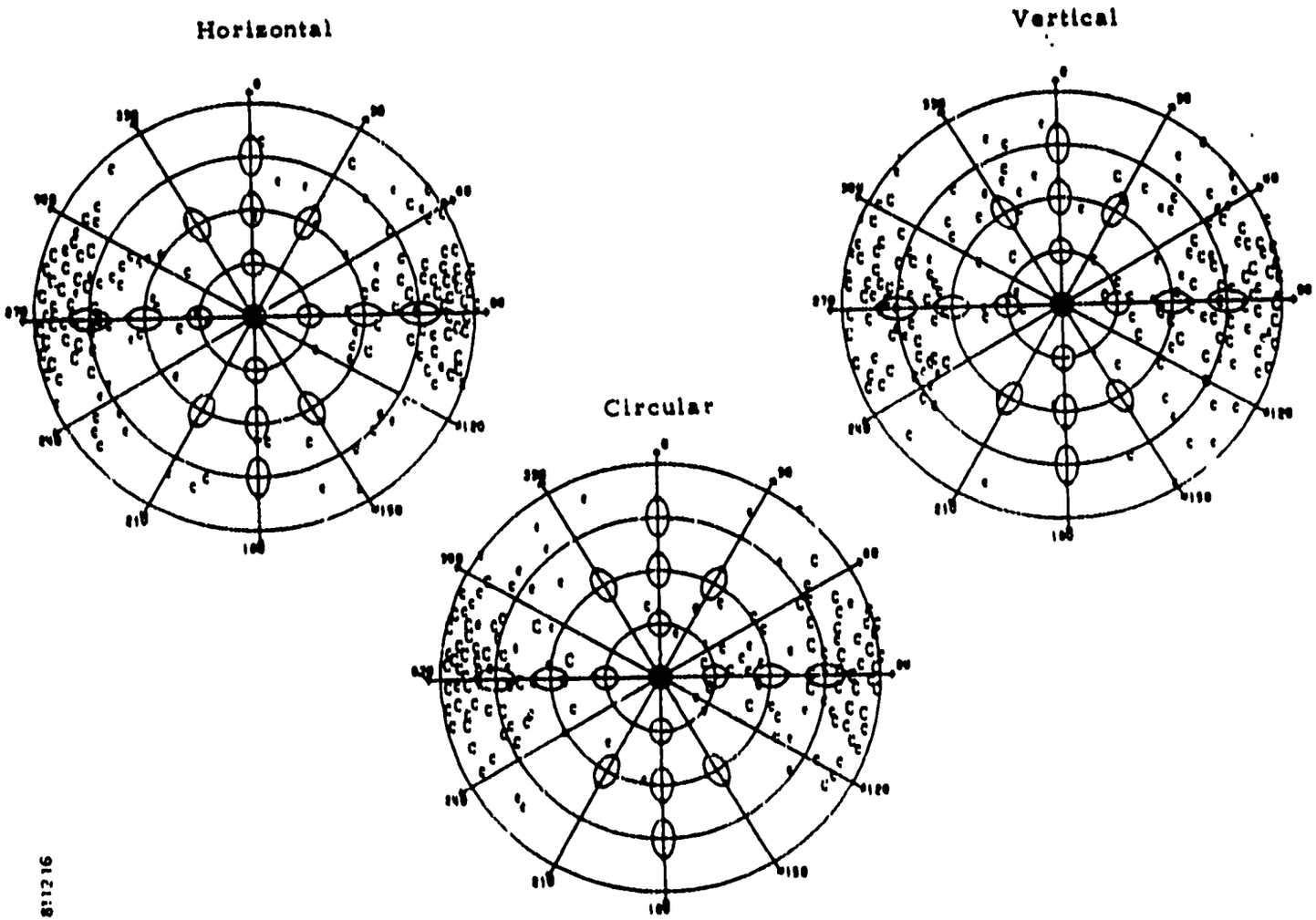

Figure A-2. Backscattered Wave Polarizations from dipoles with orientation ± 30° from horizational

$$A^{+}(\phi_1,\phi_2) = \frac{3}{8}(\phi_2-\phi_1) + \frac{1}{32}(\sin 4\phi_2 - \sin 4\phi_1) + \frac{1}{4}(\sin 2\phi_2 - \sin 2\phi_1)$$

$$B_2^{+}(\phi_1,\phi_2) = (\phi_2-\phi_1) + \frac{1}{2}(\sin 2\phi_2 - \sin 2\phi_1)$$

$$B_4^{+}(\phi_1,\phi_2) = (\phi_2-\phi_1) + \frac{1}{4}(\sin 4\phi_2 - \sin 4\phi_1)$$

$$S_2(\alpha,\beta) = \sin^2\beta - \sin^2\alpha$$

$$S_4(\alpha,\beta) = \sin^4\beta - \sin^4\alpha$$

$$E|C_1|^2 = \frac{1}{4} - \frac{1}{4\Omega}\left[B_2^{+}(\phi_1,\phi_2)\,G(\theta_1,\theta_2) - A^{+}(\phi_1,\phi_2)\,F(\theta_1,\theta_2)\right]$$

$$E|C_2|^2 = \frac{1}{4} - \frac{1}{4\Omega}\left[B_2^{-}(\phi_1,\phi_2)\,G(\theta_1,\theta_2) - A^{-}(\phi_1,\phi_2)\,F(\theta_1,\theta_2)\right]$$

$$E|C_3|^2 = \frac{1}{32\Omega}B_2^{-}(\phi_1,\phi_2)\,F(\theta_1,\theta_2)$$

$$E|D_1|^2 = \frac{1}{4}E|C_1|^2$$

$$E|D_2|^2 = \frac{1}{4}E|C_2|^2 + \frac{\cos^2\theta_1 + \cos\theta_1\cos\theta_2 + \cos^2\theta_2}{48}$$

$$E|D_3|^2 = \frac{1}{4}E|C_3|^2$$

$$E(C_1C_2^{*}) = \frac{-1}{8\Omega}S_2(\phi_1,\phi_2)\,G(\theta_1,\theta_2) + \frac{1}{16\Omega}(\cos^4\phi_2 - \cos^4\phi_1)\,F(\theta_1,\theta_2)$$

$$E(C_1C_3^{*}) = \frac{-1}{32\Omega}B_4^{-}(\phi_2,\phi_1)\,F(\theta_1,\theta_2) - \frac{\cos^2\theta_1 + \cos\theta_1\cos\theta_2 + \cos^2\theta_2}{12}$$

$$E(C_2C_3^{*}) = \frac{-1}{8\Omega}S_2(\phi_1,\phi_2)\,G(\theta_1,\theta_2) - \frac{1}{16\Omega}(\sin^4\phi_2 - \sin^4\phi_1)\,F(\theta_1,\theta_2)$$

$$E(D_1 D_2^*) = -\frac{1}{16\Omega}\left[S_2(\phi_1,\phi_2)\, G(\theta_1,\theta_2) - \frac{(\cos^4\phi_2 - \cos^4\phi_1)}{4} F(\theta_1,\theta_2)\right]$$

$$+ \frac{j}{16\Omega}\left[\frac{1}{2}(\phi_2 - \phi_1)\, S_2(\theta_1,\theta_2) - \frac{1}{8} B_2^+(\phi_1,\phi_2)\, S_4(\theta_1,\theta_2)\right]$$

$$E(D_1 D_3^*) = -E(D_1)^2 + \frac{1}{16\Omega}\left\{B_2^-(\phi_1,\phi_2)\, G(\theta_1,\theta_2) - B_2^+(\phi_1,\phi_2)\right.$$

$$\left.+\left[\frac{(\cos^5\theta_2 - \cos^5\theta_1)}{5} - \frac{(\cos^3\theta_2 - \cos^3\theta_1)}{3}\right]\right\}$$

$$- \frac{j}{64\Omega} S_2(\phi_1,\phi_2)\, S_4(\theta_1,\theta_2)$$

$$E(D_2 D_3^*) = -\frac{1}{16\Omega}\left[S_2(\phi_1,\phi_2)\, G(\theta_1,\theta_2) + S_4(\phi_1,\phi_2)\, F(\theta_1,\theta_2)\right]$$

$$+ \frac{j}{16\Omega}\left[\frac{1}{2}(\phi_2 - \phi_1)\, S_2(\theta_1,\theta_2) - \frac{1}{8} B_2^-(\phi_1,\phi_2)\, S_4(\theta_1,\theta_2)\right]$$

REFERENCES

(1) G.A. Ioannidis and D.F. Hammers, "Adaptive Antenna Polarization Schemes for Clutter Suppression and Target Identification in Processing", 2nd International Symposium on the Operator Theory of Networks and Systems, Lubbock, Texas, 1977

(2) A.J. Poelman, "Reconsideration of the Target Detection Criterion based on Adaptive Antenna Polarizations", AGARD Symposium Proceedings 1975

(3) A.J. Poelman, "Cross Correlation of Orthogonally Polarized Backscatter Components", IEE Trans. on AES, Vol 12, pp 674-682, 1976

(4) J.L. Wong, I.S. Reed, and Z.A. Kaprielian, "A Model for the Radar Echo from a Random Collection of Rotating Dipole Scatterers", IEEE Trans. on AES, Vol 3 pp 171-178, 1967.

(5) S.L. Borison, "Bistatic Cross Section of a Randomly Oriented Dipole", IEEE Trans on Antennas, Vol AP-15, pp 320-321, 1967.

(6) H. Akaike, "Autoregressive Model Fitting for Control", Ann. Inst. Statistical Math., Vol 23, pp 163-180, 1971.

(7) J. Durbin, "The Fitting of Time-Series Models", Rev. Inst. Int. Statist. Vol 28, pp 233-243, 1960.

Appendix B

LIKELIHOOD DETECTION

BINARY HYPOTHESIS TESTING

In order to make a decision whether a target is present in chaff, binary hypothesis testing is performed to determine its decision region [see Van Trees 1968]. Referring to Figure B-1, the two hypothesis H_0 and H_1 with respect to the received signal Y (with additive narrowband white noise) are:

$$\text{Hypothesis } H_0: \quad \underline{y} = Y_C + \underline{n}_o$$

$$\text{Hypothesis } H_1: \quad Y = Y_T + Y_C + \underline{n}_o$$

The input signal Y is then processed through the optimally weighted matrix G whose output Z is given by:

$$Z = G \cdot \underline{y}$$

Hence,

$$Z|H_0 = G \cdot (Y_C + N_o)$$

$$Z|H_1 = G \cdot (Y_T + Y_C + N_o)$$

and the respective covariance matrices are

$$\text{Cov}(Z|H_0) = G \cdot E[Y_C Y_C^*]G^* + G \cdot E[N_o N_o^*] \cdot G^* = R_{CN}$$

$$\text{Cov}(Z|H_1) = G \cdot E[Y_T Y_T^*]G^* + R_{CN} = R_T + R_{CN}$$

In general, the covariance matrices R_T and R_{CN} are not diagonal, and it is desirable to perform a coordinate transformation such that the resultant covariance matrices are simultaneously diagonalized. The new set of transformed random variables are now statistically independent. In order to find the desired coordinate transformation we solve the generalized eigenvalue, eigenvector problem: Find the eigenvalues μ_i and eigenvectors ϕ_i such that

$$R_T \phi_i = \mu_i R_{CN} \phi_i \qquad i = 1, \ldots k$$

is satisfied.

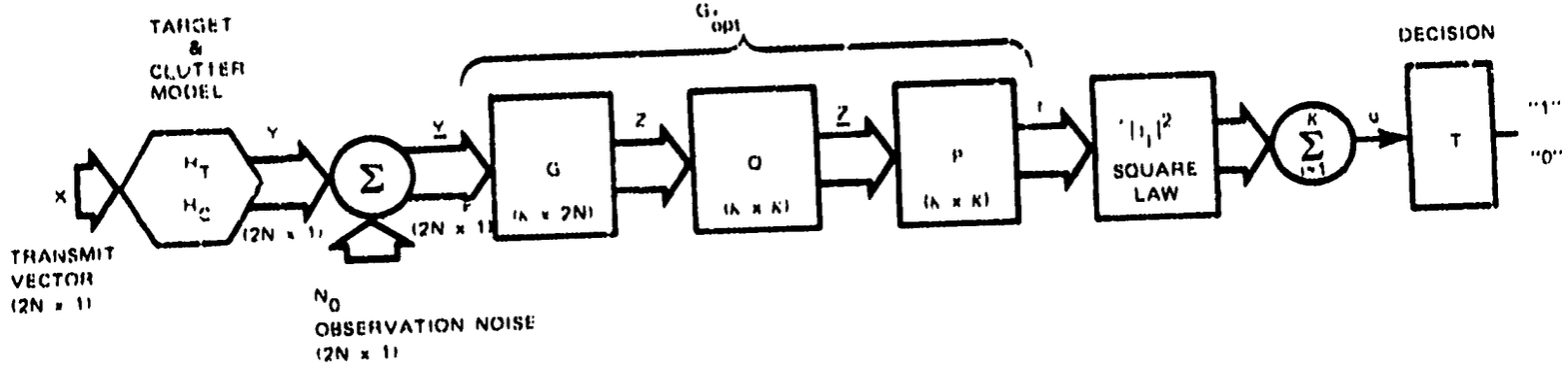

$r = G_{opt} \cdot \underline{Y}$ (POG) $\cdot \underline{Y}$

$\underline{Y} = Y + N_0$

$Y = X \cdot h$

Figure B-1. Matrix Maximum Likelihood Receiver

It is shown in Appendix D (setting $Q = \phi^*$) that solution to the above problem can expressed as follows

$$Q\ R_{cn}\ Q^* = I$$

$$Q\ R_T\ Q^* = \mu$$

where Q is the coordinate transformation matrix

I is (k x k) Identity matrix

μ is (k x k) diagonal matrix whose elements are the eigenvalues μ_i

The new set of random variables $\underline{Z}$ is

$$\underline{Z} = QZ = QG\underline{Y}$$

and the covariances under the two hypotheses are

$$cov(\underline{Z}|H_0) = I$$

$$cov(\underline{Z}|H_1) = \mu$$

RECEIVER LIKELIHOOD RATIO

In order to find the decision criteria for the binary hypothesis test we take the likelihood ratio $\Lambda(\underline{Z})$

$$\Lambda(\underline{Z}) = \ln\left(\frac{p(\underline{Z}|H_1)}{p(\underline{Z}|H_0)}\right)$$

$$= -\underline{Z}^* (\mu + I)^{-1}\ \underline{Z} + \underline{Z}^*\ I\underline{Z} - \tfrac{1}{2} \ln[\det(\mu + I)]$$

$$= \underline{Z}^* [I - (\mu + I)^{-1}] \underline{Z} - \tfrac{1}{2} \ln[\det(\mu + I)]$$

Further, we define another transformation P such that

$$\underline{r} = P \cdot \underline{Z} = P \cdot Q \cdot Z = P \cdot Q \cdot G \cdot \underline{Y}$$

and

$$P = [I - (\mu+I)^{-1}]^{1/2} = \begin{bmatrix} \sqrt{\frac{\mu_1}{1+\mu_1}} & & & 0 \\ & \sqrt{\frac{\mu_2}{1+\mu_2}} & & \\ & & \ddots & \\ 0 & & & \sqrt{\frac{\mu_k}{1+\mu_k}} \end{bmatrix}$$

then

$$\Lambda(r) = r^* r + \text{const}$$

and the decision criteria is

$$u = r^* r = \sum_{i=1}^{k} |r_i|^2 > T \qquad H_1: \text{ Target present}$$

Consequently, the probability of false alarm P_{FA} is given by

$$P_{FA} = \int_T^\infty p(u|H_0)du$$

and probability of detection is given by

$$P_D = \int_T^\infty p(u|H_1)du$$

and the optimal receiver weighting matrix is given by

$$G_{opt} = P \cdot Q \cdot G$$

THRESHOLD DETERMINATION

The general form of the probability density function p(u) is given by

$$p(u) = \sum_{i=1}^{k} \frac{1}{\prod_{\substack{j=1 \\ j \neq i}}^{k} \left(1 - \frac{\sigma_j^2}{\sigma_i^2}\right)} \frac{e^{-u/\sigma_i^2}}{\sigma_i^2} \quad : u \geq 0$$

where

$$u = \sum_{i=1}^{k} |r_i|^2$$

$$\sigma_i^2 = E|r_i|^2$$

$$p(r_1, \ldots, r_k) = \prod_{i=1}^{k} p(r_i)$$

$$p(T) = \int_T^{\infty} p(u) = \sum_{i=1}^{k} \frac{e^{-T/\sigma_i^2}}{\prod_{\substack{j=1 \\ j \neq i}}^{k} (1 - \sigma_j^2/\sigma_i^2)}$$

For a given P_{FA} the threshold T can be computed from the above equation using the Newton-Raphson iterative technique with the appropriate σ_i^2 for H_0 condition and $P_{(T)} = P_{FA}$.

Appendix C

CONSTRAINED OPTIMIZATION OF S/C

The constrained optimization problem is as follows. Given the target and clutter convariance matrices K_{YT} and K_{YC}, find the optimum W that maximizes the signal to clutter ratio defined by

$$S/C \triangleq \frac{W^* K_{YT} W}{W^* K_{YC} W} \tag{1}$$

where W is a N x1 complex column vector,
* denotes complex conjugate transpose
and K_{YT}, K_{YC} are both positive definite hermitian matrices.

This problem is equivalent to maximization of

$$W^* K_{YT} W \tag{2}$$

subject to the constraint

$$W^* K_{YC} W = 1 \tag{3}$$

Let λ be the Lagrange multiplier and define F(w) as

$$F(w) = W^* K_{YT} W - \lambda (W^* K_{YC} W - 1) \tag{4}$$

In order to use the Lagrange multiplier for maximizing F(w), both real scalar functions $W^* K_{YT} W$ and $W^* K_{YC} W$ must be differentiable with respect to W which is complex. Applying the Cauchy-Riemann Equations to test for differentiability, the test fails and it is concluded that the scalar functions are nowhere differentiable in C^N (complex N dimensional space). An alternate approach is to solve the differentiation problems in real space R^{2N}.

$$\text{Let } W = X + jY \tag{5a}$$

$$K_{YT} = \text{Re}\,[K_{YT}] + j\,\text{Im}\,[K_{YT}] \tag{5b}$$

$$K_{YC} = \text{Re}\,[K_{YC}] + j\,\text{Im}\,[K_{YC}] \tag{5c}$$

For any hermitian matrix M we have

$$M = Re[M] + j\, I_m[M]$$

$$Re[M] = (Re[M])^T,\ I_m[M] = -(I_m[M])^T$$

where superscript T denotes tranpose.

Therefore, W*MW can be rewritten as

$$\begin{aligned} W^*MW &= X^T Re[M] X + Y^T Re[M] Y + Y^T I_m[M] X - X^T I_m[M] Y \\ &\quad + j(X^T Re[M] Y - Y^T Re[M] X + X^T I_m[M] X + Y_T I_m[M] Y) \\ &= X^T Re[M] X + Y^T Re[M] Y + Y^T I_m[M] X - X^T I_m[M] Y \\ &= Re[W^*MW] \end{aligned} \tag{6}$$

Note that

$$X^T Re[M] Y = (X^T Re[M] Y)^T = (Re[M] Y)^T (X^T)^T = Y^T Re[M] X$$

and

$$X^T I_m[M] X = (X^T I_m[M] X)^T = (I_m[M] X)^T (X^T)^T = X^T (-I_m[M]) X = 0$$

W*MW can now be expressed as follows

$$W^*MW = (X^T, Y^T) \begin{bmatrix} Re[M] & -I_m[M] \\ I_m[M] & Re[M] \end{bmatrix} \begin{pmatrix} X \\ Y \end{pmatrix} = (X^T, Y^T)\, M_1 \begin{pmatrix} X \\ Y \end{pmatrix} \tag{7}$$

where M_1 is a positive definite symmetric real matrix.

Now we introduce the gradient operator ∇_W defined as

$$\nabla_W \triangleq \left(\frac{\partial}{\partial X_1}, \frac{\partial}{\partial X_2}, \cdots \frac{\partial}{\partial X_N}, \frac{\partial}{\partial Y_1}, \frac{\partial}{\partial Y_2}, \cdots, \frac{\partial}{\partial Y_N} \right) \tag{8}$$

$$\nabla_W \begin{pmatrix} X \\ Y \end{pmatrix} = \begin{bmatrix} \frac{\partial X_1}{\partial X_1} & \frac{\partial X_1}{\partial X_2} & \cdots & \frac{\partial X_1}{\partial X_N} & \frac{\partial X_1}{\partial Y_1} & \cdots & \frac{\partial X_1}{\partial Y_N} \\ \frac{\partial X_2}{\partial X_1} & & & & & & \\ \vdots & & & & & & \\ \frac{\partial X_N}{\partial X_1} & & & & & & \\ \frac{\partial Y_1}{\partial X_1} & & & & & & \\ \vdots & & & & & & \\ \frac{\partial Y_N}{\partial X_1} & & & & & & \frac{\partial Y_N}{\partial Y_N} \end{bmatrix} = \left[\nabla_W \begin{pmatrix} X \\ Y \end{pmatrix} \right]^T = I \qquad (9)$$

Then we have

$$\nabla_W (W^* MW) = \nabla_W \left[(X^T, Y^T) M_1 \begin{pmatrix} X \\ Y \end{pmatrix} \right]$$

$$= 2 \left[\nabla_W \begin{pmatrix} X \\ Y \end{pmatrix} \right]^T M_1 \begin{pmatrix} X \\ Y \end{pmatrix}$$

$$= 2 M_1 \begin{pmatrix} X \\ Y \end{pmatrix} \qquad (10)$$

To find the W that gives the extremes (min and max) of $F(W)$ we set

$$\nabla_W F(W) = 0 \qquad (11)$$

That is, from Equations (7) and (10)

$$\nabla_W F_{(W)} = \nabla_W [W^* K_{YT} W - \lambda (W^* K_{YC} W - 1)]$$

$$= 2 \left\{ \begin{bmatrix} Re[K_{YT}] & -I_m[K_{YT}] \\ I_m[K_{YT}] & Re[K_{YT}] \end{bmatrix} - \lambda \begin{bmatrix} Re[K_{YC}] & -I_m[K_{YC}] \\ I_m[K_{YC}] & Re[K_{YC}] \end{bmatrix} \right\} \begin{pmatrix} X \\ Y \end{pmatrix} = 0 \qquad (12)$$

Equation (12) is equivalent to two simultaneous equations set to zero

$$(Re[K_{YT}] - \lambda Re[K_{YC}])\, X - (I_m[K_{YT}] - \lambda I_m[K_{YC}])\, Y = 0 \qquad (13a)$$

$$(I_m[K_{YT}] - \lambda I_m[K_{YC}])\, X + (Re[K_{YT}] - \lambda Re[K_{YC}])\, Y = 0 \qquad (13b)$$

Therefore, we can express the two simultaneous equations into one as follows

$$(Re[K_{YT}] - \lambda Re[K_{YC}])X + j(I_m[K_{YT}] - \lambda I_m[K_{YC}])jY)$$

$$+j[(I_m[K_{YT}] - \lambda I_m[K_{YC}]) X + (Re[K_{YT}] - \lambda Re[K_{YC}])Y] = 0 \qquad (14)$$

or equivalently

$$[(Re[K_{YT}] - \lambda Re[K_{YC}]) + j (I_m[K_{YT}] - \lambda I_m[K_{YC}])] \cdot [X + jY] \qquad (15)$$

$$= [K_{YT} - \lambda K_{YC}] \quad W = 0$$

Thus,

$$\nabla_W F(w) = 2 (K_{YT} - \lambda K_{YC}) \cdot W = 0 \qquad (16)$$

The solution to $(K_{YT} - \lambda K_{YC}) \cdot W = 0$ can be obtained using the simultaneous diagonalization of two hermitian matrices discussed in Appendix D.

It then follows that there are N such extreme values λ_i and transformation vectors W_i (equals ϕ_i in Appendix D) that satisfies Equation (16) as given below

$$W_i^* K_{YT} W_i = \lambda_i$$

$$W_i^* K_{YC} W_i = 1 \qquad (17)$$

Substituting Equation (17) into Equation (1) yields

$$(S/C)_i = \frac{W_i^* K_{YT} W_i}{W_i^* K_{YC} W_i} = \lambda_i$$

and

$$\max_{W_i}(S/C) = \lambda_{max}$$

Hence, by selecting the largest eigenvalue $\lambda_i (= \lambda_{max})$ and the corresponding transformation vector $W_i (= W_{opt})$, then (S/C) is maximized over all W satisfying the constraint.

Appendix D

SIMULTANEOUS DIAGONALIZATION OF TWO COVARIANCE MATRICES

Let **A** and **B** be the two complex NXN covariance (positive definite and hermitian) matrices.

We show that the two covariance matrices **A** and **B** can be simultaneously reduced to a diagonal form by a NXN matrix ϕ such that,

$$\phi^* B \phi = \Lambda$$

$$\phi^* A \phi = I \tag{1}$$

where Λ is a NXN diagonal matrix whose elements are real and I is a NXN identity matrix.

The columns of ϕ are the eigenvectors ϕ_i satisfying

$$(B - \lambda_i A)\phi_i = 0 \tag{2}$$

where the λ_i are the eigenvalues of the matrix equation

$$|B - \lambda A| = 0 \tag{3}$$

where $|\cdot|$ denotes determinant of a matrix.

Simultaneous diagonalization of the matrices are performed in two steps. The first step is to diagonalize matrix **A**, that is,

$$W^* A W = \Omega \tag{4}$$

The columns of W are the eigenvectors w_i satisfying

$$A \cdot w_i = \omega_i w_i \qquad i = 1, \ldots, N \tag{5}$$

where ω_i are elements of the diagonal matrix Ω and the eigenvalues of the matrix equation

$$|A - \omega I| = 0 \tag{6}$$

Note that **A** is hermitian and thus Ω is real and W is a unitary matrix, i.e.,

$$W^* W = W^{-1} W = I \tag{7}$$

From Equation (4),

$$A = W \Omega W^* \tag{8}$$

Since **A** is hermitian, the eigenvalues ω_i are real and thus,

$$\Omega = \Omega^{1/2} \cdot \Omega^{1/2} \tag{9}$$

Now **A** can be rewritten as

$$\mathbf{A} = \mathbf{W} \cdot \Omega^{1/2} \cdot \Omega^{1/2} \cdot \mathbf{W}^* \tag{10}$$

and

$$\Omega^{-1/2} \cdot \mathbf{W}^* \cdot \mathbf{A} \cdot \mathbf{W} \cdot \Omega^{-1/2} = \mathbf{I} \tag{11}$$

Substituting Equation (10) into Equation (3) yields

$$\begin{aligned} |\mathbf{B} - \lambda\mathbf{A}| &= |\mathbf{B} - \lambda(\mathbf{W}\Omega^{1/2} \cdot \Omega^{1/2}\mathbf{W}^*)| \\ &= |\mathbf{W}\Omega^{1/2}(\Omega^{-1/2}\mathbf{W}^*\mathbf{B} \cdot \mathbf{W}\Omega^{-1/2} - \lambda\mathbf{I})\Omega^{1/2}\mathbf{W}^*| \\ &= |\mathbf{W}\Omega^{1/2}| \cdot |\Omega^{-1/2}\mathbf{W}^*\mathbf{B} \cdot \mathbf{W}\Omega^{-1/2} - \lambda\mathbf{I}| \cdot |\Omega^{1/2}\mathbf{W}^*| \\ &= 0 \end{aligned} \tag{12}$$

Both $|\mathbf{W}\Omega^{1/2}|$ and $|\Omega^{1/2}\mathbf{W}^*|$ are non-zero hence

$$|\Omega^{-1/2}\mathbf{W}^*\mathbf{B}\mathbf{W}\Omega^{-1/2} - \lambda\mathbf{I}| = 0 \tag{13}$$

Let

$$\mathbf{K} = \Omega^{-1/2}\mathbf{W}^* \cdot \mathbf{B} \cdot \mathbf{W}\Omega^{-1/2} \tag{14}$$

Note that K is also hermitian.

The second step is to diagonalize K. The same procedure as the diagonalization of matrix **A** is used.

$$\mathbf{V}^*\mathbf{K}\mathbf{V} = \Lambda \tag{15}$$

where the columns of the unitary matrix V are the eigenvectors v_i satisfying

$$\mathbf{K}\,v_i = \lambda_i\,v_i \qquad i = 1, \ldots, N \tag{16}$$

and λ_i are the eigenvalues of the matrix equation

$$|\mathbf{K} - \lambda\mathbf{I}| = 0 \tag{17}$$

Substituting K from Equation (14) into Equation (15), we have,

$$V^*\Omega^{-1/2}W^*BW \cdot \Omega^{-1/2}V = \Lambda \tag{18}$$

Premultiply and postmultiply Equation (11) by V^* and V, respectively.

$$V^*\Omega^{-1/2}W^*AW\Omega^{-1/2}V = V^*IV = V^*V = I \tag{19}$$

The last equality in Equation (19) is due to the property of a unitary matrix.

Defining the matrix operator ϕ as follows

$$\phi = W\Omega^{-1/2}V \tag{20}$$

Then Equations (18) and (19) yield

$$\phi^*B\phi = \Lambda$$

$$\phi^*A\phi = I \tag{21}$$

Appendix E

BHATTACHARYYA DISTANCE B FOR GAUSSIAN DENSITIES

It is assumed that the conditional probability densities under the two hypotheses H0 and H1 are zero mean Gaussian. It is noted that the random variable Z is complex and the real and imaginary components are independently zero mean Gaussian. Hence, the waveform is described in terms of Rayleigh distributed amplitude (envelope) and uniformly distributed phase.

The Gaussian statistical representation is a reasonable one for chaff as well as for targets of the Swerling I and II class where the target amplitude fluctuation is described by a Rayleigh distribution.

Let the two conditional probability densities $p(Z \mid H0)$ and $p(Z \mid H1)$ be zero mean Gaussian densities under the two hypotheses H0 and H1. The zero mean Gaussian densities densities are [Helstrom 1968]

$$p(Z \mid H0) = \frac{1}{(2\pi)^k \quad |K_{Z0}|^{1/2}} \cdot \exp\left[-\frac{Z^* K_{Z0}^{-1} Z}{2}\right] \tag{1}$$

$$p(Z \mid H1) = \frac{1}{(2\pi)^k \quad |K_{Z1}|^{1/2}} \cdot \exp\left[-\frac{Z^* K_{Z1}^{-1} Z}{2}\right] \tag{2}$$

where K_{Z0}, K_{Z1} are the kXk covariance matrices of H0 and H1.

Note that $|\cdot|$ denotes the absolute value of the determinant of a matrix.

Substituting Equations (1) and (2) into the integrand of Equation (3-34) in Section 3, the integrand becomes

$$I(Z) = [p(Z \mid H0) \cdot p(Z \mid H1)]^{1/2} = \frac{1}{(2\pi)^k \quad |K_{Z1}|^{1/2} \cdot |K_{Z0}|^{1/2}} \cdot \exp\left[-\tfrac{1}{2} Z^* \left(\frac{K_{Z0}^{-1} + K_{Z1}^{-1}}{2}\right) Z\right] \tag{3}$$

and evaluation of J using Equation (3) yields

$$J = \int_{\Omega} I(Z)dZ = \frac{\left|\frac{K_{Z0}^{-1} + K_{Z1}^{-1}}{2}\right|^{-1}}{|K_{Z0}|^{1/2} \cdot |K_{Z1}|^{1/2}} \cdot \int_{\Omega} \frac{1}{(2\pi)^k \left|\frac{K_{Z0}^{-1} + K_{Z1}^{-1}}{2}\right|^{-1}}$$

$$\cdot \exp\left[-\tfrac{1}{2}Z^*\left(\frac{K_{Z0}^{-1} + K_{Z1}^{-1}}{2}\right)Z\right] \cdot dZ$$

$$= \frac{\left|\frac{K_{Z0}^{-1} + K_{Z1}^{-1}}{2}\right|^{-1}}{|K_{Z0}|^{1/2} \cdot |K_{Z1}|^{1/2}} \tag{4}$$

The term in the numerator of Equation (4) $(K_{Z0}^{-1} + K_{Z1}^{-1})$ can be rewritten as

$$(K_{Z0}^{-1} + K_{Z1}^{-1}) = K_{Z0}^{-1}(I + K_{Z0}K_{Z1}^{-1}) = K_{Z0}^{-1}(K_{Z1} + K_{Z0})K_{Z1}^{-1}$$

Then, the determinant of $(K_{Z0}^{-1} + K_{Z1}^{-1})$ becomes

$$|K_{Z0}^{-1} + K_{Z1}^{-1}| = |K_{Z0}^{-1}(K_{Z1} + K_{Z0})K_{Z1}^{-1}| = |K_{Z0}|^{-1} \cdot |K_{Z1} + K_{Z0}| \cdot |K_{Z1}|^{-1} \tag{5}$$

Hence, substituting Equation (5) into Equation (4) yields

$$J = \left|\frac{K_{Z0} + K_{Z1}}{2}\right|^{-1} \cdot |K_{Z0}|^{1/2} \cdot |K_{Z1}|^{1/2} \tag{6}$$

The Bhattacharyya distance B is given by

$$B = -\ln J = -\ln\left[\left|\frac{K_{Z0} + K_{Z1}}{2}\right|^{-1} \cdot |K_{Z0}|^{1/2} \cdot |K_{Z1}|^{1/2}\right]$$

$$= \ln\left[\frac{|K_{Z0} + K_{Z1}|}{2^k |K_{Z0}|^{1/2} \cdot |K_{Z1}|^{1/2}}\right] \tag{7}$$

as shown in Equation (3-35).

Equation (7) can be further rewritten as

$$B = \tfrac{1}{2}\ell n \frac{|K_{Z0} + K_{Z1}|^2}{|K_{Z0}| \cdot |K_{Z1}|} + k/2\ \ell n\ \tfrac{1}{4} \tag{8}$$

In Equation (3-36) K_{Z1} and K_{Z0} are given by

$$K_{Z1} = W K_{yT} W^* + W K_{yc} W^* \tag{9}$$

$$K_{Z0} = W K_{yc} W^* \tag{10}$$

Substituting $K_{Z0} = W K_{yc} W^*$ for **A** and $W K_{yT} W^*$ for **B** in Appendix D, it is shown that there exists a coordinate transformation matrix ϕ such that

$$\phi^* B \phi = \phi^* (W K_{yT} W^*) \phi = \Lambda \tag{11}$$

$$\phi^* A \phi = \phi^* (W K_{yc} W^*) \phi = I \tag{12}$$

Let $Z = \phi z$

With this coordinate transformation, we get

$$Z^* K_{Z1} Z = Z^* W K_{yT} W^* Z = z^* \phi^* W K_{yT} W^* \phi z = z^* \Lambda z \tag{13}$$

$$Z^* K_{Z0} Z = Z^* W K_{yc} W^* Z = z^* \phi^* W K_{yc} W^* \phi z = z^* I z \tag{14}$$

Substituting Equations (13) and (14) into Equations (1) and (2),

$$K_{z1} = \Lambda + I \tag{15}$$

$$K_{z0} = I \tag{16}$$

Substituting Equations (15) and (16) into Equation (18) yields

$$B = \tfrac{1}{2}\ell n \left[\frac{|(\Lambda + I) + I|^2}{\Lambda + I} \right]$$

$$= \tfrac{1}{2}\ell n \frac{|\Lambda + 2I|^2}{|\Lambda + I|} + k/2\ \ell n\ \tfrac{1}{4} \tag{17}$$

Λ is a diagonal matrix whose elements are the eigenvalues λ_i, $i = 1, \ldots, k$. Therefore the determinants of $(\Lambda + 2I)$ and $(\Lambda + I)$ can be expressed in the product form as follows

$$|\Lambda + 2I| = \prod_{i=1}^{k} (\lambda_i + 2) \tag{18}$$

$$|\Lambda + I| = \prod_{i=1}^{k} (\lambda_i + 1) \tag{19}$$

Finally we obtain the desired result

$$\begin{aligned} B &= \tfrac{1}{2} \ln \left[\frac{\prod_{i=1}^{k} (\lambda_i + 2)^2}{\prod_{i=1}^{k} (\lambda_i + 1)} \right] + k/2 \ln \tfrac{1}{2} \\ &= \tfrac{1}{2} \sum_{i=1}^{k} \ln \left[\frac{(\lambda_i + 2)^2}{(\lambda_i + 1)} \right] + k/2 \ln \tfrac{1}{2} \\ &= \tfrac{1}{2} \sum_{i=1}^{k} \ln \left[(\lambda_i + 1) + \frac{1}{\lambda_i + 1} + 2 \right] + k/2 \ln \tfrac{1}{2} \end{aligned} \tag{20}$$

Equation (20) is the result shown in Equation (3-37) in Section 3.

Ref: Heistrom, C.W. "Statistical Theory of Signal Detection," Appendix D. Pergamon Press, 1968

Appendix F

AUTOREGRESSIVE MODELING

The Autoregressive Process

Without lack of generality we consider a scalar random process u_t with zero mean and variance σ_u^2. A second process $\{X_t\}$ is defined to be an autoregressive process (AR) of order m if

$$X_t = \alpha_1 X_{t-1} + \ldots + \alpha_m X_{t-m} + u_t \tag{1}$$

For the first order case, i.e., m = 1, we have

$$X_t = \alpha_1 X_{t-1} + u_t \tag{2}$$

Therefore by successive substitution

$$X_t = \alpha_1^2 [\alpha_1 X_{t-3} + u_{t-2}] + \alpha_1 u_{t-1} + u_t$$

Then X_t can be expressed as

$$X_t = u_t + \alpha_1 u_{t-1} + \alpha_1^2 u_{t-2} + \ldots\ldots$$

That is, X_t is expressible as an infinite order ***moving average*** process.

For the general order case we define the operator

$$B^k X_t = X_{t-k} \text{ for all } k$$

Then Equation (1) becomes

$$[1-\alpha_1 B - \ldots - \alpha_m B^m] X_t = u_t$$

Set

$$f(B) = [1-\alpha_1 B - \ldots - \alpha_m B^m]^{-1} \tag{3}$$

$$= 1 + \beta_1 B + \ldots + \beta_m B^m + \ldots \text{ (say)} \tag{4}$$

We find

$$X_t = f(B)\, u_t \tag{5}$$

It then follows that $E\, X_t = 0$ and the variance is finite as soon as $\Sigma\, \beta_i^2$ is convergent.

Yule-Walker Equations

Let us assume the process to be stationary. Then multiplying Equation (1) by X_{t-k} and taking the expectation, we find for each $k>0$:

$$\zeta(k) = \alpha_1\, \zeta(k-1) + \ldots\ldots + \alpha_m\, \zeta(k-m) \tag{6}$$

where ζ is the autocorrelation function of the process. The set of Equation (6) is the well known ***Yule-Walker equations***.

The Yule-Walker equations are particularly useful in estimating parameters of an AR process, that is, to estimate the parameters $\alpha_1, \ldots\ldots, \alpha_m$, given the observations $X_1, X_2, \ldots\ldots, X_N$, (say) of the process $\{X_t\}$. It is evident from Equation (6) that we can solve for the α_j's by substituting the sample autocorrelation functions into the first m Yule-Walker equations. Let us next consider two recursive methods of solving for the coefficients of the AR process; one for the scalar (Durbin's Method) case and the other for the vector case.

Durbin's Scalar Recursive Algorithm

In fitting a stochastic (stationary) process with an autoregressive process, the order of the process N must be decided. The criteria may be the least squares fitness to the model, where the mean squared error terminates the process when it becomes smaller than some predetermined threshold.

The conventional method of solving for the coefficients is to form N simultaneous Yule-Walker equations and solve for the A_i's by matrix inversion. However, with this method, each time the order of the AR process is increased, an NXN matrix inversion is required. A more efficient method is to use the Durbin's Recursive Algorithm described below.

The Algorithm

Given the N-1 coefficients $(A_{N-1,1}, \ldots\ldots A_{N-1,N-1})$ for the N-1 order AR process, the N coefficients $(A_{N,1}, \ldots\ldots A_{N,N})$ of the N^{th} order AR process is obtained from the two recursive equations.

$$\alpha_{NN} = \frac{\rho_N - \tilde{A}_{N-1} \cdot R_{-(N-1)}}{\rho_0 - \tilde{A}_{N-1} \cdot R_{N-1}} \tag{7}$$

$$A_N = \begin{pmatrix} A_{N-1} \\ 0 \end{pmatrix} - \alpha_{NN} \begin{pmatrix} A_{-(N-1)} \\ -1 \end{pmatrix} \tag{8}$$

where

$$\tilde{A}_N = (\alpha_{N1}, \alpha_{N2}, \ldots\ldots, \alpha_{NN})$$

$$\tilde{A}_{-N} = (\alpha_{NN}, \alpha_{NN-1}, \ldots\ldots, \alpha_{N1})$$

$$\tilde{R}_N = (\rho_1, \rho_2 \ldots\ldots, \rho_N)$$

$$\tilde{R}_{-N} = (\rho_N, \rho_{N-1} \ldots\ldots, \rho_1)$$

~ denotes transpose

The mean square error of the Nth order AR process is

$$\sigma_N^2 = \rho_0 - A_N \cdot R_N = \rho_0 \sum_{i=1}^{N} \alpha_{Ni} \rho_i = \sigma_{N-1}^2 (1 - \alpha_{NN}^2) \tag{9}$$

The initial conditions are

$$N = 1, \quad \alpha_{1,1} = \rho_1/\rho_0, \ \sigma_1^2 = \rho_0 (1 - \rho_1^2/\rho_0^2)$$

Proof

For the N-1th order AR process, the matrix equation is given by

$$\begin{Bmatrix} \rho_1 \\ \cdot \\ \cdot \\ \cdot \\ \cdot \\ \rho_{N-1} \end{Bmatrix} = \begin{Bmatrix} \rho_0 & & \rho_{N-2} \\ \cdot & & \\ \cdot & & \\ \cdot & & \\ \cdot & & \\ \rho_{N-2} & & \rho_0 \end{Bmatrix} \begin{Bmatrix} \alpha_{N-1,\,1} \\ \cdot \\ \cdot \\ \cdot \\ \cdot \\ \alpha_{N-1,N-1} \end{Bmatrix}$$

or in brief notation

$$R_{N-1} = P_{N-1} \cdot A_{N-1} \text{ or } R_{-(N-1)} = P_{N-1} A_{-(N-1)} \tag{10}$$

where the coefficients of A_{N-1} are known. Note that P matrix is positive definite.

The matrix form of the Nth order Process is thus given by

$$R_N = P_N \cdot A_N \tag{11}$$

This can be rewritten as

$$\begin{pmatrix} R_{N-1} \\ \rho_N \end{pmatrix} = \begin{pmatrix} P_{N-1} & R_{-(N-1)} \\ \tilde{R}_{-(N-1)} & \rho_0 \end{pmatrix} \begin{pmatrix} \underline{A}_N \\ \alpha_{NN} \end{pmatrix}$$

where

$$\tilde{\underline{A}}_N \triangleq (\alpha_{N1}, \ldots, \alpha_{N,N-1})$$

Then, we have

$$R_{N-1} = P_{N-1} \cdot \underline{A}_N + R_{-(N-1)} \cdot \alpha_{N,N} \tag{12}$$

$$\rho_N = \tilde{R}_{-(N-1)} \underline{A}_N + \alpha_{N,N} \rho_0 \tag{13}$$

From Equation (13)

$$\alpha_{N,N} \rho_0 = \rho_N - \tilde{R}_{-(N-1)} \cdot \underline{A}_N \tag{14}$$

From Equations (12 and 10)

$$\underline{A}_N = P_{N-1}^{-1} (R_{N-1} - R_{-(N-1)} \alpha_{N,N})$$

$$= A_{N-1} - \alpha_{N,N} P_{N-1}^{-1} R_{-(N-1)}$$

$$= A_{N-1} - \alpha_{N,N} A_{-(N-1)} \tag{15}$$

Substituting Equation (15) into Equation (14) yields

$$\alpha_{N,N}\rho_0 = \rho_N - \tilde{R}_{-(N-1)} \cdot A_{N-1} + \alpha_{N,N} \cdot \tilde{R}_{-(N-1)} \cdot A_{-(N-1)}$$

and

$$\alpha_{N,N} = \frac{\rho_N - \tilde{R}_{-(N-1)} \cdot A_{N-1}}{\rho_0 - \tilde{R}_{-(N-1)} \cdot A_{(N-1)}} = \frac{\rho_N - \tilde{A}_{N-1} \cdot R_{-(N-1)}}{\rho_0 - \tilde{A}_{N-1} \cdot R_{N-1}} \qquad (16)$$

From Equation (15) and $\alpha_{N,N}$, we form

$$\underline{A}_N = A_{N-1} - \alpha_{N,N} \cdot A_{-(N-1)}$$

$$\alpha_{N,N} = 0 + \alpha_{N,N}$$

and it follows that

$$A_N = \begin{pmatrix} \underline{A}_N \\ \alpha_{N,N} \end{pmatrix} = \begin{pmatrix} A_{N-1} \\ 0 \end{pmatrix} - \alpha_{N,N} \begin{pmatrix} A_{-(N-1)} \\ -1 \end{pmatrix} \qquad (17)$$

Equations (16) and (17) are the recursive equations of Equations (7 and 8). The mean squared error is obtained from

$$\sigma_N^2 \triangleq E\left[X(t) - \sum_{i=1}^{N} \alpha_i X(t-i)\right]^2 = E\left[X(t) - \sum_{i=1}^{N} \alpha_i X(t-i)\right) \cdot X(t)]$$

which yields

$$\sigma_N^2 = \rho_0 - \sum_{i=1}^{N} \alpha_i \rho_i \qquad (18)$$

Hence

$$\sigma_N^2 = \rho_0 - \tilde{A}_N \cdot R_N \qquad (19)$$

Substituting Equation (17) for A_N above yields

$$\sigma_N^2 = \rho_0 - (\tilde{A}_{N-1} R_{N-1} - \alpha_{N,N} \tilde{A}_{-(N-1)} R_{N-1} + \alpha_{N,N}\rho_N)$$

$$= \rho_0 - \tilde{A}_{N-1} R_{N-1} - \alpha_{N,N} (\rho_N - \tilde{A}_{-(N-1)} \cdot R_{N-1})$$

$$= \rho_0 - \tilde{A}_{N-1} \cdot R_{N-1} - \alpha_{N,N} (\rho_N - \tilde{A}_{N-1} \cdot R_{-(N-1)})$$

and from Equation (16)

$$\sigma_N^2 = \rho_0 - \tilde{A}_{N-1} R_{N-1} - \alpha_{N,N}^2 \cdot (\rho_0 - \tilde{A}_{N-1} R_{N-1})$$

$$= (\rho_0 - \tilde{A}_{N-1} \cdot R_{N-1}) (1 - \alpha_{N,N}^2)$$

$$= \sigma_{N-1}^2 (1 - \alpha_{N,N}^2) \qquad (20)$$

which is the result of Equation (9)

Matrix Recursive Algorithm

For the general case, the multivariate stochastic process can be modeled by a Vector autoregressive process Z(t).

Consider the following Nth order vector autoregressive process Z(t)

$$Z(t) = \sum_{i=1}^{N} A_{N,i} Z(t-i) + U(t) \qquad (21)$$

where

$$\tilde{Z}(t) = [z_1(t)\ z_2(t) \ldots\ldots z_p(t)$$

$A_{N,i}$ pxp matrix coefficients of the Nth order AR process.

U(t)px1 vector of independently distributed zero mean white noise process.

and

~ denotes transpose

The matrix coefficients A_i can be computed from the matrix Yule-Walker equations

$$K_m = \sum_{i=1}^{N} A_{N,i} K_{m-i} \qquad m = 1, \ldots\ldots N \qquad (22)$$

where K_m is a covariance matrix (hermitian) given by

$$K_m = \frac{1}{L} \sum_{k=1}^{L-m} Z(n+k) \cdot Z^*(n) \qquad m = 0, 1, 2 \ldots$$

$$K_m = K_{-m}^*$$

Superscript * denotes complex conjugate transpose

The mean squared error $\sum_N^a$ of the AR process may be obtained from Equation (21)

$$\sum_N^a = K_0 - \sum_{i=1}^{N} A_{N,i} K_i \tag{23}$$

Real Process

The matrix recursive algorithm solving for the $A_{N,i}$ is derived below for a real valued multivariate stochastic process. For complex case, see the next subsection on complex processes.

The mean squared error $\sum_N^a$ of Equation (23) combined with the N Yule-Walker Equations of Equation (22) can be expressed in matrix form as follows

$$[I, -A_{N,1}, -A_{N,2}, \ldots, -A_{N,N}] \begin{bmatrix} K_0 & K_1 & \ldots & K_N \\ K_{-1} & K_0 & & K_{N-1} \\ \cdot & & & \cdot \\ \cdot & & & \cdot \\ \cdot & & & \cdot \\ K_{-N} & K_{-(N-1)} & & K_0 \end{bmatrix} = \left[\sum_N^a, 0, \ldots, 0\right]$$

or in brief notation

$$[I, -\underline{A}_N] \cdot K_N = [\sum_N^a, 0, \ldots, 0] \tag{24}$$

For N+1th order, we pick an α_N such that

$$[I, -\underline{A}_N, 0]\, K_{N+1} = [\sum_N^a, 0, \ldots, 0, \alpha_N] \tag{25}$$

which is the representation of Equation (24) and

$$K_{N+1} - A_{N,1} K_N - A_{N,2} K_{N-1} - \cdots - A_{N,N} K_1 - 0 \cdot K_0 = \alpha_N$$

or

$$\alpha_N = K_{N+1} - \sum_{i=1}^{N} A_{N,i} \cdot K_{N+1} \tag{26}$$

We note that if $\alpha_N = 0$, then $\underline{\underline{A}}_{N+1} = (\underline{\underline{A}}_N, 0)$ and the desired solution is obtained. If this does not happen, α_N must be forced to zero. In order to do this, we introduce the backward (adjoint) equation.

$$Z(t-N) = \sum_{i=1}^{N} B_{N,i} Z(t-N+i)$$

$$[0, -B_{N,N}, -B_{N,N-1}, \cdots -B_{N,1}, 1] \cdot K_{N+1} = [\beta_{N,0}, \cdots, 0, \quad \Sigma_N^b]$$

or in brief notation

$$[0, -\underline{\underline{B}}_N, 1] \; K_{N+1} = [\beta_{N,0}, \cdots, 0, \Sigma_N^b] \tag{27}$$

which is a representation of

$$[-\underline{\underline{B}}_N, 1] \cdot K_N = [0, \ldots \quad , 0, \Sigma_N^b]$$

and

$$\beta_N = K_{-(N+1)} - \sum_{i=1}^{N} B_{N,i} K_{i-N-1} \tag{28}$$

We now form a weighted combination of Equations (25) and (27).

$$\left\{[1, -\underline{\underline{A}}_N, 0] + Q_N^a [0, -\underline{\underline{B}}_N, 1]\right\} \cdot K_{N+1}$$

$$= [\Sigma_N^a + Q_N^a \beta_N, 0, \ldots, 0, \alpha_N + Q_N^a \Sigma_N^b] \tag{29}$$

By setting the last element of the vector on the RHS

$$\alpha_N + Q_N^{\alpha} \Sigma_N^b = 0$$

or

$$Q_N^{\alpha} = -\alpha_N [\Sigma_N^b]^{-1} = 0 \tag{30}$$

then we have the solution for $\underline{\underline{A}}_{N+1}$ in the form of Equation (24) for N provided we have $\underline{\underline{B}}_N$, and Σ_N^b

$$[I, -\underline{\underline{A}}_{N+1}] = [I, -\underline{\underline{A}}_N, 0] + Q_N^{\alpha} [0, -\underline{\underline{B}}_N, I] \tag{31}$$

and

$$\Sigma_{N+1}^a = \Sigma_N^a + Q_N^a \beta_N \tag{32}$$

In order to obtain the $\underline{\underline{B}}_N$ and Σ_N^b, we perform a similar operation as in Equation (29) as follows

$$\left\{[0, -\underline{\underline{B}}_N, I] + Q_N^b [I, -\underline{\underline{A}}_N, 0]\right\} \cdot K_{N+1}$$

$$= [\beta_N + Q_N^b \Sigma_N^a, 0, \ldots, 0, \Sigma_N^b + Q_N^b \alpha_N] \tag{33}$$

from which we get

$$\beta_N + Q_N^b \Sigma_N^a = 0$$

or

$$Q_N^b = -\beta_N [\Sigma_N^a]^{-1} \tag{34}$$

and it follows that

$$[-\underline{\underline{B}}_{N+1}, I] = [0, -\underline{\underline{B}}_N, I] + Q_N^b [I, -\underline{\underline{A}}_N, 0] \tag{35}$$

$$\Sigma_{N+1}^b = \Sigma_N^b + Q_N^b \alpha_N$$

The matrix recursive algorithm is stated as follows: Given $(\underline{\underline{A}}_N; \Sigma^a_N; \alpha_N)$ and $(\underline{\underline{B}}_N; \Sigma^b_N; \beta_N)$ for the Nth order AR process. $(\underline{\underline{A}}_{N+1}; \Sigma^a_{N+1}; \alpha_{N+1})$ and $(\underline{\underline{B}}_{N+1}; \Sigma^b_{N+1}; \beta_{N+1})$ for the N+1th iteration is obtained from the following matrix recursive equations

$$1a)\quad Q^a_N = -\alpha_N \left[\Sigma^b_N\right]^{-1}$$

$$2a)\quad [I, -\underline{\underline{A}}_{N+1}] = [I, -\underline{\underline{A}}_N, 0] + Q^a_N\ [0, -\underline{\underline{B}}_N, I]$$

$$3a)\quad \Sigma^a_{N+1} = \Sigma^a_N + Q^a_N \cdot \beta_N$$

$$4a)\quad \alpha_{N+1} = K_{N+2} - \sum_{i=1}^{N+1} A_{N+1,i} \cdot K_{N+2-i}$$

$$1b)\quad Q^b_N = -\beta_N \left[\Sigma^a_N\right]^{-1}$$

$$2b)\quad [-\underline{\underline{B}}_{N+1}, I] = [0, -\underline{\underline{B}}_N, I] + Q^b_N\ [I, -\underline{\underline{A}}_N, 0]$$

$$3b)\quad \Sigma^b_{N+1} = \Sigma^b_N + Q^b_N \cdot \alpha_N$$

$$4b)\quad \beta_{N+1} = K_{-(N+2)} - \sum_{i=1}^{N+1} B_{N+1,i} \cdot K_{i-N-2}$$

The initial conditions are

$$\Sigma^a_0 = K_0 = \Sigma^b_0 : \alpha_0 = K_1 \text{ and } \alpha_0 = K_1 \text{ and } \beta_0 = K_{-1} = \tilde{K}_1$$

we note that $\alpha_N = \tilde{\beta}_N$. i.e., an adjoint relationship

Complex Process

In dealing with a complex random variable $z = x + jy$, we note that z is in fact comprised of bivariate random variables x, y , and hence a complex scalar stochastic process must be treated as a real vector of dimension two. For a complex N dimensional process, the multivariate dimension is 2N.

As described earlier, in the process of generating an AR model, the matrix coefficients of A_i must be determined when the stochastic process is complex, special care must be taken in formulating the matrix equations.

Thus the following rule must be observed

1) Given a NxN complex matrix M, decompose this matrix into the real and imaginary parts.

$$M = R_e[M] + j\, I_m[M]$$

2) Define a 2Nx2N real matrix $\underline{M}$ where

$$\underline{M} = \begin{bmatrix} R_e[M], & I_m[M] \\ -I_m[M], & R_e[M] \end{bmatrix}$$

3) Substitute $\underline{M}$ for M

The complex form of the matrix Yule-Walker Equation of Equation (22) can be rewritten as

$$\underline{K}_m = \sum_{i=1}^{N} \underline{A}_{N,i} \cdot \underline{K}_{m-i}$$

$$K_{m,i} = \sum_{i=1}^{N} A_{N,i} \cdot K_{m-i}$$

can be rewritten as

$$R_e[K_m] + j\, I_m[K_m] = \sum_{i=1}^{N} (R_e[A_{N,i}] + j\, I_m[A_{N,i}]) \cdot (R_e[K_{m-i}] + j\, I_m[K_{m-i}])$$

$$= \sum_{i=1}^{N} \Big\{ (R_e[A_{N,i}] \cdot R_e[K_{M-i}] - I_m[A_{N,i}] \cdot I_m[K_{m-i}]) + j(I_m[A_{N,i}] \cdot R_e[K_{m-i}] + R_e[A_{N,i}] \cdot I_m[K_{m-i}]) \Big\}$$

and

$$\underline{K}_m = \sum_{i=1}^{N} \underline{A}_{N,i} \cdot \underline{K}_{m-i}$$

can also be rewritten as

$$\begin{bmatrix} R_e[K_m] & I_m[K_m] \\ -I_m[K_m] & R_e[K_m] \end{bmatrix} = \sum_{i=1}^{N} \begin{bmatrix} R_e[A_{N,i}] & I_m[A_{N,i}] \\ -I_m[A_{N,i}] & R_e[A_{N,i}] \end{bmatrix} \cdot \begin{bmatrix} R_e[K_{m-i}] & I_m[K_{m-i}] \\ -I_m[K_{m-i}] & R_e[K_{m-i}] \end{bmatrix}$$

$$= \sum_{i=1}^{N} \begin{bmatrix} R_e[A_{N,i} \cdot K_{m-i}] & I_m[A_{N,i} \cdot K_{m-i}] \\ -I_m[A_{N,i} \cdot K_{m-i}] & R_e[A_{N,i} \cdot K_{m-i}] \end{bmatrix}$$

MISSION
of
Rome Air Development Center

RADC plans and executes research, development, test and selected acquisition programs in support of Command, Control Communications and Intelligence (C^3I) activities. Technical and engineering support within areas of technical competence is provided to ESD Program Offices (POs) and other ESD elements. The principal technical mission areas are communications, electromagnetic guidance and control, surveillance of ground and aerospace objects, intelligence data collection and handling, information system technology, ionospheric propagation, solid state sciences, microwave physics and electronic reliability, maintainability and compatibility.